Investigation of the molecular machinery underlying sleep homeostasis in *Drosophila melanogaster.*



Seoho (Michael) Song

Supervisor: Professor Gero Miesenböck

St. John's College

University of Oxford

This report is submitted in partial fulfilment for the degree of

Doctor of Philosophy

Trinity 2017

Abstract

Though universal and highly conserved, the biological function of sleep remains largely mysterious. One approach to solving this mystery is to study the neural mechanisms that regulate sleep and waking. There are two such mechanisms: the circadian clock, which synchronizes sleep with periodic changes in the external environment, and the sleep homeostat, which responds to (still largely unknown) internal changes that require sleep to reset. Understanding this second, homeostatic control system will likely offer important clues to the biological function of sleep.

In the fruit fly, *Drosophila melanogaster*, a homeostatic sleep switch has been discovered in a cluster of two dozen neurons with projections to the dorsal fan-shaped body (dFB) in the central brain. The electrical activity of these cells induces sleep and is antagonistically modulated by two potassium currents: Shaker-based A-type currents promote sleep, whereas Sandman-based leak currents inhibit sleep. The potassium conductances are, in turn, regulated by Rho GTPase activating proteins such as Crossveinless-c (Cv-c). How this molecular machinery logs a fly's sleep history and responds by altering the electrical properties of the dFB neuronal membrane is currently unknown.

In this study, two molecular mechanisms were identified that signal changes in sleep drive within dFB neurons. The first mechanism involves Rho GTPases and their regulators. Catalytically 'dead' Cv-c was found to be unable to rescue the short-sleeping phenotype of *cv-c* mutants, implicating the GTPase cycle of a small G protein of the Rho family in sleep regulation. Through behavioural screens, Rho1 was identified as a candidate Cv-c substrate, and Rac1 as a Rho1 antagonist. Targeted ablations of Rho1 and Rac1 in the dFB neurons of *cv-c* mutants rescued and exacerbated sleep deficits,

respectively. Thus, active Rac1 and Rho1 promote sleep and wakefulness in a mutually antagonistic fashion.

The second mechanism involves the action of oxidation by-products on Hyperkinetic (Hk), a beta subunit of the potassium channel Shaker whose function in dFB neurons is important for sleep. Hk is a functional aldo-keto reductase and senses cellular redox levels. This redox sensing capacity is required to restore sleep in short-sleeping Hk^{1} mutants. Mitochondrial respiration is a primary source of reactive oxygen species (ROS). *In vivo* measurements of mitochondrial ROS in sleep deprived flies revealed that sleep pressure correlated with ROS concentrations in dFB neuron dendrites. Elevating ROS in dFB neurons by overexpressing mutant superoxide dismutase (Sod1) increased sleep, whereas overexpressing wild type Sod1, which neutralizes ROS, decreased sleep. These effects were occluded in the absence of functional Hk, which implicates it as the site of redox modulation of membrane excitability. Thus, ROS acts as a potential link between energy metabolism, oxidation, and sleep.

Acknowledgements

First and foremost, I would like to thank my supervisor, Gero Miesenböck, for the priceless opportunity to work with him and mature under his mentorship. Six years ago, I contacted Gero as a complete novice, fresh out of my undergraduate degree. Gero took me in without hesitation and introduced me to his team and his work. Initially, I struggled as I troubleshot experiment after experiment, most of which failed, but Gero was ever patient. He always made time to offer me his guidance, and by following his advice, I emerged out of the darkness towards the light. He assisted and endorsed me in all my endeavours, from writing letters of recommendations for my various applications to reviewing and editing my thesis. His ability to attend to my needs in his busy schedule always amazed me. I could not have found a supervisor as reliable and generous as Gero. One of the most important lessons he taught me was to be direct and not to shy away when opportunity presents: "go for the jugular!" Gero would say. I am proud to be Gero's student, and I am eternally grateful for his trust in me.

Additionally, I would like to acknowledge the current and former members of the Miesenböck group for their incredible camaraderie. In particular, I am grateful to Jeffrey Donlea, Anissa Kempf, Diogo Pimentel, Clifford Talbot, Jan Kropf, Shamik DasGupta, and Evan Harrell for their advice and generous help. Jeff introduced me to sleep and my first batch of fruit flies, and he also taught me all the essential skills I needed to know for my behavioural experiments. During his time in Oxford, Jeff was the kindest and most attentive collaborator and friend that I could have. Anissa offered me valuable advice and guidance as a collaborator and friend. I continue to work with her closely, and I have learned so much from her mentorship. Diogo has helped me understand electrophysiology, which became so key to interpreting my results, and he has also kindly proofread my thesis. Cliff and Jan have helped me with all sorts of technical difficulties. Shamik has

offered me with immense intellectual support and frequently advised me in all manners of difficulties. Evan taught me a great deal in molecular biology. He also showed me how to make the best of my time at Oxford. During times of struggles, it was the kind words and insightful assistance of these colleagues and friends that diverted me from despair to optimism. In addition, I extend my warm gratitude to the other members of the Miesenböck group and by extension the CNCB.

I also acknowledge Lukas Groschner and Laura Chan Wah Hak, my fellow graduate students in the Miesenböck group, for their support. They are incredible colleagues and friends. I am also greatly indebted to Katerina Christodoulou, current technician and soon-to-be graduate student, for the selfless hours she devoted to help me with many of my experiments. Not only did she share the laborious task of setting up and conducting the experiments, but she was a great companion and helped to transform these duties into much more enjoyable activities.

I am also grateful to Donald Mitchell and Kevin Duffy, my first mentors, who encouraged me to pursue a path in science. Even after my undergraduate graduation, they welcomed me with open arms whenever I visited them and continued to offer me valuable advice. I thank them for helping me start my scientific career. Without them, I would not have been able to make it to the "Land of Soap and Water." (This one is for you Donald!)

Moreover, I would like to acknowledge my parents for their everlasting support in all my endeavours. Despite their hopes for me to enter medicine, they did not lose faith in me even when I chose graduate studies over medical school. They have always been the greatest fans of my work, and I am eternally grateful to them for helping and encouraging me to follow my passion.

Finally, I would like to show my deepest appreciation for the Commonwealth Scholarship Commission (CSC) for its generous financial support. I am honoured to join

the CSC's illustrious global network of scholars, and I am grateful for the many friendships I made as part of this community.

Besides these named individuals, there is an even longer list of unsung heroes who have vitally influenced my path to completing this manuscript. I am forever grateful to have had such a caring and friendly palette of acquaintances.

Sir Isaac Newton famously stated that "if I have seen further, it is by standing on the shoulders of giants." My academic journey embodies this ethos, and so I begin my thesis by echoing these words to show my recognition and gratitude for the invaluable support I received to venture this far into my career.

Table of Contents

Abstract.....2

Acknowledgements 4

Chapter 1: Introduction 10

1.1 The mystery of sleep. 10

1.2 An operational definition of sleep. 12

1.3 A two-process model of sleep regulation. 13

1.3.1 Circadian regulation of sleep. 13

1.3.2 Homeostatic regulation of sleep. 14

1.4 The biological functions of sleep. 18

1.4.1 Sleep promotes memory consolidation. 18

1.4.2 Sleep promotes synaptic scaling. 20

1.4.3 Sleep promotes metabolic recovery. 21

1.5 *Drosophila melanogaster* as a model of sleep regulation. 25

1.5.1 A powerhouse for behavioural genetics. 25

1.5.2 The dorsal fan-shaped body: a locus for the sleep homeostat. 26

Chapter 2: Results.....32

2.1 How does Cv-c regulate sleep in the dFB neurons? 32

2.1.1 Cv-c's GAP activity is necessary for sleep regulation in the dFB neurons. 32

2.1.2 Behavioural screen for sleep regulatory Rho GTPases. 43

2.1.3 Rac1 promotes sleep whereas Rho1 promotes wakefulness. 52

2.2 What is the sleep regulatory role of Hk? 61

2.2.1 *Sh* and its interacting partners, *Hk* and *sss*/*qvr,* are required for sleep regulation in the dFB neurons. 61

2.2.2 Redox sensing via Hk's aldo-keto reductase domain is necessary for sleep. 65

2.2.3 Sleep deprivation causes oxidative stress in dFB neurons. 69

2.2.4 ROS levels in dFB neurons modulate sleep. 75

2.2.5 Hk mediates the sleep-promoting effect of ROS in dFB neurons. 87

Chapter 3: Discussion 98

3.1 Sleep homeostasis in the dorsal fan-shaped body: a recap. 98

3.2 Sleep regulation via Rho GTPases. 99

3.2.1 A model for sleep regulation via Rho GTPases in the dFB neurons. 99

3.2.2. The wild type genetic background is unsuitable for behavioural assays of Rho GTPase dynamics. 99

3.2.3 Processes upstream and downstream to sleep regulatory Rho GTPases. 100

3.2.4 Future directions. 102

3.3 Sleep regulation via neuronal redox states. 104

3.3.1 A model for sleep regulation via redox modulation in the dFB neurons. 104

3.3.2 Sources of mitochondrial ROS production. 104

3.3.3 Oxidative regulation of membrane biophysics. 106

3.3.4 Future directions. 108

Chapter 4: Materials and Methods 111

4.1 Drosophila strains. 111

4.2 Molecular biology. 114

4.3 Confocal microscopy. 115

4.4 Behavioural analyses. 116

4.4.1 Sleep measurements using *Drosophila* Activity Monitors. 116

4.4.2 Sleep deprivation using SNAP. 116

4.4.3 Arousal threshold measurements. 117

4.5 Functional imaging of redox state. 118

4.6 Statistical analyses. 120

Bibliography 121

Appendix 130

Chapter 1: Introduction

1.1 The mystery of sleep.

Sleep is vital and universal, yet its biological function(s) remain(s) mysterious. Among the countless figures who have grappled with the enigma of sleep, the 2nd Century Roman physician Galen stands out as the earliest documented scholar who focused on the brain as the seat of perception and waking activity[1].

Galen's views on sleep strike us as particularly perceptive from a modern perspective. He inquired into the mechanics of sleep in his attempt to understand its purpose and its medicinal value[2]. In contrast to his Hippocratic predecessors, who argued that sleep's purpose was to facilitate digestion[2,3], Galen imagined sleep as a rest response that allows our brain to escape from the rigours of our waking experience[1]. Galen claimed that while awake, the brain actively engages in perception, and he proposed this to be one of the brain's primary functions[4]. Galen believed that the brain is connected via humorous conduits called *dunamis* to the *prôton aisthêtikon*, the sensory organs[4]. According to this conjecture, vigilance during periods of wakefulness draws fresh *dunamis* from the brain to the senses, and while this flow is bidirectional, the taxing demands incurred by perception heavily favour the efflux of *dunamis* from the brain[4]. To Galen, *dunamis* was a physical symbol of neural activity[2].

Prolonged periods of perception would drain the brain of *dunamis*, at which point it could no longer maintain wakefulness. According to Galen, sleep was the brain's response to such a depletion[4]. By minimizing perception, sleep restores the brain's *dunamis* by retrogradely transporting it from the sense organs[4]. Accordingly, Galen argued that the duration of sleep is subject to the intensity of the waking experience[4].

Galen's model, while mostly conjectural, offers two valuable insights. First, he pointed out that prolonged periods of wakefulness are energetically demanding for the

brain. Second, Galen predicted that the cumulative magnitude of this demand determines the duration and depth of sleep. Galen arrived at these conclusions purely through predictions based on observations at his clinic.

Galen proclaimed that a complete understanding of sleep would:

παμπόλλης μὲν τῆς ζητήσεως δεόμενον, ἴσως δ' οὐδ' εὑρεθῆναι δυνάμενον

require a very long process of inquiry, and perhaps even then it cannot be found out[2,5].

1800 years have elapsed since Galen's time, and we are still tackling the same question that challenged him.

1.2 An operational definition of sleep.

A significant portion of our modern understanding of sleep has been possible thanks to extensive work on animal models. Sleep has been reported in every animal species placed under careful behavioural scrutiny[6,7], and while animals sleep in diverse manners[8], many commonalities can be extracted from a comparative analysis of different species. These common features not only indicate that sleep is highly conserved, but they also provide a set of behavioural criteria for an operational definition of sleep[7].

1. State reversibility: it must be possible for a sleeping organism to be woken up with sufficiently intense stimulation.

2. Heightened arousal thresholds: when asleep, an organism is less responsive to stimuli, thus stimuli of higher intensities are required to elicit behavioural responses.

3. Distinctive immobile posture: organisms are immobile during sleep, and they assume a species-specific posture to accommodate this.

4. Regulation (circadian and homeostatic): the timing and amount of sleep in an organism are regulated through circadian and homeostatic mechanisms, respectively.

These criteria offer a reference to standardize and evaluate sleep across species. That these behavioural features are shared across species moreover suggests that the biological mechanisms that give rise to them are also likely conserved. Thus, by examining sleep in animal models, where behavioural, genetic, and physiological analyses are more easily feasible than in humans, it is possible to gain mechanistic insights into sleep and its biological role(s) that are likely to be general.

1.3 A two-process model of sleep regulation.

To address why an organism sleeps, it is important first to identify the biological mechanisms of sleep regulation. In 1982, Alexander Borbély proposed a model of sleep regulation that has been influential in guiding the field's progress[9]. According to this model, sleep is regulated by two mechanistic arms: one circadian and the other homeostatic (in **Figure 1.1**, these are indicated as C and S, respectively)[9].

1.3.1 Circadian regulation of sleep.

The circadian system attunes the organism to periodic changes in external stimuli (especially light and temperature) that arise from the Earth's rotation[10]. The energetic and neural costs of waking activity can be recovered during sleep (See **1.4.3**). Yet, disconnecting an organism's senses from environmental stimuli and, moreover, immobilizing it is a large risk, especially for those that must avoid predation. The circadian rhythm helps to mitigate this problem by restricting sleep to periods of the day when most organisms (especially the predators) are inactive[10]. Thus, by synchronizing its sleep and activity to that of its natural predators, an organism's sleep is no longer life threatening[10]. Therefore, the circadian clock facilitates the biological advantages of sleep by minimizing the ecological risks stemming from sleep's behavioural restrictions.

At the molecular level, the circadian clock operates as a transcriptional feedback system. Some of the first evidence for this system was discovered in the fruit fly, *Drosophila melanogaster*[11], and near identical counterparts have been reported in mammals, thus illustrating that the circadian system is highly conserved[12,13]. In *Drosophila*, "clock genes" such as *clock* (*clk*) and *cycle* (*cyc*), a pair of heterodimeric transcription factors, accumulate during the day[13]. Once formed, Clk/Cyc activate the transcription of *period* (*per*) and *timeless* (*tim*), which dimerize to form an additional

layer of transcriptional control[13]. This Per/Tim complex then suppresses the transcription of Clk and Cyc, thus completing a negative feedback loop[14]. The subsequent reduction in Clk/Cyc, in turn, lifts the transcriptional activation of *per* and *tim*, ultimately clearing Per/Tim from the system[13]. This liberates Clk and Cyc from the feedback inhibition imposed upon them by their peptide products, thus resetting the system for a new cycle. Cryptochrome is a photoreceptor which responds to blue light by accelerating the degradation of Tim, thus facilitating the accumulation of Clk and Cyc during the day and entraining the oscillation to the day-night cycle[15,16]. The final outcome of this multi-layered system of transcriptional control is an autonomous clock that allocates sleep and wakefulness to designated periods in a 24-hour cycle.

1.3.2 Homeostatic regulation of sleep.

The homeostatic system adjusts the organism to currently unknown internal cues thought to accumulate during waking activity[9,17]. When this sleep debt surpasses a set threshold, sleep begins until this debt is cleared and a new cycle starts[17]. The sleep homeostat thus allocates sleep amount (and depth) as a function of an organism's sleep history.

Homeostatic control is best revealed through sleep deprivation. When an organism is deprived of sleep, it will sleep more deeply and for an extended time at the next opportunity when sleep is possible[7,18]. This rebound sleep is the prime demonstration of a homeostatic response[18]. Knowing the molecular mechanism through which the brain accounts for its sleep debt will be vital, as it may divulge a crucial clue towards the coveted biological role of sleep.

In contrast to the detailed literature available for the circadian arm of sleep regulation, comparatively little is known about the molecular "nuts and bolts" of the sleep homeostat. Early investigations have suggested several candidate mechanisms such as

chaperones[19], potassium channel subunits[20], synaptic plasticity[21,22], steroid hormones[23], but the most comprehensive description thus far can be found in *Drosophila*. Homeostatic sleep regulation in flies involves the reciprocal modulation of two potassium currents of opposing consequences within a select cluster of sleep promoting neurons[24]. This forms a sleep switch that records and translates the flies' sleep history into electrical events at the membranes of specific neurons[24,25]. This mechanism and the neurons in which it operates will be discussed in greater detail in **1.5.2**.

Thus, we are beginning to uncover a cohesive molecular framework that explains what signals or cells the brain uses to keep track of sleep need. In order to advance our understanding of sleep, it is imperative to characterize the molecular currency that lodges and homeostatically monitors an organism's sleep history.

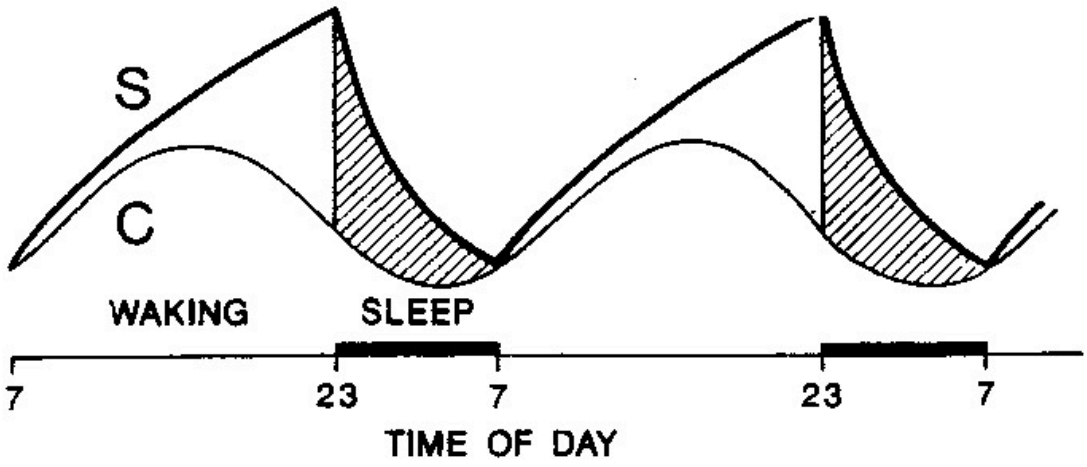

Figure 1.1 Two-process model of sleep regulation[9]

Figure 1.1 Two-process model of sleep regulation[9]

A graphical representation of Alexander Borbély's two-process model of sleep regulation[9]. The homeostatic (S) and circadian (C) regulatory arms are overlapped above a time course on the abscissa. The homeostatic system illustrates an initially linear increase in the sleep drive during wakefulness followed by a rapid, decline following the exceedance of a threshold. The circadian system demonstrates a sinusoidal fluctuation of sleep and wakefulness as a function of light and dark periods during a 24-hour cycle.

1.4 The biological functions of sleep.

Where should one look for the sleep homeostat? Perhaps it is possible to work backwards to the homeostat's location by examining processes that lie downstream from it. There are numerous biological outcomes that result from sleep; these range from synaptic modifications [22,26-28] to the removal of metabolic waste[29]. If a central homeostat were to exist, it must lie at the nexus between at least three processes: (1) memory consolidation, (2) synaptic scaling, and (3) metabolic recovery. While independent, these functions are not mutually exclusive.

1.4.1 Sleep promotes memory consolidation.

Memory represents an organism's capability to log previous experiences to optimize its future encounters with similar instances[30]. The registration of memory in the brain is thought to involve three stages: encoding, consolidation, and retrieval[30]. When an organism encounters novel stimuli of behavioural significance, the brain encodes this information as a fresh memory[30]. Next, during consolidation, this labile memory is stabilized for either short term or long term storage[30,31]. Once the memory is reliably catalogued and stored, it can later be retrieved during a new encounter with familiar stimuli.

That sleep is essential for memory consolidation is perhaps one of the most easily accepted truths. Aside from our personal anecdotes of poor memory performance following a lack of sleep, there is a wealth of studies that have investigated the connection between sleep and memory[30,32]. Two primary lines of experimental evidence support this link. First, sleep deprivation following training is detrimental for memory consolidation. This is a near universal observation that has been reported across countless species from humans to fruit flies. In humans, for instance, sleep deprivation following a spatial

learning task resulted in the participants to underperform compared to control participants[33]. Similarly, experiments with fruit flies showed that male flies fail to express their learned courtship avoidance when their training is followed by a night of sleep deprivation[34]. This study also demonstrated that the converse prediction was also true; that is, post-training sleep boosts the efficiency of memory consolidation and increases subsequent memory performance[34]. Sleep – from fruit flies to humans – removes an organism from environmental stimuli and shields its memory from the interfering influences of external inputs. Sleep deprivation leaves an organism vulnerable to such inputs and, thus, compromises its memory.

The second line of evidence in support of sleep's active facilitation of memory consolidation came through *in vivo* physiological studies of sleeping brains. Most notably, Wilson and McNaughton recorded from the hippocampal CA1 place cells in rats during periods of wakefulness and sleep[35]. When an awake rat explores a novel environment, ensembles of place cells fire in a characteristically correlated manner[36]. Recordings from the hippocampi of sleeping rats revealed correlated firing within these neuronal ensembles that closely mimicked the activity observed in the same cells in the awake animal[35]. Comparable reactivations of neuronal ensembles were also observed in the dentate gyrus during sleep following spatial training[37]. Curiously, these reactivations coincided with slow-wave sleep, the characteristic waveform that underlies homeostatic sleep in mammals[35,37].

These results speak to a role of sleep in memory consolidation. Not only does sleep protect memory, but it also actively strengthens it. The search for a mechanistic link, however, continues.

1.4.2 Sleep promotes synaptic scaling.

Persistent wakeful experience involves dynamic, cohesive activity amongst vast neuronal populations[38]. Perceptual processing and filtering of environmental stimuli, encoding novel stimuli into memory, and maintaining the attention to support these are all essential to enhance an organism's adaptability to its surroundings. These processes demand the detection of vast quantities of "suspicious coincidences" that are each encoded in the connections between neurons[38,39]. The collective expenditure of this widespread networking activity levies a substantial toll on neurons[38]. Once this burden surpasses a threshold, the organism can no longer afford to remain awake, and thus sleep is considered as "the price the brain pays for plasticity"[38].

Synapses are the principal sites of interneuronal communication and the foundation of all neuronal processes, ranging from sensory transduction to higher order cognition. The Hebbian rule states that "neurons that fire together, wire together," and thus synapses within neural circuits that display correlated activity are strengthened both structurally and functionally[40]. This form of synaptic plasticity forms the foundation of the synaptic homeostasis hypothesis of sleep (SHY). Proposed by Giulio Tononi and Chiara Cirelli in 2003, the SHY suggests that wakefulness involves a great deal of coherent activity between diverse constellations of neurons, and this fortifies the underlying synapses[41,42]. The SHY assumes that the awake brain experiences widespread correlated excitation rather than inhibitions, and this would lead to synaptic upscaling on a global scale[41,42].

To counter this cost of remaining awake, sleep offers the brain an opportunity for synaptic downscaling[41,42]. During sleep, wide-scale, correlated excitation is no longer present, synaptic upscaling ceases[41,42], and an opportunity arises to prune non-essential synapses[41,42]. This synaptic downscaling optimizes neuronal connectivity, for the end

result is the persistence of connections with the most up-to-date information[41,42]. This is critical for adaptive processes such as memory[30]. The consolidation stage of memory formation requires a refinement step, which is akin to sleep-dependent synaptic downscaling[30]. Thus, according to the SHY, sleep promotes memory consolidation through synaptic pruning.

Experimentally, the SHY has been difficult to demonstrate, for neuronal dynamics in awake and sleeping animals are more diverse and less dichotomous than assumed by the SHY (for instance, the SHY neglects the inhibitory connections that are present in awake animals[38,43]), and it is technically challenging to measure synaptic strength across the whole brain. Nonetheless, there is some supporting evidence from fruit flies and rodents. In *Drosophila*, wakefulness or sleep deprivation is correlated with increased labelling for synaptic biomarkers (e.g. synaptotagmin or bruchpilot)[22,26] whereas sleep is associated with decreased detection of these markers[22,26,34,44]. A recent study even demonstrated that sleep deprivation primes the sleep drive in *Drosophila* by increasing excitatory glutamatergic receptor expression in the membrane of sleep regulatory cells while rebound sleep following the deprivation downscales the excitability of these synapses[45]. In rodents, sleep causes structural modifications of some, but not all, synapses[28]. As the SHY would predict, smaller synapses were preferentially pruned[28].

Thus, the current literature contains some correlative evidence in support of the SHY, but closer inquiry is required for a mechanistic model of how sleep regulation is directly tied to synaptic scaling.

1.4.3 Sleep promotes metabolic recovery.

All cellular events have an energetic cost. Thus, for a cell to function as a component of a larger tissue, organ, or system, its metabolism is inevitably tied to its activity and the

role it needs to fulfil. Neurons are no exception to this rule. Action potentials are thermodynamically expensive cellular processes[46-48]. Energy (in the form of adenosine triphosphate [ATP]) is required to restore the intracellular sodium and potassium concentrations through the sodium-potassium pump, and the synthesis of all the necessary proteins represents an additional energetic cost for the cell[49]. Thus, in order to perform such a costly function, neuronal metabolism must be optimized[50,51]. ATP synthesis in the mitochondria is the cell's primary source of energy production, and this is powered by the transfer of electrons from reducing agents (e.g. nicotinamide adenine dinucleotide [NADH]), which are produced during glycolysis and the tricarboxylic acid cycle, to molecular oxygen.

Remaining awake is therefore costly for the brain. Perhaps sleep's function is to temporarily reduce this cost through metabolic homeostasis. Strikingly, investigations of gene expression in *Drosophila* and rodents at different behavioural states revealed a similar trend: extended periods of wakefulness involve wide scale downregulation of genes involved in metabolic pathways[52-55]. Examples of these genes include components of carbohydrate metabolism and oxidative phosphorylation as well as catabolic cascades for amino acids, lipids, and aldehydes[54,55]. Curiously, these genes are upregulated during sleep[54]. In particular, the genes that experience some of the largest fold changes in their expression levels are those encoding mitochondrial proteins. For instance, components of the electron transport chain, the cell's primary harnessers of metabolic energy for ATP synthesis, are highly upregulated during sleep[54,56]. This supports the view that sleep restocks the brain's energetic stores in preparation for the next episode of wakefulness.

How do disturbances in energy homeostasis trigger sleep? One hypothesis for the mechanism underlying this behavioural switch involves cellular stress. Protracted energy expenditure by any cell would inevitably lead to metabolic stress[57]. Since wakefulness

requires persistent neuronal activity, this might contribute to cellular stress in vast populations of neurons[56]. Perhaps it is this cellular stress that triggers the transition to sleep. This hypothesis is partially supported by studies in *Drosophila* and rodents. Wakefulness and sleep deprivation result in the upregulation of heat shock proteins such as molecular chaperones[52,58,59]. These proteins respond to various stress factors such as intracellular calcium, oxidation, misfolded proteins, glucose depletion, and others, and they are induced by the unfolded protein response in the endoplasmic reticulum[60]. Errors in protein biosynthesis comprise one of the principal causes of cellular stress, and removing these misfolded proteins is a default defence mechanism for cells to manage their stress[60].

More specifically, it would be important to know what type of cellular stress neurons are exposed to when the organism is awake. If this stress mechanism directly triggers sleep, this could potentially represent the input that feeds into the sleep homeostat, and further, this could be the long-sought after biological substrate for sleep. One candidate stress signal is reactive oxygen species (ROS). These molecules are by-products of reduction-oxidation reactions (i.e. processes that involve the exchange of electrons) involving highly electronegative – and thus reactive – elements such as oxygen[57]. Due to its high affinity for electrons, molecular oxygen, if left lingering for sufficient periods in the intracellular milieu, will extract electrons from nearby species to create ROS such as superoxide anions[57]. Such ROS will react with and damage nearby cellular infrastructure and lead to oxidative stress, a state in which the cell cannot manage its level of intracellular oxidation[57]. ROS are produced by two sources: the mitochondrial electron transport chain and NADPH oxidase in the plasma membrane[61]. The former site represents the greater manufacturing source[57], and it links ROS generation to cellular energy metabolism.

ROS involvement in sleep has been demonstrated in both *Drosophila* and mammals. Injecting oxidized glutathione, an oxidant (i.e. a chemical that mimics the activity of ROS)[57], into ventricles of rabbits increased sleep, suggesting that sleep can be affected by cellular redox conditions[62]. Similar results were observed with the infusion of the oxidant *tert*-butyl-hydroperoxide into the third ventricles of rats[63]. In flies, restricted sleep either due to deprivation or age-related sleep fragmentation resulted in increased ROS levels in the brain as well as increased gene expression of neuroprotective and antioxidant mechanisms[64]. Further to these findings, a recent meta-analysis evaluated 266 studies and concluded with high statistical confidence that sleep deprivation promotes oxidative stress, a state in which oxidants overwhelm the internal machinery that removes them[65]. Conversely, sleep is antioxidizing and helps to reduce this oxidative burden[65]. This is particularly convincing given that the studies analysed here used numerous model organisms and diverse sleep deprivation procedures. Collectively, these investigations suggest that ROS accumulation promotes sleep, and through sleep, the brain removes toxic chemicals that result from the metabolic duress of remaining awake for extended periods of time. What still remains unanswered is the molecular link that ties energy homeostasis to sleep.

1.5 *Drosophila melanogaster* as a model of sleep regulation.

Solving the enigma of sleep will require the identification of candidate molecules that convey homeostatic signals. Thus, an optimal model system for these analyses ought to facilitate reliable behavioural measurements of sleep that satisfy the criteria mentioned above. Simultaneously, such a model should accommodate highly precise and diverse strategies to enable biochemical manipulations in specific cells.

The fruit fly, *Drosophila melanogaster*, offers an optimal platform for convergent molecular and behavioural analyses of sleep. Flies fulfil the four behavioural criteria for sleep mentioned in **1.2**[7,19,66]. Moreover, sleep in flies is genetically comparable to that in mammals, as evidenced by the near identical regulation of similar gene families during different behavioural states[52,67,68]. In addition, learning impairments following post-training sleep deprivation is observed in both flies and mammals[69]. Thus, sleep in flies is highly similar to mammalian sleep. And, of course, that behavioural features of sleep are so closely shared between mammals and flies suggests that the molecular mechanisms underlying sleep regulation may also be conserved across these different model systems.

1.5.1 A powerhouse for behavioural genetics.

One of the greatest strengths of *Drosophila* stems from unparalleled genetic access to reliably identifiable cells and the ability to conduct saturating forward genetic strategies to link mutations in specific genes to behavioural changes[70]. This comprehensive approach uncovered countless genes important for sleep regulation. Examples include *per*[11], *tim*[71], *Sh*[67], *Hk*[72] and many others. Of particular note is the discovery and subsequent mechanistic dissection of *per* and *tim*, for this laid the foundation for understanding the molecular clockwork enabling circadian timekeeping[13].

Another strength of *Drosophila* behavioural genetics is the mature, versatile techniques for precisely targeted gene expression. Originally engineered from yeast, the *GAL4/UAS* system is the most widely used transgenic platform in *Drosophila* research[73,74]. It is a binary system consisting of two components. The GAL4 driver is a yeast derived transcriptional activator protein that binds to a UAS (upstream activator sequence) and initiates the transcription of the sequence controlled by the UAS only in cells expressing GAL4, despite the UAS being ubiquitously present[74]. The specificity of the GAL4 driver is determined by the sequences located immediately upstream of the driver coding sequence[75-77]. These regulatory DNA sequences are typically fragments derived from the promoters of genes, and the resulting driver would express in cells demarcated by these promoter fragments[75-77]. With the availability of the full genomic sequence for *Drosophila melanogaster*[78], exhaustive efforts by multiple institutions around the globe have led to the generation of vast libraries of GAL4 drivers and UAS constructs[77]. This has made it possible to ectopically target a diverse list of genes in diverse but specific cell populations in *Drosophila*. Moreover, the availability of additional transgenic platforms such as the LexA/LexAop and QF/QUAS systems further expands the scope of genetic manipulation in the fruit fly[79].

1.5.2 The dorsal fan-shaped body: a locus for the sleep homeostat.

These general benefits aside, perhaps the single greatest unique advantage of *Drosophila* in sleep neurobiology is the fact that we currently know a locus for sleep homeostasis in the fly brain (See below for evidences). The dorsal fan-shaped body (dFB) is comprised of a cluster of cells in the central complex (**Figure 1.2**). The cell bodies of dFB neurons are located laterally, with processes projecting medially and dorsally to form dendritic tufts and ventrally to create an axonal arch. While the anatomy of the central complex

was thoroughly established by early investigations[80-82], it was only recently that the dFB neurons have entered the spotlight of sleep neurobiology.

In 2011, Donlea et al. discovered that artificial activation of these neurons was sufficient to put flies to sleep[34]. By measuring the flies' arousal thresholds, these researchers were able to verify that the behavioural effect of dFB activation is genuinely sleep and not merely a cessation of locomotion[34]. In addition, it was observed that sleep induced via dFB activation enhanced performance on a courtship learning task[34].

Subsequent studies found that the electrical activity of dFB neurons is directly connected to the fly's behavioural state. Electrophysiological recordings from dFB neurons revealed that these cells exist in two discrete activity states; they are electrically active (ON, **Figure 1.2**) when the fly is asleep, and they are quiescent (OFF, **Figure 1.2**) when the fly is awake[25]. This intriguingly suggests that these cells contain machinery to initiate the switch between sleep and wakefulness. Further investigations revealed that the arousal-promoting effect of dopamine[83] is mediated by dFB neurons[24]. Specifically, dopaminergic input to dFB neurons switches the cells to the electrically silent (OFF) state by reciprocally modulating two types of potassium currents[24]. Dopamine attenuates voltage-dependent A-type currents through Shaker, which are critical for repetitive spiking, and enhances leak potassium currents through Sandman, a two-pore domain potassium channel[24]. During sleep, these currents are regulated in the opposite directions: increased A-type and decreased leak conductance[24]. These results indicate that the dFB neurons possess the functional architecture of an electrical switch for transitioning between behavioural states.

dFB neurons regulate sleep homeostatically. Sleep deprivation in flies results in an enhanced sleep drive that is encoded as heightened membrane excitability of dFB neurons[25]. This is a remarkably elegant mechanism: The biophysical excitability switch

acts as the lever that switches the fly's behavioural state when sleep need surpasses a threshold[25].

The signalling cascades within dFB neurons that constitute the gears of the sleep homeostat remain largely unknown. One intriguing lead, however, is the finding that mutations in *crossveinless-c* (*cv-c*), a gene encoding a Rho family GTPase activating protein (GAP), permanently prevent dFB neurons from spiking[25]. These mutant flies exhibit severe insomnia and its cognitive consequences, and they are incapable of rebound sleep following sleep deprivation[25].

What is the molecular composition of the sleep homeostat in the dFB neurons? I approached this question with a two-pronged strategy to identify the upstream signals and the downstream targets that comprise this sleep regulatory network. Based on previous results that Cv-c is necessary for regulating membrane excitability in the dFB neurons (and in turn, sleep in flies)[25], I hypothesized that Cv-c (acting as a Rho GAP) and its substrate (a Rho GTPase) are upstream sleep regulatory signals. I sought to elucidate whether Cv-c's catalytic activity regulates sleep and, in turn, identify its substrate.

The integration of these signals must then influence the electrical activity in the dFB neurons, ultimately by modulating the activity of ion channels in the neuronal membrane[24,25]. Accordingly, from the downstream end of this signalling cascade, I searched for the ion channels in the dFB neuronal membrane that are involved in sleep regulation. Building on the finding that potassium conductance through the Shaker ion channel promotes sleep, I chose to dissect how this conductance is regulated. A genetic screen revealed that knocking down the beta subunits or the auxiliary modulators of the Shaker complex mimics the knock down of the alpha subunit, suggesting that they are necessary for the whole channel to function properly. Specifically, I focused on identifying a regulatory locus in Hyperkinetic, a beta subunit of the Shaker complex.

Curiously, Hyperkinetic is an aldo-keto reductase, and it senses cellular reduction-oxidation potentials[84]. Thus, I predicted that Hyperkinetic's sleep regulatory role involves its ability to modulate cellular redox potentials. Accordingly, I investigated whether the dFB neurons respond to changes in cellular oxidation and whether this response requires Hyperkinetic.

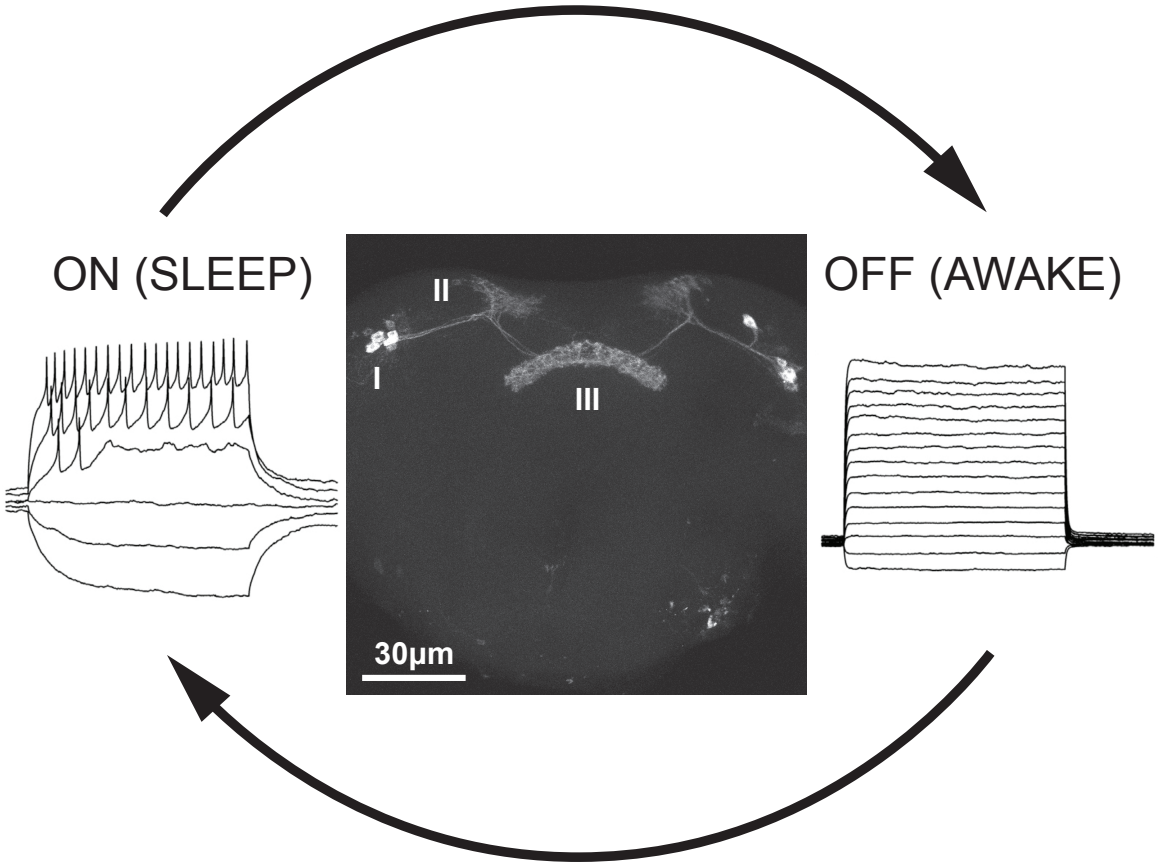

Figure 1.2 Electrical activity in the dFB neurons is linked to behavioural states in flies.

Figure 1.2 Electrical activity in the dFB neurons is linked to behavioural states in flies. The anatomy of the dFB neurons is indicated through a representative image in the centre of the diagram. Cell bodies (I) are located laterally on either side of the brain with projections connecting them to the dorsal dendritic tufts (II) and the medial axonal arch (III) in the central brain. Biphasic electrical activity in the dFB neurons is connected to sleep and wakefulness in flies. The traces are current clamp recordings of the dFB neurons at different behavioural states. When the dFB neurons are electrically active (ON), the flies sleep. When the dFB neurons are electrically silent (OFF), the flies are awake. Pimentel et al. showed that such electrical activity precedes transitions into the following behavioural states, which suggests that it is this electrical signature that initiates the fly to transition between sleep and wakefulness and vice versa[24].

Chapter 2: Results

2.1 How does Cv-c regulate sleep in the dFB neurons?

Previous work has established that predicted Rho-GAP Crossveinless-c (Cv-c) regulates sleep by modulating the membrane excitability of dFB neurons[25]. Yet, the molecular nature of this regulation is unknown; in particular, it is unclear whether the Rho-GAP activity of Cv-c is required. The work documented in this section helps to address this issue.

2.1.1 Cv-c's GAP activity is necessary for sleep regulation in the dFB neurons.

Cv-c is structurally complex. It is comprised of 1017 amino acids with three conserved domains[85]. These are the GTPase activating protein (GAP), sterile α motif (SAM), and steroidogenic acute regulatory protein (START) domains[85]. Commonly, Cv-c is categorized as a GAP that deactivates Rho family GTPases[85], yet this is not to say that its other domains can be ignored. In fact, Rho GAPs partake in pathways independent of their GAP activity but rather dependent on their immediate microenvironment[86-88]. Does Cv-c function as a GAP when it performs its sleep-regulatory role in dFB neurons?

To test this, I created a UAS-driven transgene encoding wild type Cv-c ($cv\text{-}c^{WT}$), which could be expressed in specific cell populations via the GAL4/UAS system. Moreover, I also created a catalytically 'dead' construct wherein the GAP domain is rendered inactive ($cv\text{-}c^{R601Q}$) via a point mutation in arginine 601 (for glutamine), which is critical for the GAP activity[85]. For both constructs, I created untagged as well as C-terminal HA (hemagglutinin) tagged variants.

Expressing *cv-c*^{R601Q} in the dFB neurons of wild type flies mimics the *cv-c* mutation.

By driving transgene expression in the dFB neurons via *R23E10-GAL4*, I overexpressed *cv-c*^{WT} and *cv-c*^{R601Q} in wild type flies. The expression patterns of the constructs were validated immunohistochemically by labelling the HA tagged Cv-c^{WT} and Cv-c^{R601Q} (**Figures 2.1.1-A** and **B**). Untagged constructs were generated using the identical vector backbone, which is expected to confer identical expression. Behavioural experiments involved these untagged constructs. **Figures 2.1.2-A** and **B** show that targeted overexpression of *cv-c*^{WT} in dFB neurons did not significantly change the flies' sleep. [Throughout this report, significant behavioural differences are only considered if the experimental group differs from both parental controls: responder and driver]. However, overexpressing the catalytically inactive construct in the dFB neurons significantly decreased sleep, mimicking the short-sleeping phenotype of the *cv-c* mutants (*cv-c*^{MB3717}/*cv-c*^{C524}) (**Figures 2.1.1 C** and **D**). Thus, *cv-c*^{R601Q} is a dominant negative mutation, underscoring the importance of the GAP domain in Cv-c's sleep regulatory function in the dFB neurons.

R23E10-GAL4 > UAS-mCD8::GFP,
UAS-cv-c$^{WT-CTHA}$

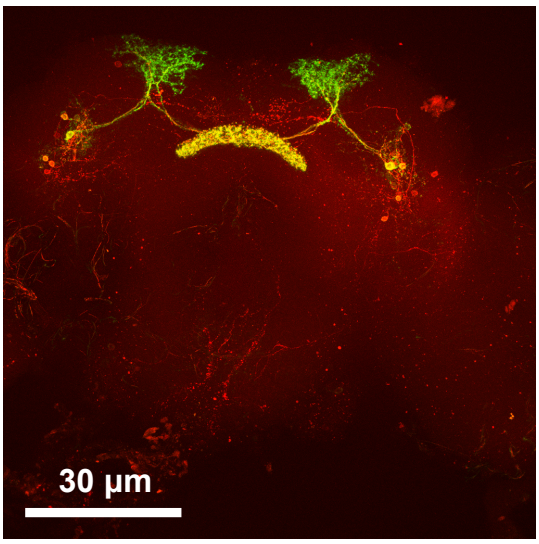

R23E10-GAL4 > UAS-mCD8::GFP,
UAS-cv-c$^{R601Q-CTHA}$

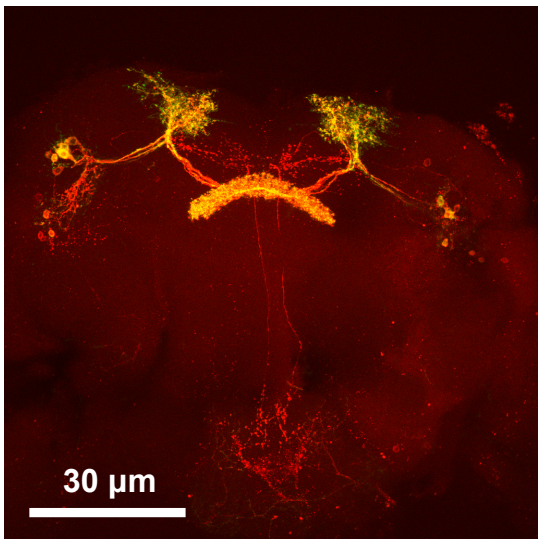

Figure 2.1.1 *cv-c$^{WT-CTHA}$* and *cv-c$^{R601Q-CTHA}$* expression in the dFB neurons.

Figure 2.1.1 *cv-c*$^{WT\text{-}CTHA}$ and *cv-c*$^{R601Q\text{-}CTHA}$ expression in the dFB neurons.

R23E10-GAL4 driven expression of mCD8::GFP with either *cv-c*$^{WT\text{-}CTHA}$ or *cv-c*$^{R601Q\text{-}CTHA}$ in wild type dFB neurons. The membrane bound GFP was used to highlight the location of the dFB neurons (green) and the HA tagged Cv-c constructs were labelled via immunohistochemistry (red). Immunohistochemically prepared brains were imaged using confocal microscopy. The scale bars represent 30 μm.

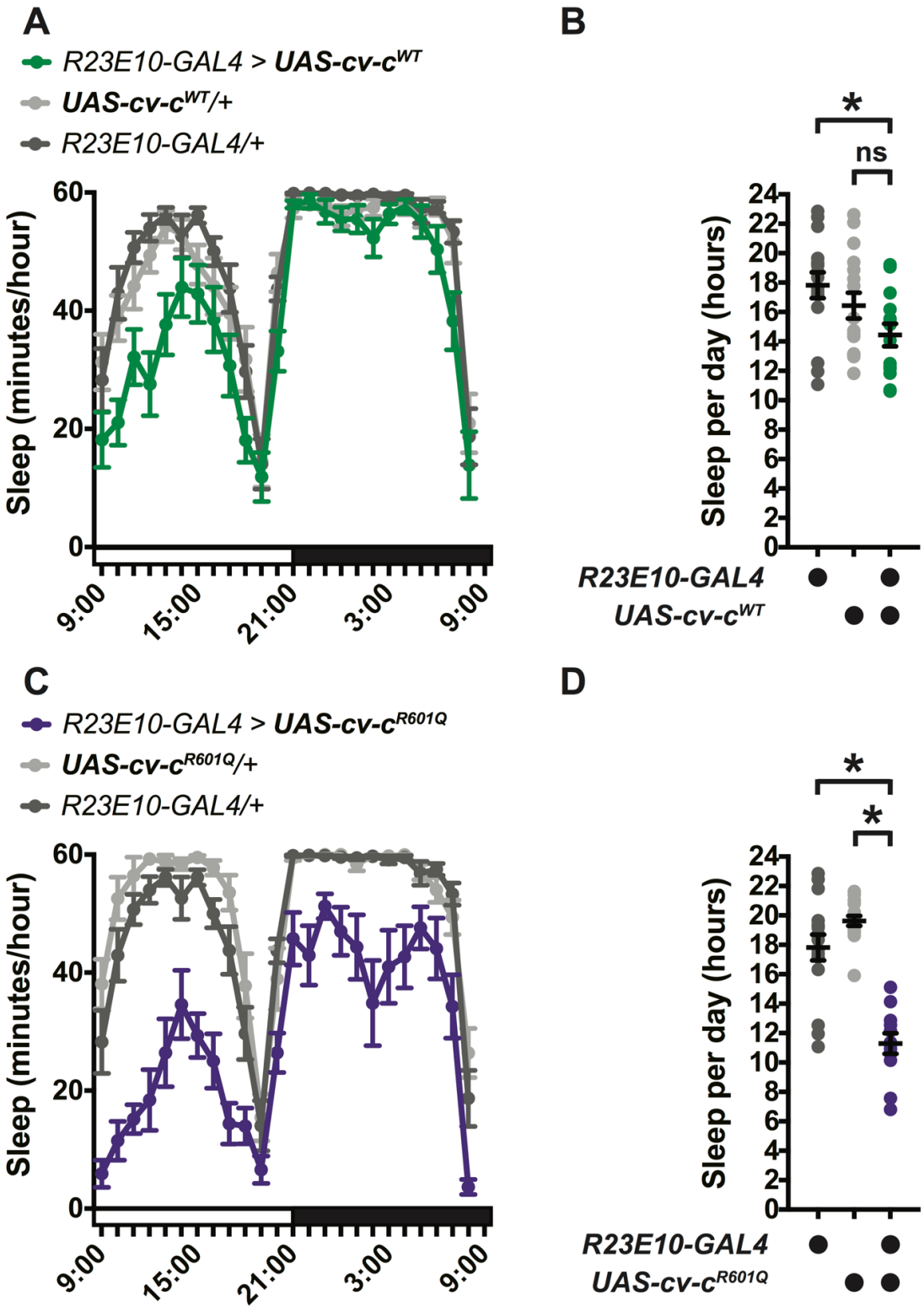

Figure 2.1.2 Sleep following the overexpression of *cv-c*^{WT} or *cv-c*^{R601Q} in the dFB neurons.

Figure 2.1.2 Sleep following the overexpression of *cv-c*^{WT} or *cv-c*^{R601Q} in the dFB neurons.

(A) *R23E10-GAL4* driven expression of *cv-c*^{WT} slightly decreases sleep during a 24-hour day (mean ± SEM, n = 16 per group). Two-way repeated measures ANOVA detected significant main effects for genotype and time ($F_{(2,43)} = 9.309$, $\boldsymbol{p = 0.0004}$, $\eta^2 = 0.043$; $F_{(23,989)} = 64.590$; $\boldsymbol{p < 0.0001}$; $\eta^2 = 0.499$) as well as a significant genotype × time interaction ($F_{(46,989)} = 1.895$, $\boldsymbol{p = 0.0004}$, $\eta^2 = 0.029$).

(B) Total sleep time per day in wild type flies overexpressing *cv-c*^{WT} in the dFB neurons differed significantly from only the responder control and not the driver control. One-way ANOVA detected significant differences ($F_{(2,43)} = 3.886$, $\boldsymbol{p = 0.028}$, $\eta^2 = 0.153$), but post-hoc Holm-Šídák comparisons revealed that the experimental group was significantly different from the responder control ($t_{(43)} = 2.781$, $\boldsymbol{p = 0.016}$, $d = 0.718$) and not the driver control ($t_{(43)} = 1.643$, $\boldsymbol{p = 0.108}$, $d = 0.424$).

(C) *R23E10-GAL4* driven expression of *cv-c*^{R601Q} decreases sleep throughout a 24-hour day. (mean ± SEM, n = 16 per group). Two-way repeated measures ANOVA detected significant main effects for genotype and time ($F_{(2,41)} = 71.270$, $\boldsymbol{p < 0.0001}$, $\eta^2 = 0.228$, $F_{(23,943)} = 57.940$, $\boldsymbol{p < 0.0001}$, $\eta^2 = 0.382$) as well as a significant interaction ($F_{(46,943)} = 3.907$, $\boldsymbol{p < 0.0001}$, $\eta^2 = 0.052$).

(D) Total sleep time per day in wild type flies overexpressing *cv-c*^{R601Q} in the dFB neurons differed significantly from both responder and driver controls. One-way ANOVA detected significant differences ($F_{(2,41)} = 38.040$, $\boldsymbol{p < 0.0001}$, $\eta^2 = 0.650$), and post-hoc Holm-Šídák comparisons revealed that the experimental group was significantly different from both the driver ($t_{(41)} = 8.446$, $\boldsymbol{p < 0.0001}$, $d = 2.157$) and the responder controls ($t_{(41)} = 6.615$; $\boldsymbol{p < 0.0001}$; $d = 1.768$).

$cv\text{-}c^{WT}$, but not $cv\text{-}c^{R601Q}$, rescues the *cv-c* mutation.

Next, I examined whether the GAP domain is necessary to rescue the *cv-c* mutation. Previously, Donlea et al. demonstrated that sleep in $cv\text{-}c^{MB03717}/cv\text{-}c^{C524}$ mutants can be restored (i.e. increased to wild type levels) by rescuing $cv\text{-}c^{WT}$ only in the mutants' dFB neurons[25]. I repeated and expanded this experiment using the reagents I created. *R23E10-GAL4* driven overexpression of $cv\text{-}c^{WT}$ in the mutant background corrected the short-sleeping phenotype (**Figures 2.1.3-A** and **B**), but the rescue failed when $cv\text{-}c^{R601Q}$ was used instead (**Figures 2.1.4-A** and **B**). In both cases, total daily sleep analyses involved controls that contained the heterozygous mutation. Given that the $cv\text{-}c^{WT}$ rescue involved a steep increase in sleep compared to the parental controls, I further examined whether this might be due to a locomotor deficit. An analysis of the flies' daytime and nighttime activities revealed that flies expressing the $cv\text{-}c^{WT}$ rescue construct showed greater waking activity during the day and night than controls (**Figure 2.1.3-C**). Flies in which $cv\text{-}c^{R601Q}$ was used for the rescue did not exhibit such enhanced activity. Hence, Cv-c's GAP domain and, by extension, its involvement in the Rho GTPase pathway is necessary for sleep regulation in dFB neurons.

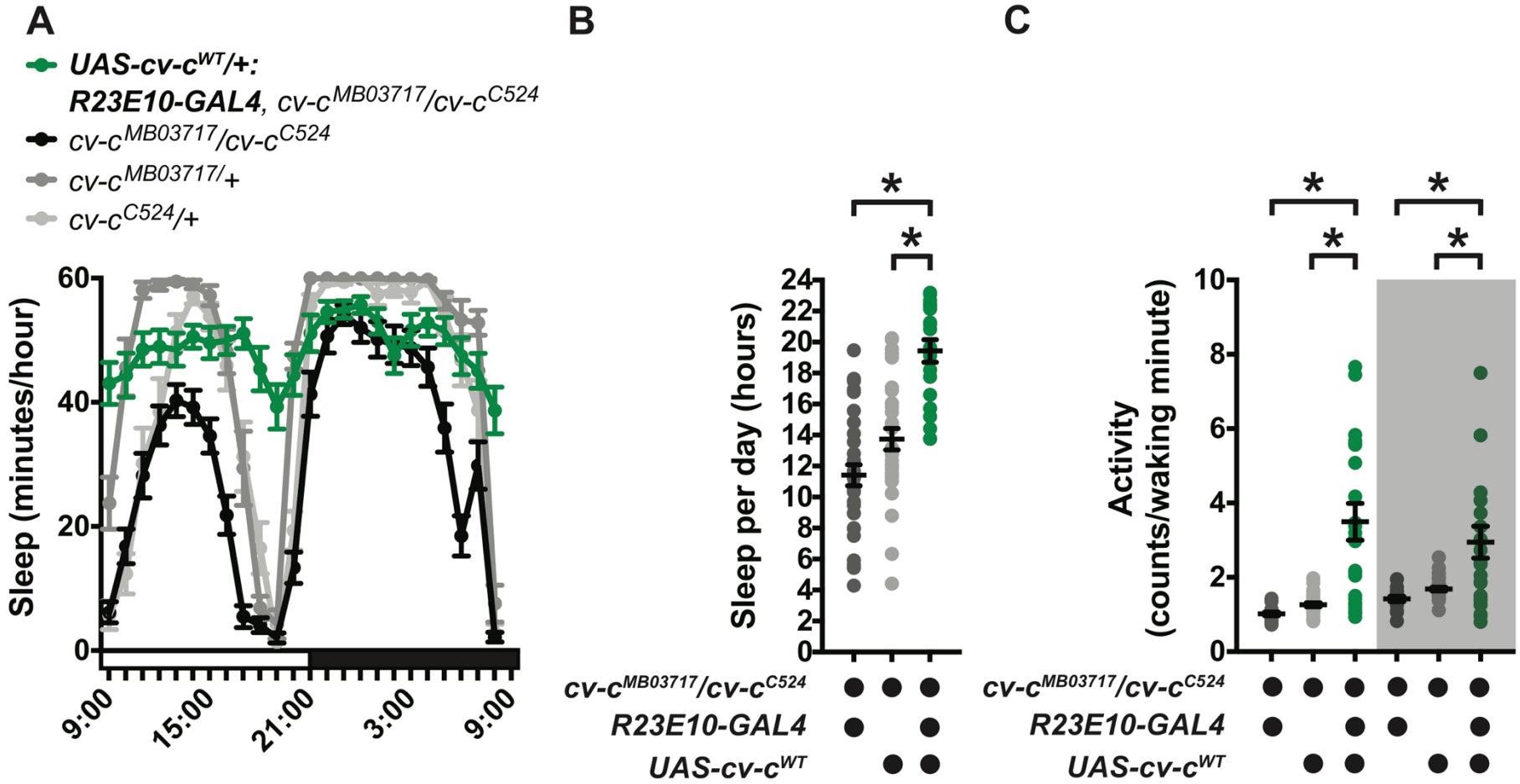

Figure 2.1.3 Sleep following the rescue of *cv-c*^{WT} in the dFB neurons of the *cv-c* mutants.

Figure 2.1.3 Sleep following the rescue of *cv-c*^{WT} in the dFB neurons of the *cv-c* mutants.

(A) *R23E10-GAL4* driven rescue of the *cv-c*^{MB03717}/*cv-c*^{C524} mutation with wild type *cv-c* restores sleep in the mutants over a 24-hour day. (mean ± SEM, n = 21 – 32 per group). Two-way repeated measures ANOVA detected significant main effects for genotype ($F_{(3,85)}$ = 37.000, $\boldsymbol{p < 0.0001}$, η^2 = 0.136) and time ($F_{(23,1955)}$ = 129.200; $\boldsymbol{p < 0.0001}$, η^2 = 0.384) as well as a significant genotype × time interaction ($F_{(69,1955)}$ = 13.580, $\boldsymbol{p < 0.0001}$, η^2 = 0.121).

(B) Total sleep time per day in *cv-c*^{MB03717}/*cv-c*^{C524} mutants carrying the *cv-c*^{WT} rescue in the dFB neurons differed significantly from both the responder and driver controls. Kruskal-Wallis test detected significant differences (H = 34.530, $\boldsymbol{p < 0.0001}$), and post-hoc Dunn's comparisons revealed that the experimental group was significantly different from both the responder (Z = 3.891; $\boldsymbol{p = 0.0001}$) and the driver controls (Z > 3.891, $\boldsymbol{p < 0.0001}$).

(C) Activity is higher in *cv-c*^{MB03717}/*cv-c*^{C524} mutants carrying the *cv-c*^{WT} rescue in the dFB neurons (daytime and nighttime activities are positioned in the light and dark regions, respectively). Kruskal-Wallis tests detected significant differences for both daytime (H = 29.050; $\boldsymbol{p < 0.0001}$) and nighttime activities (H = 14.32; $\boldsymbol{p = 0.0008}$). Post-hoc Dunn's comparisons between the experimental group and the driver and responder controls were significant for the daytime period (Z = 3.432, $\boldsymbol{p = 0.0006}$; Z > 3.891, $\boldsymbol{p < 0.0001}$). During the night, the experimental group significantly differed from the driver control (Z = 3.616, $\boldsymbol{p = 0.0003}$) but not the responder control (Z = 1.774, $\boldsymbol{p = 0.076}$).

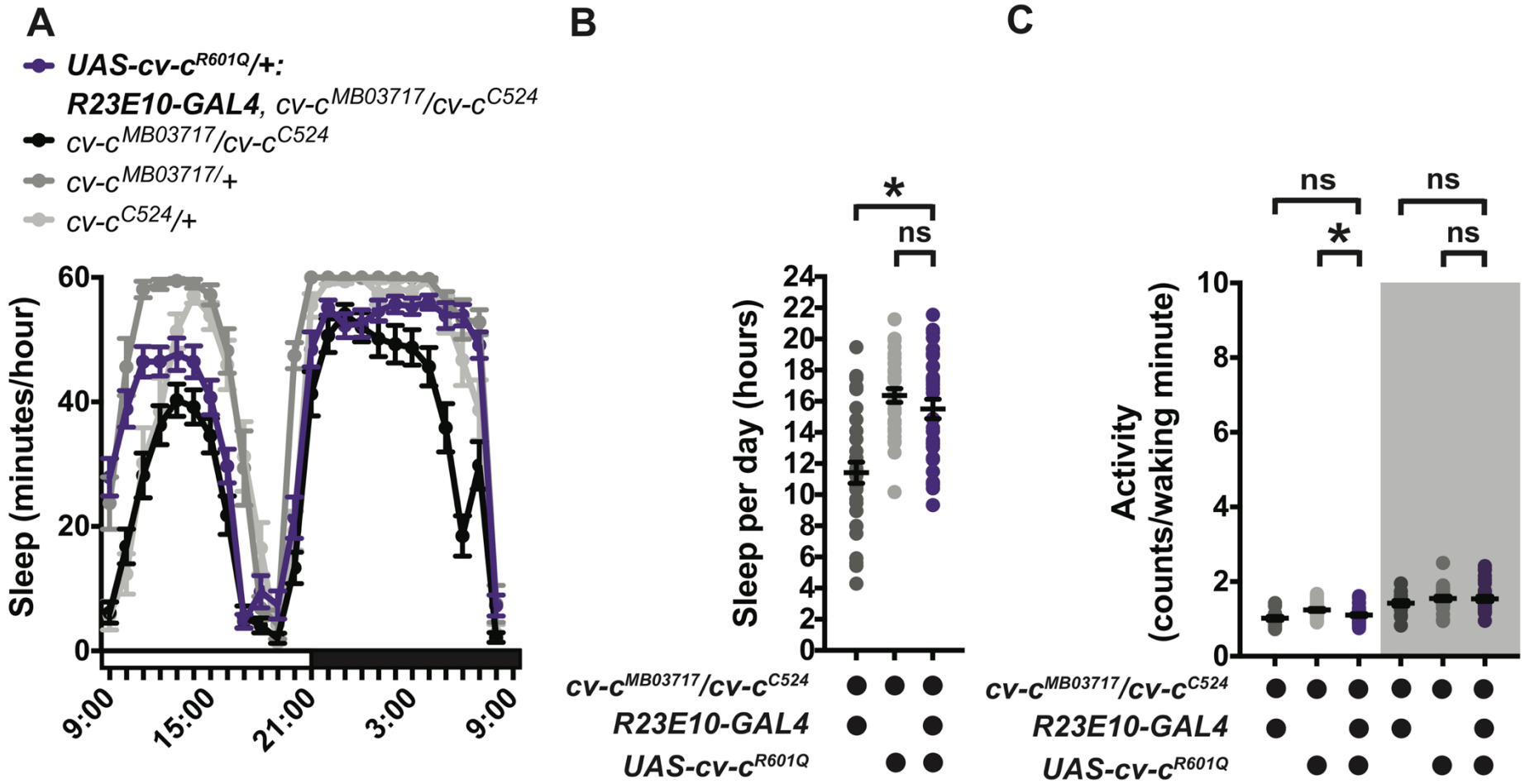

Figure 2.1.4 Sleep following the rescue of *cv-c*^{R601Q} in the dFB neurons of the *cv-c* mutants.

Figure 2.1.4 Sleep following the rescue of *cv-c*^{R601Q} in the dFB neurons of the *cv-c* mutants.

(A) *R23E10-GAL4* driven rescue of the *cv-c*^{MB03717}/*cv-c*^{C524} mutation with the catalytically inactive *cv-c* fails to restore sleep in the mutants over a 24-hour day. (mean ± SEM, n = 32 per group). Two-way repeated measures ANOVA detected significant main effects for genotype and time ($F_{(3,92)} = 26.060$, $\mathbf{p < 0.0001}$, $\eta^2 = 0.073$; $F_{(23,2116)} = 201.100$, $\mathbf{p < 0.0001}$, $\eta^2 = 0.504$) as well as a significant genotype × time interaction ($F_{(69,2116)} = 7.750$, $\mathbf{p < 0.0001}$; $\eta^2 = 0.058$).

(B) Total sleep time per day in *cv-c*^{MB03717}/*cv-c*^{C524} mutants carrying the *cv-c*^{R601Q} rescue in the dFB neurons differed significantly only from the driver control. Kruskal-Wallis test detected significant differences ($H = 26.020$, $\mathbf{p < 0.0001}$). However, post-hoc Dunn's comparisons revealed that the experimental group was significantly different from the driver control ($Z = 3.719$, $\mathbf{p = 0.0002}$) but not the responder control ($Z = 0.423$, $\mathbf{p = 0.672}$).

(C) Attempted rescue with *cv-c*^{R601Q} do not alter activity in the flies (daytime and nighttime activities are positioned in the light and dark regions, respectively). One-way ANOVA detected significant differences during the day ($H = 29.050$; $\mathbf{p < 0.0001}$). Post-hoc Holm-Šídák comparisons for daytime activities revealed significant differences between the experimental group and the responder control ($t_{(77)} = 2.653$, $\mathbf{p = 0.019}$, $d = 0.469$) but not the driver control ($t_{(77)} = 1.373$; $\mathbf{p = 0.174}$; $d = 0.280$). Kruskal-Wallis test of nighttime activities detected no significant differences ($H = 1.618$; $\mathbf{p = 0.445}$).

2.1.2 Behavioural screen for sleep regulatory Rho GTPases.

What is Cv-c's substrate? Sato et al. demonstrated using cell-free assays that Cv-c had the highest affinity for Rho1 and partial affinities for Cdc42 and Rac1[89]. I decided to check whether these tendencies are true in dFB neurons and thus, I sought to identify the Rho family GTPases relevant for sleep regulation. The *D. melanogaster* genome contains 7 Rho family GTPases, which are positively regulated by 20 GTP exchange factors (GEF) and negatively regulated by 21 GAPs[90]. To identify potential Cv-c substrates, I expressed wild type or mutant versions of various Rho GTPases in dFB neurons via *R23E10-GAL4* and measured sleep. In addition, I also completed a genetic knockdown screen of the 7 Rho GTPases.

Overexpressing mutant Rac1 in dFB neurons of wild type flies reduces sleep.

I examined three broad categories of Rho GTPase constructs: wild type, constitutively active mutants, and dominant negative mutants. The wild type construct overexpresses the unaltered Rho GTPase. A constitutively active mutant Rho GTPase lacks its intrinsic GTPase activity, which is needed to hydrolyse bound GTP to GDP and thereby switch the protein to its inactive form. The dominant negative mutation, on the other hand, acts not on the GTPase but on surrounding GEFs, quenching them, thereby preventing them from activating endogenous GTPases.

This library of constructs covered four major Rho GTPases: Cdc42, Rho1, Rac1, and Rac2[91-94]. Each construct was expressed in the dFB neurons of wild type flies. Here, as above, I searched for meaningful constructs by isolating only those for which the experimental group differed significantly from both the responder and driver controls. This selection criterion narrowed the list to constructs encoding mutant versions of Rac1 (**Figure 2.1.5**). Curiously but confusingly, overexpressing the constitutively active or

dominant negative Rac1 both resulted in decreased sleep. *R23E10-GAL4* driven expression of wild type Rac1 did not significantly affect the flies' sleep.

Knocking down *Rac1* in the dFB neurons of wild type flies reduces sleep.

Employing the same screening strategy as above, I examined the impacts of *R23E10-GAL4* driven RNA interference of the 7 Rho GTPases. For this experiment, I also included *R23E10-GAL4* driven *UAS-cv-c*^{RNAi} as an additional control, for this mimics the *cv-c* mutant phenotype[25]. **Figure 2.1.6** illustrates the results of this screen, which highlight that sleep is significantly and consistently decreased when *Rac1* is knocked down in the dFB neurons of wild type flies. Additionally, silencing the expression of other Rho GTPase genes (e.g. *Rac2*, *RhoBTB*, *RhoU*, and *Rho1*) also decreased fly sleep. Yet, the results for *Rac1* were replicable using two separate, independently generated RNAi constructs. Hence, the results for *Rac1* were most credible and also consistent with the aforementioned results.

Conditional, post-developmental, overexpression of Rac1 constructs reduces sleep.

Rho GTPases play an active role in neuronal development, and the earliest explorations of their mechanisms reported developmental defects as consequences of manipulating and mutating these proteins[95]. The above results, while suggestive, do not exclude the involvement of developmental consequences as contributing factors to the observed sleep phenotypes. To test this, I paired select candidates from the above screens with a temperature sensitive suppressor of GAL4 activity (GAL80^{TS}). At 18 °C, this transcriptional suppressor is active, and at 31 °C, it is inactivated. Hence, flies were reared at 18 °C from birth, and during experimentation (which occurred when the flies were ~ 3 days old), they were divided into two groups, one for each temperature. By normalizing

the total amount of sleep at 31 °C relative to the average of the respective group kept at 18 °C, the post-developmental effects of manipulating Rho GTPase expression could be isolated.

The constitutively active and dominant negative Rac1 mutations (*Rac1*^{V12} and *Rac1*^{L89}, respectively[91,92]; **Figure 2.1.7**) significantly decreased sleep after they were expressed. Yet, *Rac1*^{N17}, a different dominant negative Rac1, which decreased sleep when constitutively expressed, failed to produce a significant effect. Moreover, *Rac1*^{RNAi} increased rather than decreased sleep, contrary to observations made in **Figure 2.1.6**. In addition, new candidate constructs were identified through this screen (e.g. *Cdc42*^{N17} [dominant negative Cdc42], *Rho1*^{V14} [constitutively active Rho1], and *Rho1*^{N19} [dominant negative Rho1][91,93]).

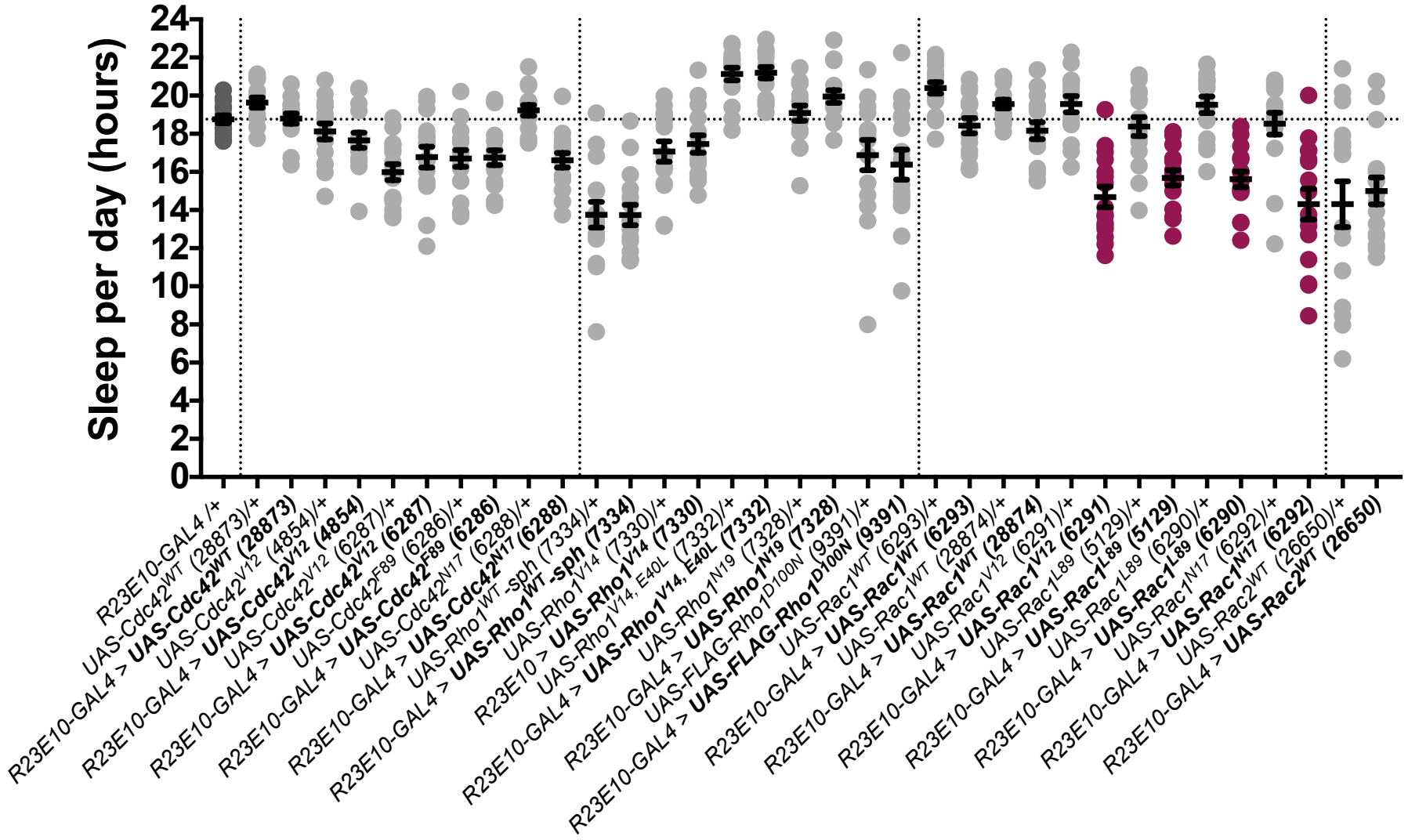

Figure 2.1.5 Sleep in flies overexpressing wild type or mutant Rho GTPases in the dFB neurons.

Figure 2.1.5 Sleep in flies overexpressing wild type or mutant Rho GTPases in the dFB neurons.

R23E10-GAL4 driven overexpression of Rho GTPase constructs in wildtype flies (mean ± SEM, n = 16 per group). One-way ANOVA detected significant differences ($F_{(34,525)} = 16.450$, $\boldsymbol{p < 0.0001}$, $\eta^2 = 0.516$). Post-hoc Holm-Šídák comparisons revealed significantly decreased sleep (compared to parental controls) in flies overexpressing the constitutively active $Rac1^{V12}$ and the dominantly negative $Rac1^{L89}$ and $Rac1^{N17}$ (burgundy; $t_{(525)} \geq 3.717$, $\boldsymbol{p \leq 0.005}$, $d \geq 0.929$).

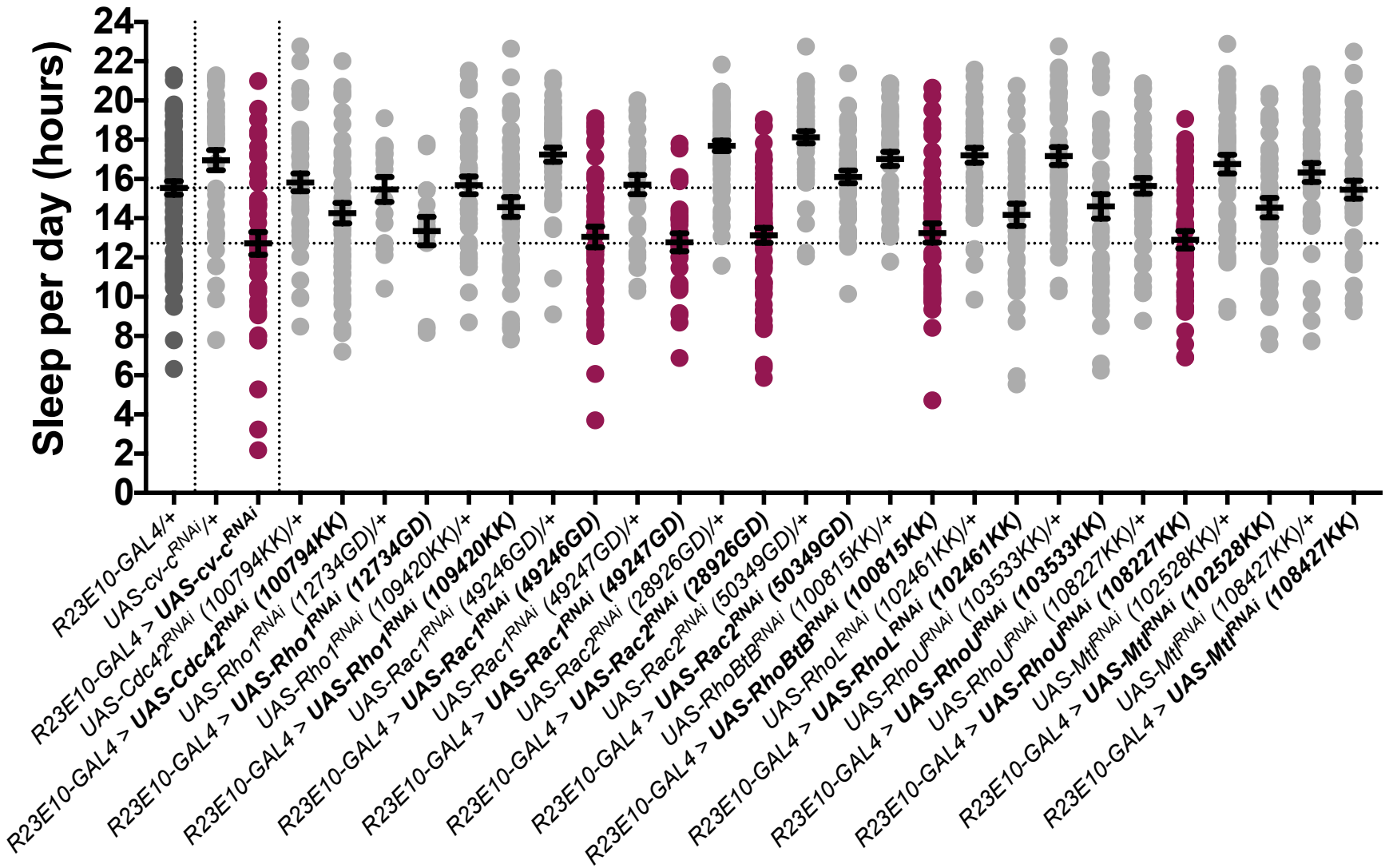

Figure 2.1.6 Sleep in flies expressing Rho GTPase RNAi in the dFB neurons.

Figure 2.1.6 Sleep in flies expressing Rho GTPase RNAi in the dFB neurons.

R23E10-GAL4 driven RNAi knockdown of Rho GTPases (mean ± SEM, n = 16 – 83 per group). One-way ANOVA detected significant differences ($F_{(28,1310)} = 12.820$, $\boldsymbol{p < 0.0001}$, $\eta^2 = 0.215$). Post-hoc Holm-Šídák comparisons identified the Rho GTPases, which when knocked down, significantly decreased sleep in the experimental group when compared to both parental controls (burgundy; $t_{(1310)} \geq 3.738$, $\boldsymbol{p \leq 0.003}$; $d > 0.501$). Among the Rho GTPases with multiple, independent RNAi's, only those targeting *Rac1* produced consistent results between the different constructs.

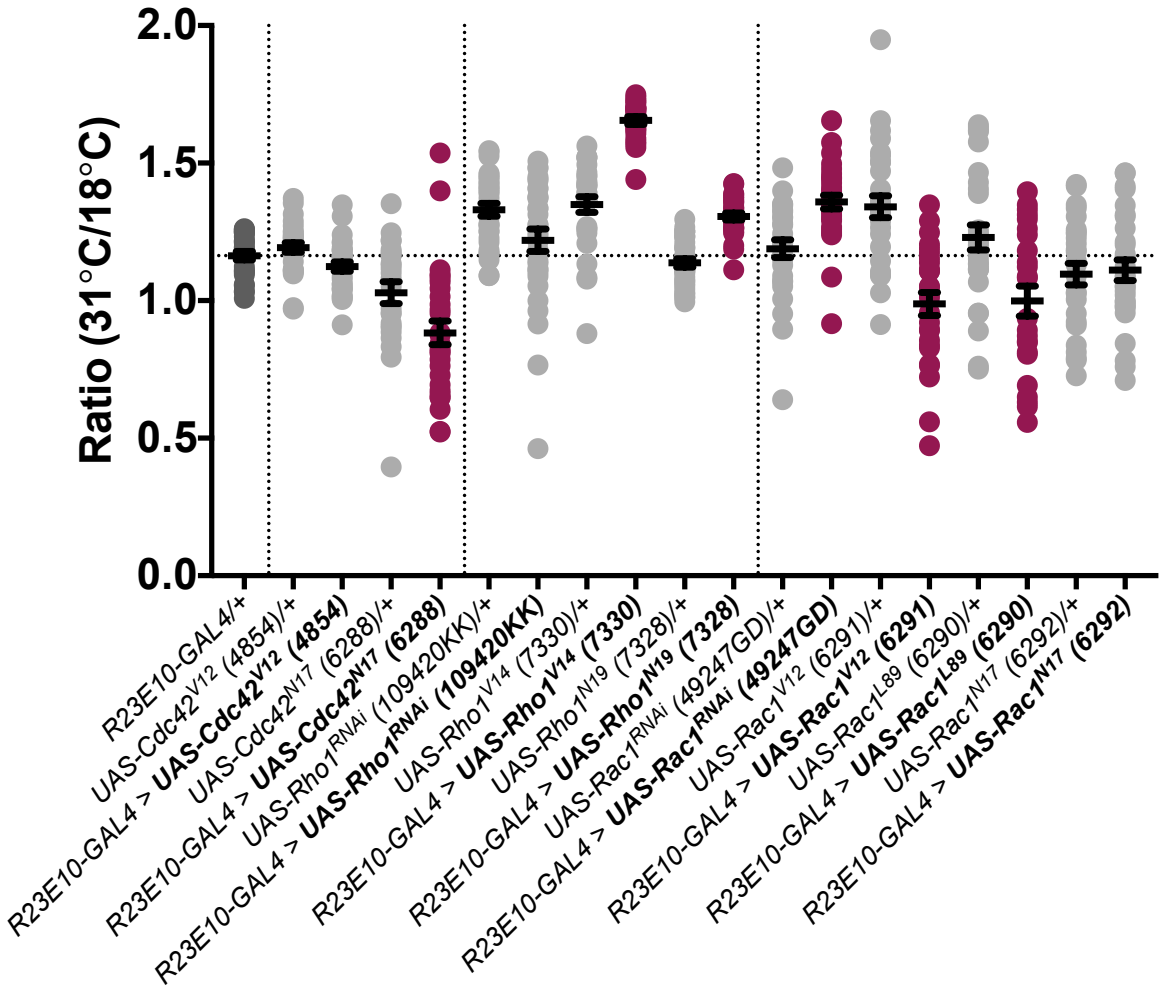

Figure 2.1.7 Sleep in flies with GAL80^{TS} controlled expression of Rho GTPase constructs and RNAi in the dFB neurons.

Figure 2.1.7 Sleep in flies with GAL80^{TS} controlled expression of Rho GTPase constructs and RNAi in the dFB neurons.

R23E10-GAL4 driven expression of Rho GTPase constructs and RNAi was thermally modulated via GAL80^{TS} (mean ± SEM, n = 32 per group). Flies were reared at 18 ºC (gene suppression via active GAL80^{TS}) and split into 2 groups, one of which was kept and monitored at 18 ºC and the other, which was transferred to 31 ºC (gene expression via inactivation of GAL80^{TS}). One-way ANOVA on the ratio of sleep in these 2 conditions detected significant differences ($F_{(18,529)} = 27.140$, $\boldsymbol{p < 0.0001}$, $\eta^2 = 0.480$). Post-hoc Holm-Šídák comparisons identified Rho GTPase constructs and RNAi's that yielded significantly different 31 ºC/18 ºC ratios of sleep in the experimental group when compared to both parental controls (burgundy; $t_{(529)} \geq 3.100$, $\boldsymbol{p \leq 0.003}$; $d > 0.576$).

2.1.3 Rac1 promotes sleep whereas Rho1 promotes wakefulness.

Screening for sleep regulatory Rho GTPases in a wild type background provided partially inconsistent results. Wild type Rho GTPases cycle dynamically between their active and inactive states, and their balance between these two states is integral to their function as cell biological switches[95]. The equilibria are adjusted by the various GEFs and GAPs that activate and inactivate GTPases, respectively (**Figure 2.1.8-A**)[95]. The effects of silencing the expression or overexpressing mutant variants of Rho GTPases therefore reflect complex interactions between the targeted GTPase, other GTPases, and their modulating proteins rather than a simple consequence of manipulating a single Rho GTPase. Disentangling these factors in the wild type background is difficult.

***Rho1* knock down rescues the *cv-c* mutant phenotype.**

To bypass the limitations of influencing Rho GTPase activity in the wild type genetic background, I decided to clamp the system in a fixed state to isolate the effects of modulating single GTPases. *cv-c* mutants lack a functional GAP that inactivates Rho1, which keeps it constitutively active (**Figure 2.1.8-B**). To test whether Rho1 truly lay downstream of Cv-c in dFB neurons, I knocked down Rho1 expression via *R23E10-GAL4* in $cv\text{-}c^{MB03717}/cv\text{-}c^{C524}$ mutants. As **Figure 2.1.9-A** shows, this is sufficient to restore sleep in the *cv-c* mutants, which suggests that an abnormally large pool of active Rho1 underlies the *cv-c* mutant phenotype. This indicates that Rho1 is the substrate for Cv-c and that active Rho1 promotes arousal.

Dominant negative Rac1 exacerbates the *cv-c* mutant phenotype.

Rho1, in its active state, is reported to be mutually antagonistic with Rac1[95-98] (**Figure 2.1.8-C**). Thus, in *cv-c* mutants, constitutively active Rho1 should suppress the activity

of Rac1 (**Figure 2.1.8-D**). I tested whether this mutual antagonism also exists in dFB neurons by overexpressing inactive $Rac1^{L89}$ in the *cv-c* mutant background. As **Figure 2.1.9-B** indicates, disrupting Rac1 activity by biasing its equilibrium towards the inactive state further exacerbated sleep loss. These results indicate that not only are Rho1 and Rac1 in the dFB neurons mutually antagonistic, but given Rho1's arousal promoting effect, Rac1 must promote sleep to oppose Rho1 activity.

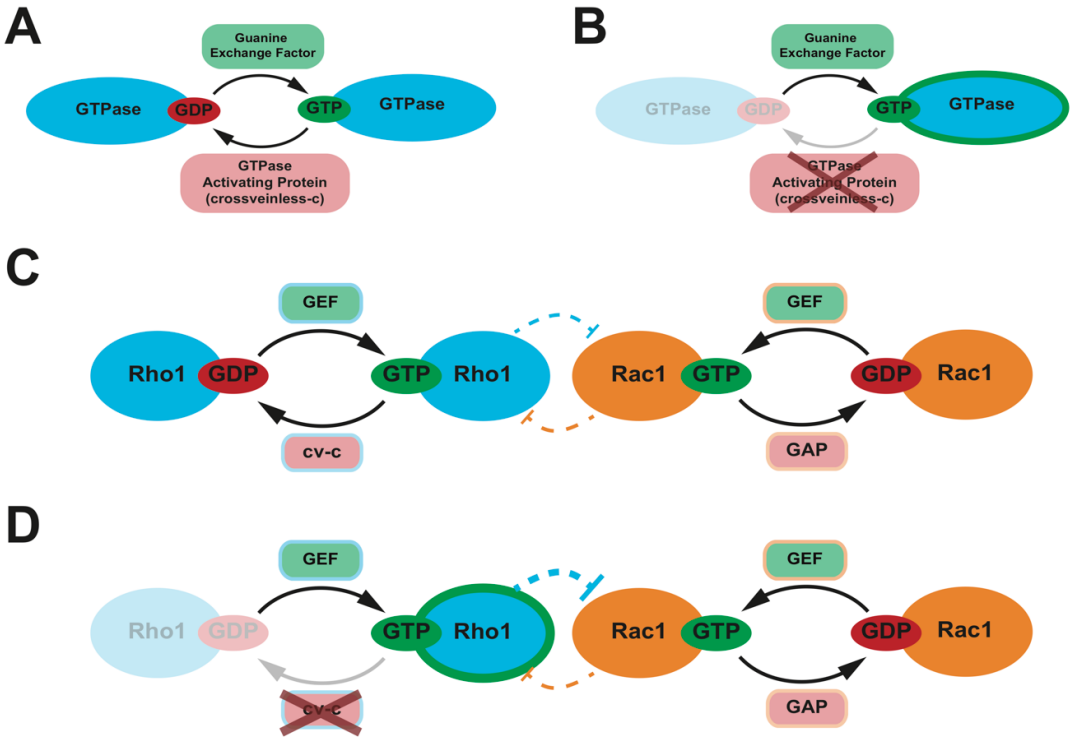

Figure 2.1.8 Regulation of Rho1 and Rac1 by GEFs and GAPs.

Figure 2.1.8 Regulation of Rho1 and Rac1 by GEFs and GAPs.

(A) Rho GTPases exist in two dynamically interchanging states: ON (GTP bound) and OFF (GDP bound). They are activated by guanine nucleotide exchange factors (GEF), which replace the bound GDP with GTP. GTPase Activating Proteins (GAP) act antagonistically by hydrolysing the bound GTP to inactivate the GTPase.

(B) The absence of a GAP (e.g. Cv-c) clamps the GTPase in a state of perpetual activity (green contours around ON state and opacity in the OFF state).

(C) Rho1 and Rac1 are both cyclically regulated by GEFs and GAPs. Based on *ex-situ* observations, Cv-c is predicted to be a GAP for Rho1[89]. Rho1 and Rac1 are also mutually inhibitory (dotted lines emphasize that this inhibition is indirect)[95-98].

(D) In Cv-c mutants, Rho1 is predicted to be clamped in a state of constitutive activity, and this would also strengthen Rho1's inhibitory pressure on Rac1 activity.

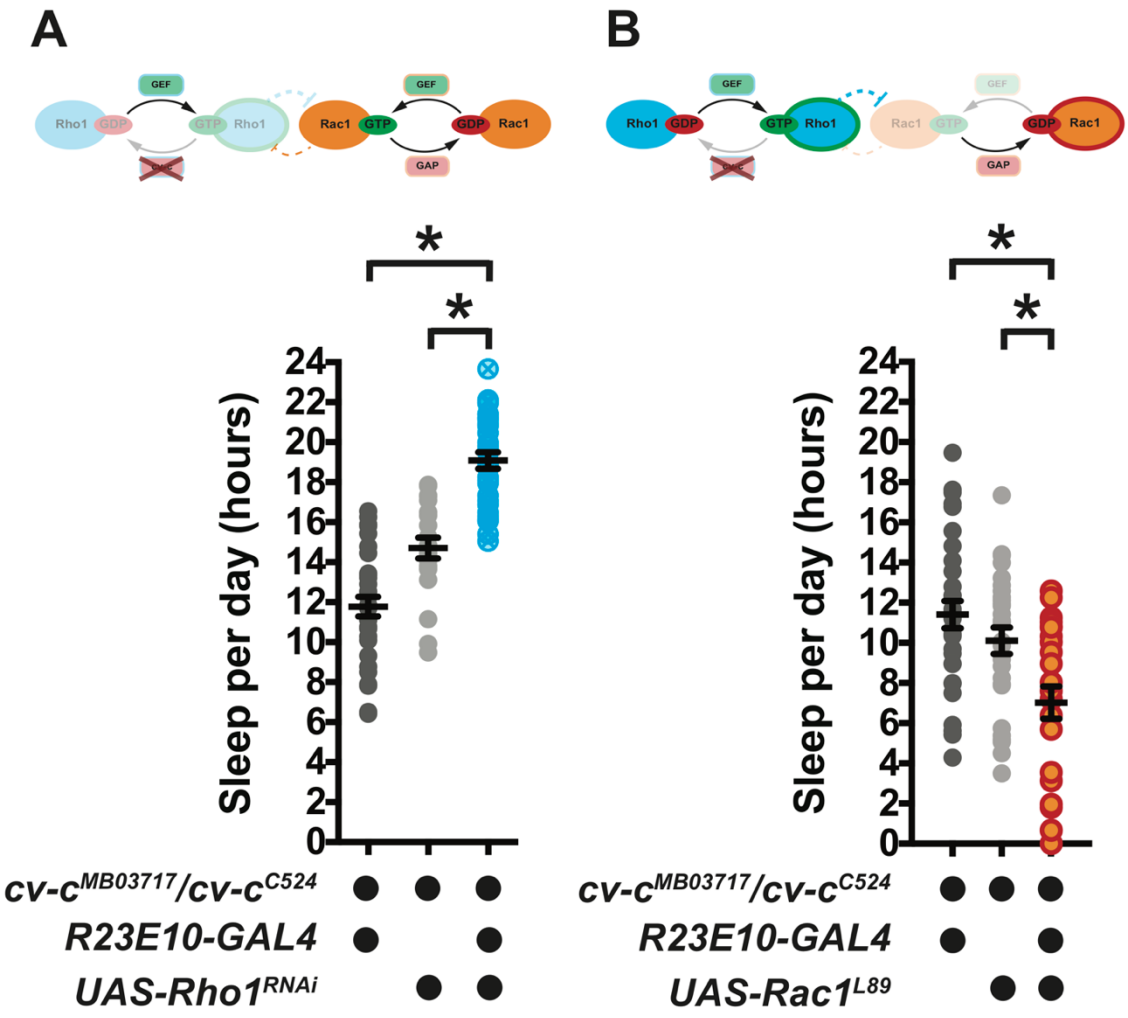

Figure 2.1.9 Rac1 and Rho1 have opposing roles in sleep regulation.

Figure 2.1.9 Rac1 and Rho1 have opposing roles in sleep regulation.

(A) *R23E10-GAL4* driven expression of $Rho1^{RNAi}$ restores total daily sleep in the $cv\text{-}c^{MB03717}/cv\text{-}c^{C524}$ mutants. One-way ANOVA detected significant differences ($F_{(2,82)}$ = 68.100, $\boldsymbol{p < 0.0001}$, η^2 = 0.624). Post-hoc Holm-Šídák comparisons revealed that the experimental group significantly differed from both responder and driver controls ($t_{(82)}$ = 6.192, $\boldsymbol{p < 0.0001}$, d = 1.203; $t_{(82)}$ = 11.610, $\boldsymbol{p < 0.0001}$, d = 2.052). The schematic above the graph illustrates the predicted molecular dynamics. Opacity in Rho1 (in both ON and OFF states) reflects the effect of decreased expression due to RNA interference.

(B) *R23E10-GAL4* driven expression of $Rac1^{L89}$ further depletes total daily sleep in the $cv\text{-}c^{MB03717}/cv\text{-}c^{C524}$ mutants. Kruskal-Wallis test detected significant differences (H = 13.610, $\boldsymbol{p = 0.001}$). Post-hoc Dunn's test revealed that the experimental group significantly differed from both responder and driver controls (Z = 2.342, $\boldsymbol{p = 0.019}$; Z = 3.432; $\boldsymbol{p = 0.0006}$). The schematic above the graph illustrates the hypothesized molecular dynamics. The red contour indicates Rac1 clamped in the OFF state, and opacity in GTP bound Rac1 symbolizes its failure to enter the ON state.

Cdc42 has no clear sleep regulatory functions in dFB neurons.

In **Figures 2.1.6** and **2.1.7**, I observed decreased sleep when Cdc42 was perturbed in the dFB neurons. Accordingly, I next examined whether Cdc42 is genuinely involved in sleep regulation in the dFB neurons. I tested this by employing *R23E10-GAL4* to drive the expression of constitutively active or dominant negative Cdc42 mutations ($Cdc42^{V12}$ and $Cdc42^{N17}$, respectively) in *cv-c* mutants. These experiments revealed that the overexpression of neither construct altered sleep in the *cv-c* mutant background (**Figures 2.1.10-A** and **B**). This is highly suggestive that Cdc42 does not affect Rho1 or Rac1 activity, let alone regulate the excitability of dFB neurons and, therefore, sleep. Also, the lack of a Cdc42 involvement demonstrates the substrate specificity of sleep regulation within the dFB neurons and highlights the significance of the phenotypes obtained from expressing $Rho1^{RNAi}$ and $Rac1^{L89}$ in the *cv-c* mutant background.

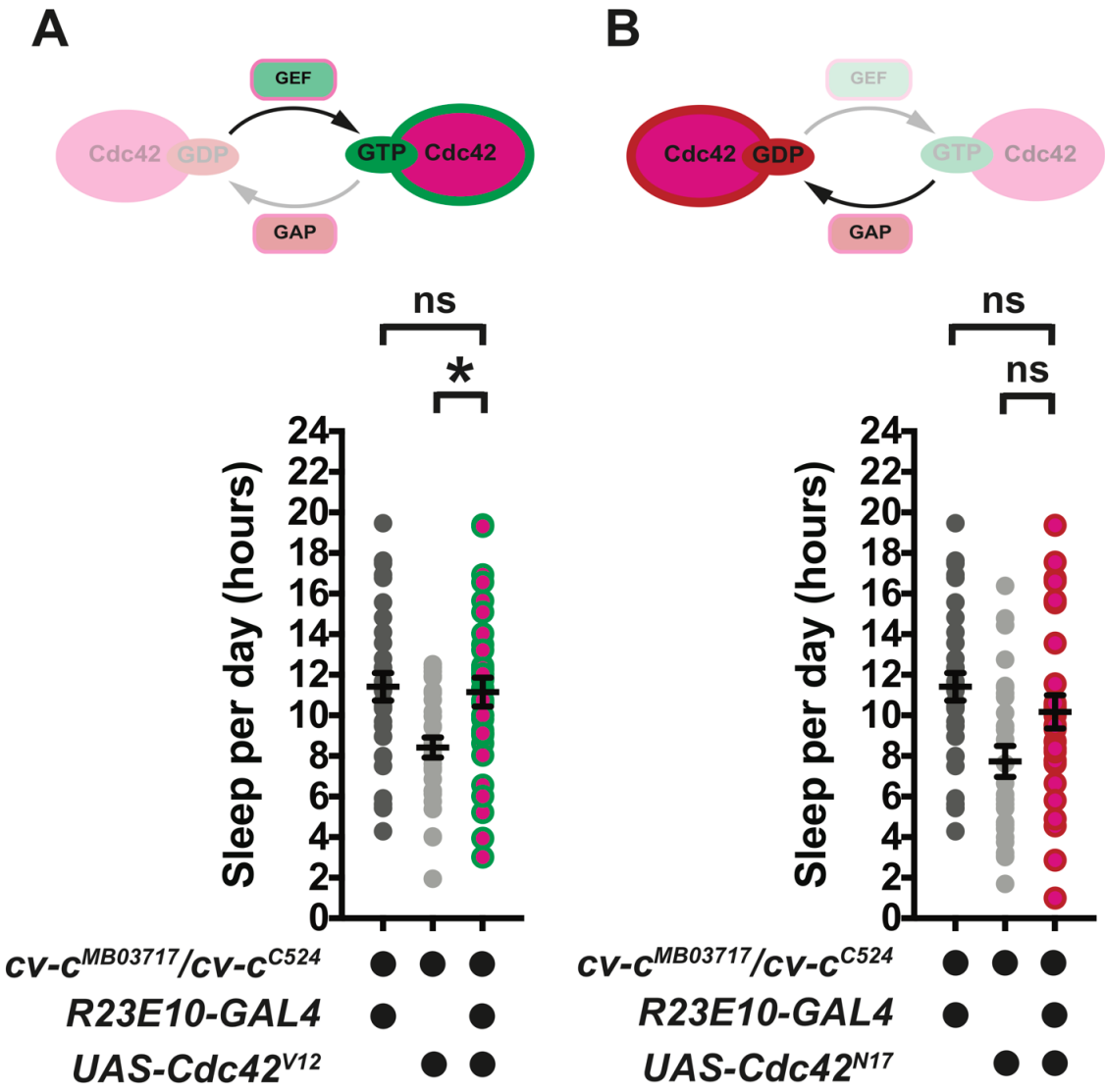

Figure 2.1.10 Cv-c does not regulate Cdc42.

Figure 2.1.10 Cv-c does not regulate Cdc42.

(A) *R23E10-GAL4* driven expression of $Cdc42^{V12}$ does not significantly affect total daily sleep in the $cv\text{-}c^{MB03717}/cv\text{-}c^{C524}$ mutants. One-way ANOVA detected significant differences ($F_{(2,82)} = 6.563$, $\boldsymbol{p = 0.002}$, $\eta^2 = 0.126$). Post-hoc Holm-Šídák comparisons revealed that the experimental group significantly differed from the responder control ($t_{(82)} = 3.001$, $\boldsymbol{p = 0.007}$, $d = 0.539$) but not the driver control ($t_{(82)} = 0.292$, $\boldsymbol{p = 0.771}$, $d = 0.052$). The schematic above the graph illustrates the predicted molecular dynamics. **(B)** *R23E10-GAL4* driven expression of $Cdc42^{N17}$ does not significantly affect total daily sleep in the $cv\text{-}c^{MB03717}/cv\text{-}c^{C524}$ mutants. One-way ANOVA detected significant differences ($F_{(2,87)} = 6.081$, $\boldsymbol{p = 0.003}$, $\eta^2 = 0.123$). Post-hoc Holm-Šídák comparisons revealed that the experimental group significantly differed from neither the responder control ($t_{(87)} = 2.153$, $\boldsymbol{p = 0.053}$, $d = 0.418$) nor the driver control ($t_{(87)} = 1.182$, $\boldsymbol{p = 0.240}$, $d = 0.212$). The schematic above the graph illustrates the predicted molecular dynamics.

2.2 What is the sleep regulatory role of Hk?

Membrane excitability connects molecular events in dFB neurons (e.g. ion channel regulation or modulation of small GTPase signaling by Cv-c) to behavioural outcomes (i.e. modulation of sleep)[25]. The electrical activity of dFB neurons tightly mirrors the flies' behavioural state: sleep is linked to spiking activity whereas wakefulness coincides with electrical quiescence of dFB neurons[24,25].

2.2.1 *Sh* and its interacting partners, *Hk* and *sss*/*qvr,* are required for sleep regulation in the dFB neurons.

Potassium conductances set the neuronal resting potential, shape the action potential waveform, and are important determinants of synaptic integration and tonic activity. Mutations in potassium ion channel genes or genes encoding accessory proteins, such as *Shaker (Sh)*, *Hyperkinetic (Hk)*, and *sleepless*/*quiver* (*sss*/*qvr*), lead to pronounced sleep impairments that are independent of the flies' circadian rhythmicity[20,67,72,99]. These findings underscore the importance of potassium conductance in modulating the electrical activity that ultimately translates to homeostatic changes in the flies' behavioural state. Yet, two central questions remain open. First, in which neurons do these potassium conductances function to regulate sleep? And second, through what mechanism(s) are the potassium conductances regulated?

Given that the electrical activity of dFB neurons correlates with the flies' behavioural state, I decided to screen for potassium ion channels and related proteins that might affect activity in these cells, using *R23E10-GAL4* to drive RNAi against candidate transcripts. The results demonstrated dramatic decreases in sleep with the knock down of *Sh* family genes: *Sh*, *Hk*, and *sss*/*qvr*, as well as *Shab*, a delayed rectifier (**Figure 2.2.1**). That dFB-restricted interference with the expression of these genes would mimic the sleep

deficits observed in genomic mutants strongly suggested that these cells are an important site of the sleep regulatory action of these potassium conductance[24]. Furthermore, the results of this screen contributed to the recent discovery that modulations of A-type potassium currents in the dFB neurons underlie states of sleep and wakefulness[24].

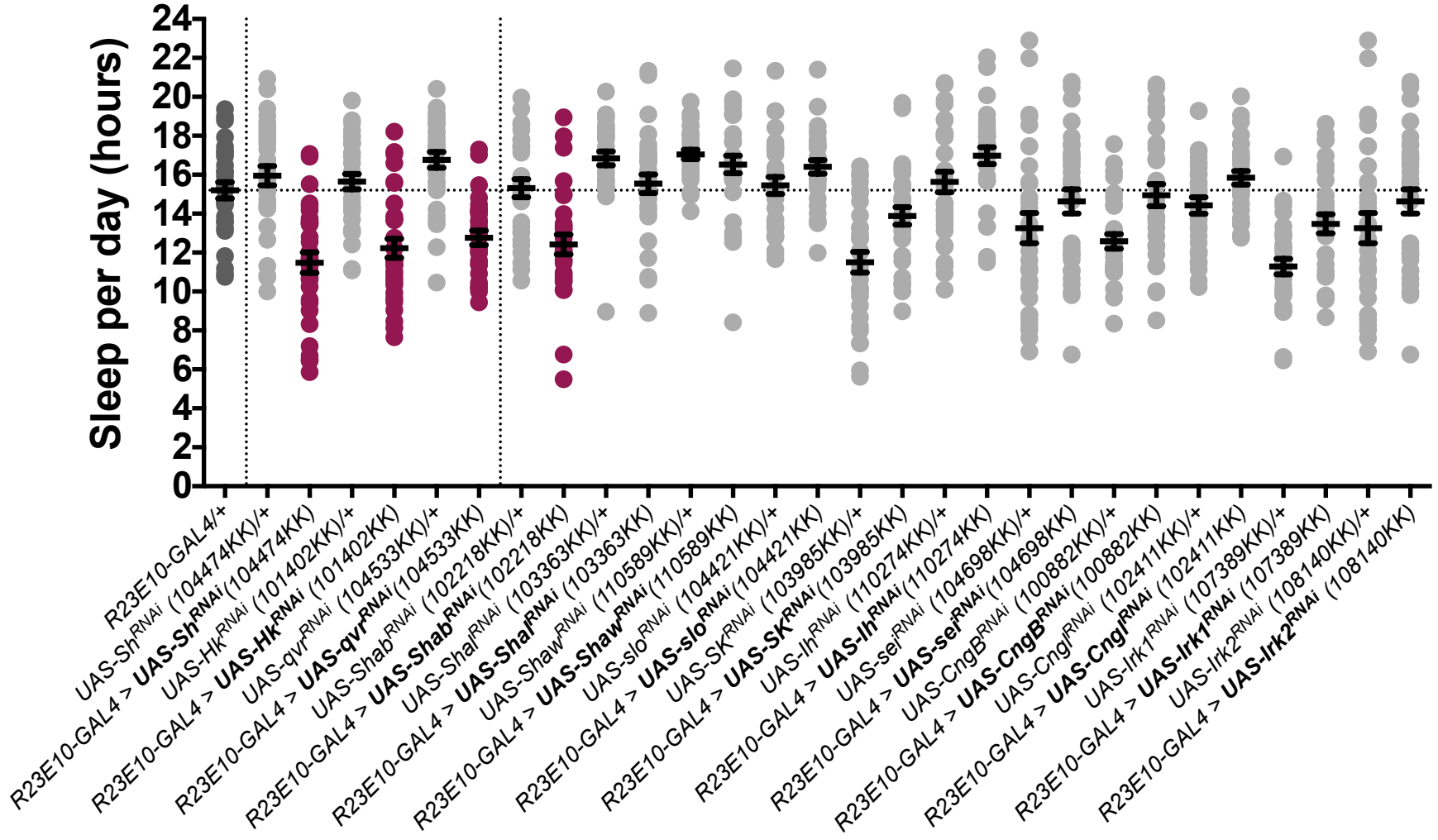

Figure 2.2.1 Sleep in flies expressing K^+ channel RNAi in the dFB neurons.

Figure 2.2.1 Sleep in flies expressing K^+ channel RNAi in the dFB neurons.

R23E10-GAL4 driven RNAi knockdown of K^+ channels in the dFB neurons (mean ± SEM, n = 29 – 32 per group). One-way ANOVA detected significant differences ($F_{(28,884)} = 13.480$, $\boldsymbol{p < 0.0001}$, $\eta^2 = 0.299$). Post-hoc Holm-Šídák comparisons revealed that sleep was significantly decreased (compared to parental controls) upon the suppressed expression of *Sh*, *Hk*, *qvr*/*sss*, and *Shab* (burgundy; $t_{(884)} \geq 3.444$, $\boldsymbol{p \leq 0.002}$, $d > 0.629$). Protein products of the former three genes comprise the Sh complex.

2.2.2 Redox sensing via Hk's aldo-keto reductase domain is necessary for sleep.

The *Sh* family genes encode pore-forming or accessory subunits of a tetrameric voltage-gated A-type potassium channel. *Sh* and *Hk* encode the alpha and beta subunits, whereas *sss*/*qvr* encodes an auxiliary modulator. Much is known about Sh, the alpha subunit that constitutes the pore of the ion channel. Exhaustive structural and functional studies have mapped domains that contribute to the pore[100-103], voltage-sensor[104] as well as regions for binding other subunits and regulators[104,105]. Most of these structural features are highly conserved across species[106].

In contrast, knowledge about Hk, the beta subunit in the Sh complex, is limited. Hk binds to Sh's cytoplasmic T1 domain[105,107] and provides fast activation as well as fast inactivation of the conductance[84]. Structurally and functionally, Hk is an aldo-keto reductase (AKR), a highly-conserved class of enzymes that modulates cellular oxidation by reducing carbonyl compounds into alcohols through a hydride transfer from reduced nicotinamide adenine dinucleotide phosphate (NADPH)[84,108]. NADPH is bound to the AKR in the crystal structure of Hk via two critical amino acid residues: aspartic acid at position 260 and lysine at position 289[108-110]. When NADPH is bound to Hk, the Sh conductance exhibits fast inactivation[84,110]. Oxidation of bound NADPH and subsequent release of $NADP^+$ potentiate the potassium current, as the inactivation gate is inhibited in the absence of NADPH[108,110]. In addition to its electrical contributions, Hk also affects the cell's oxidative state. Mutant *Hk* with a catalytically inactive AKR not only disrupts a cell electrically, but also increases its oxidative level (i.e. the concentration of intracellular oxidizing agents)[111]. Hence, the potassium channel beta subunit Hk can potentially tie a cell's excitability to its redox state, but whether this mechanistic link is important for the regulation of sleep is currently unexplored.

To test whether Hk's redox sensing ability is important for sleep, I attempted a rescue of the Hk^{1} mutant using *R23E10-GAL4* driven expression of wild type Hk (Hk^{WT}) or Hk carrying a point mutation at lysine-289, which disrupts NADPH binding (Hk^{K289M}). Hk^{1} is a widely studied, well characterized hypomorphic allele that greatly reduces the A-type potassium current conducted by $Sh^{112-115}$. This mutant also has a sleep deficit[72]. While targeted rescue of Hk^{WT} in the dFB neurons restored the sleep of Hk^{1} mutants to wild-type levels (**Figures 2.2.2-A** and **B**), a comparable rescue involving Hk^{K289M} failed to correct the sleep phenotype (**Figures 2.2.2-C** and **D**). The successful restoration of sleep in Hk^{1} mutants by rescuing Hk^{WT} only in dFB neurons complements the dFB-restricted RNAi results shown in **Figure 2.2.1** and establishes these cells as an important sleep-regulatory site for Hk. Moreover, the necessity of Hk's redox sensing capacity to restore sleep in the Hk^{1} background points to the importance of redox state in regulating sleep and suggests a biophysical mechanism by which this type of regulation might be accomplished.

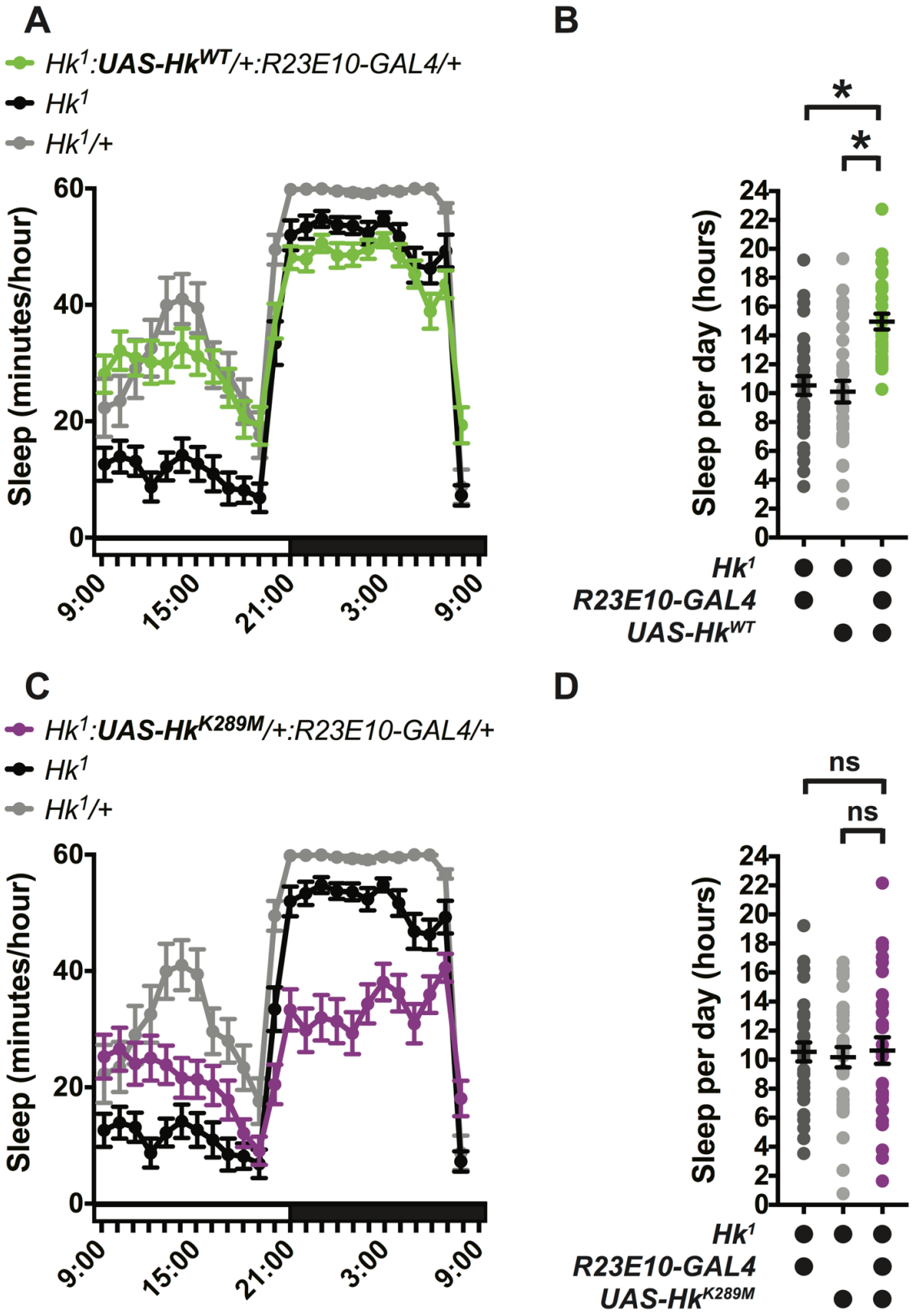

Figure 2.2.2 Redox sensing via Hk is necessary for sleep regulation in the dFB neurons.

Figure 2.2.2 Redox sensing via Hk is necessary for sleep regulation in the dFB neurons.

(A) *R23E10-GAL4* driven rescue of Hk^{1} with wildtype *Hk* restores sleep in the mutants over a 24-hour day. (mean ± SEM, n = 31 – 32 per group). Two-way repeated measures ANOVA detected significant main effects for genotype ($F_{(2,75)} = 17.200$, $\boldsymbol{p < 0.0001}$, $\eta^2 = 0.050$) and time ($F_{(23,1725)} = 111.800$, $\boldsymbol{p < 0.0001}$, $\eta^2 = 0.447$) as well as a significant genotype × time interaction ($F_{(46,1725)} = 7.910$, $\boldsymbol{p < 0.0001}$, $\eta^2 = 0.063$).

(B) Total sleep time per day in Hk^{1} mutants carrying the Hk^{WT} rescue in the dFB neurons differed significantly from both parental controls. One-way ANOVA detected significant differences ($F_{(2,91)} = 16.550$, $\boldsymbol{p < 0.0001}$, $\eta^2 = 0.2668$), and post-hoc Holm-Šídák comparisons revealed that the experimental group was significantly different from both parental controls ($t_{(91)} \geq 4.720$, $\boldsymbol{p < 0.0001}$, $d \geq 0.848$).

(C) *R23E10-GAL4* driven rescue of Hk^{1} with Hk^{K289M} fails to restore sleep in the mutants over a 24-hour day. (mean ± SEM, n = 31 – 32 per group). Two-way repeated measures ANOVA detected significant main effects for genotype and time ($F_{(2,76)} = 15.320$, $\boldsymbol{p < 0.0001}$, $\eta^2 = 0.073$; $F_{(23,1748)} = 97.490$, $\boldsymbol{p < 0.0001}$, $\eta^2 = 0.360$) as well as a significant genotype × time interaction ($F_{(46,1748)} = 12.200$, $\boldsymbol{p < 0.0001}$, $\eta^2 = 0.091$).

(D) Total sleep time per day in Hk^{1} mutants carrying the Hk^{K289M} rescue in the dFB neurons did not differ significantly from either parental control. One-way ANOVA failed to detect significant differences ($F_{(2,92)} = 0.101$, $\boldsymbol{p = 0.904}$, $\eta^2 = 0.002$).

2.2.3 Sleep deprivation causes oxidative stress in dFB neurons.

Given that redox sensing via Hk appears necessary for sleep regulation, I investigated whether prolonged waking is accompanied by an accumulation of reactive oxygen species. To do so I used MitoTimer, a Timer protein targeted to the mitochondrial matrix[116]. Timer is a mutant DsRed (DsRed1-E5) that fluoresces green (emission peak: 500nm) when first synthesized but shifts its emission to red (emission peak: 580nm) as it is oxidized[116,117]. Notably, MitoTimer responds primarily to oxidation from reactive oxygen species (ROS) with unpaired (radical) electrons[116]. Thus, the cell's oxidative state and, by extension, its ROS content can be evaluated by comparing red and green fluorescence.

Following sleep deprivation, ROS levels increase in the dendrites of the dFB neurons.

MitoTimer was expressed in dFB neurons with the help of *R23E10-GAL4* and imaged *in vivo* using a two-photon microscope. Different subcellular compartments of the dFB neurons (dendrites, axon, and soma) were analyzed separately. There was a trend for a higher red:green ratio in the evening (4PM - 6PM) compared to the morning (8AM - 11AM), consistent with increased cumulative ROS exposure during waking; however, this trend failed to reach statistical significance (**Figure 2.2.3-B**; **Figures 2.2.4-A** and **B)**. To explore the potential connection between the accumulation of sleep pressure and a build-up of ROS under more tightly controlled conditions, I quantified the MitoTimer fluorescence emission ratio in flies that had been mechanically sleep-deprived[118] for 24 hours. The red:green ratio of dendritically localized MitoTimer in these flies significantly exceeded that of non-deprived controls (**Figures 2.2.3-A** and **B**), consistent with an accumulation of ROS during sleep deprivation.

Baseline sleep in flies expressing *R23E10-GAL4* driven MitoTimer was reduced compared to parental controls (**Figures 2.2.3-C** and **D**). This initially surprising finding can be explained by MitoTimer acting as a scavenger of mitochondrial ROS[116].

Sleep deprivation does not accumulate oxidative levels in other regions of the dFB neurons or in the mushroom body.

Sleep deprivation did not result in significantly higher cumulative ROS exposures in the somatic and axonal compartments of dFB neurons (**Figures 2.2.4-A** and **B**). MitoTimer based red:green ratios in the different compartments of the dFB neurons were further analyzed to include neuronal compartment as a factor in a two-way ANOVA (**Table A28** in **Appendix**). Even in this more rigorous analysis (owing to more stringent thresholds for statistical significance from the familywise error rate), the dendrites had significantly higher ROS exposure in the sleep deprived group compared to the non-deprived controls (8AM – 11AM and 4PM – 6PM). No significant difference in ROS exposure was detected between the sleep deprived and non-deprived groups in the axons or soma.

Kenyon cells of the mushroom bodies (MBs) are involved in learning and memory[119] and also contribute to sleep[120]. Thus, I quantified the MitoTimer emission ratio in different compartments of the MB neurons (the dendritic calyx and axonal lobes). No significant differences in the cumulative redox history of these compartments were detected (**Figures 2.2.4-C**, **D**, and **E**). Consistent results were obtained from a broader, more conservative analysis that included neuronal compartment as a factor in a two-way ANOVA (**Table A32**).

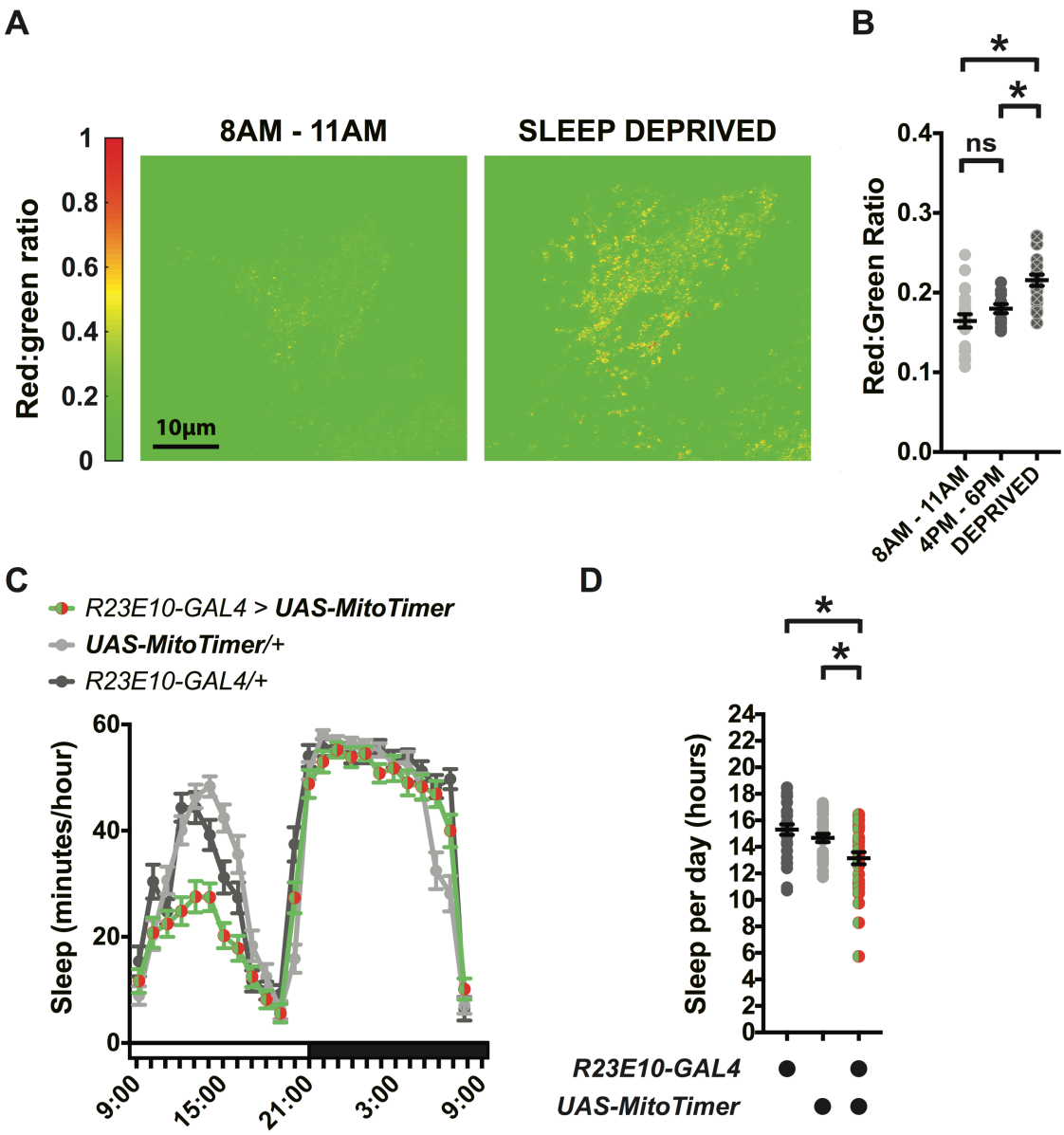

Figure 2.2.3 Sleep deprivation accumulates oxidative levels in the dFB dendrites.

Figure 2.2.3 Sleep deprivation accumulates oxidative levels in the dFB dendrites.

(A) Heat maps of oxidative levels (measured as the ratio between red and green MitoTimer fluorescence) in the dendrites of the dFB neurons. Oxidative levels in sleep deprived flies (right panel) is compared to control flies examined in the morning (left panel). The scale bar represents 10μm.

(B) Dendritic red/green ratios of sleep deprived and control flies (mean ± SEM, n = 6 – 11 per group); the latter was measured at two different time points (8AM – 11AM and 4PM – 6PM). Kruskal-Wallis test detected significant differences (H = 18.490; $\boldsymbol{p < 0.0001}$). Post-hoc Dunn's comparisons revealed significant differences between the sleep deprived flies and both controls ($Z \geq 2.346$, $\boldsymbol{p \leq 0.019}$). The two control groups did not differ significantly ($Z < 0.0001$, $\boldsymbol{p > 0.9999}$).

(C) *R23E10-GAL4* driven expression of MitoTimer decreases sleep over a 24-hour day. (mean ± SEM, n = 31 – 32 per group). Two-way repeated measures ANOVA detected significant main effects for genotype and time ($F_{(2,91)} = 7.951$, $\boldsymbol{p = 0.0007}$, $\eta^2 = 0.011$; $F_{(23,2093)} = 198.200$, $\boldsymbol{p < 0.0001}$, $\eta^2 = 0.602$) as well as a significant interaction ($F_{(46,2093)} = 7.712$, $\boldsymbol{p < 0.0001}$, $\eta^2 = 0.047$).

(D) Total sleep time per day in wild type flies expressing MitoTimer in the dFB neurons differed significantly from both responder and driver controls. One-way ANOVA detected significant differences ($F_{(2,91)} = 7.951$, $\boldsymbol{p = 0.0007}$, $\eta^2 = 0.1488$), and post-hoc Holm-Šídák comparisons revealed that the experimental group was significantly different from both parental controls ($t_{(91)} \geq 2.768$, $\boldsymbol{p \leq 0.007}$, $d \geq 0.493$).

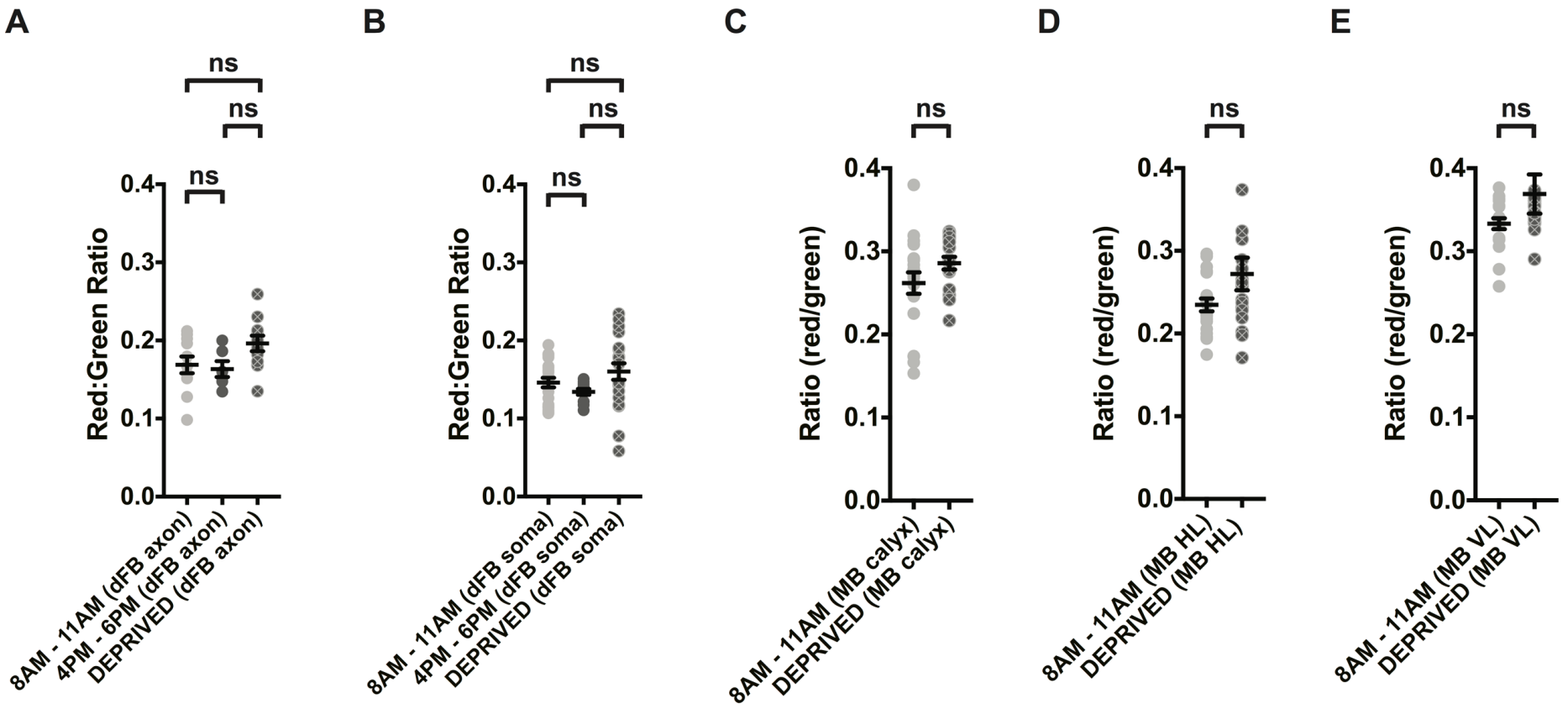

Figure 2.2.4 ROS imaging analyses in other subcellular compartments of the dFB neurons or in the mushroom body.

Figure 2.2.4 ROS imaging analyses in other subcellular compartments of the dFB neurons or in the mushroom body.

(A) Axonal red/green ratios in the dFB neurons of sleep deprived and control flies (mean ± SEM, n = 6 – 11 per group); the latter was measured at two different time points (8AM – 11AM and 4PM – 6PM). One-way ANOVA detected no significant differences ($F_{(2,25)} = 2.763$, $\boldsymbol{p = 0.082}$, $\eta^2 = 0.181$).

(B) Somatic red/green ratios in the dFB neurons of sleep deprived and control flies (mean ± SEM, n = 6 – 11 per group); the latter was measured at two different time points (8AM – 11AM and 4PM – 6PM). Kruskal-Wallis test detected no significant differences ($H = 4.923$, $\boldsymbol{p = 0.085}$).

(C) Calyx red/green ratios in the mushroom body neurons of sleep deprived and control flies (mean ± SEM, n = 9 per group); the latter measured was at 8AM – 11AM. Welch's t-test detected no significant difference ($t_{(30.41)} = 1.582$, $\boldsymbol{p = 0.124}$, d = 0.363).

(D) Horizontal lobe (HL) red/green ratios in the mushroom body neurons of sleep deprived and control flies (mean ± SEM, n = 9 per group); the latter measured was at 8AM – 11AM. Mann-Whitney test detected no significant difference ($U = 127$, $\boldsymbol{p = 0.126}$).

(E) Vertical lobe (VL) red/green ratios in the mushroom body neurons of sleep deprived and control flies (mean ± SEM, n = 9 per group); the latter measured was at 8AM – 11AM. Mann-Whitney test detected no significant difference ($U = 120$, $\boldsymbol{p = 0.082}$).

2.2.4 ROS levels in dFB neurons modulate sleep.

Sleep deprivation results in increased ROS exposures of dFB neuron dendrites. To test whether these increases in ROS are causally related to sleep, I artificially manipulated the redox state of dFB neurons. This was accomplished by overexpressing wild type or mutant superoxide dismutase 1 (Sod1) subunits. Under conditions of oxidative stress, the Sod1, some of which is localized to the mitochondrial intermembrane space, reduces the levels of the highly reactive superoxide anion (O_2^-) by conversion to hydrogen peroxide, which is readily converted into water and molecular oxygen by catalase[57].

Decreasing ROS levels via *hSod1^{WT}* expression in dFB neurons decreases sleep. Overexpression of human wild type Sod1 (*hSod1^{WT}*) in flies has been shown to boost – in a tissue specific manner – the animals' resistance to oxidative stress[121-124]. When overexpressed in dFB neurons, *hSod1^{WT}* significantly reduced sleep (**Figures 2.2.6 A** and **B**). Yet, overexpressing the flies' endogenous Sod1 did not alter sleep (**Figure 2.2.5**). The former effect mirrors that of expressing MitoTimer (**Figures 2.2.4 C** and **D)**, which is also expected to act as an antioxidant by capturing mitochondrial ROS, in the same neurons.

Increasing ROS levels via *hSod1^{A4V}* expression in the dFB neurons increases sleep. To examine the consequences of the converse manipulation — a possible enhancement of sleep by increasing ROS levels in dFB neurons — I used *hSod1^{A4V}*, a widely-studied mutation of *hSod1* implicated in familial amyotrophic lateral sclerosis[125]. This mutant allele leads to increased oxidative stress not via a dysfunction of its dismutation activity but rather through enhanced free radical generation[126,127]. While wild type Sod1 predominantly functions as a dismutase of superoxide anion, it also catalyzes a peroxidase

side reaction — the Fenton reaction — which converts H_2O_2 to hydroxyl radicals (·OH). ·OH is the most reactive among all ROS and a principal source of oxidative stress. In the *hSod1*^{A4V} mutant, the K_M for peroxidation is significantly lowered and hydroxyl radical generation accordingly facilitated[125-127].

R23E10-GAL4 driven overexpression of *hSod1*^{A4V} increased sleep in flies (**Figures 2.2.6-C** and **D**). Accordingly, greater intracellular oxidation in the dFB neurons sufficiently drives sleep, and this is consistent with the accumulation of ROS in the dFB dendrites following sleep deprivation. Thus, the sleep drive may signal through ROS.

Since the present behavioural assay for sleep is based on locomotion, it must be evaluated whether the detected decreases in locomotion could be due to causes other than sleep. To test whether the behaviour I recorded through this assay was genuinely sleep, I measured the arousal thresholds of the aforementioned flies using methods outlined by van Alphen et al[128]. As **Figures 2.2.7-A** and **B** indicate, the arousability of experimental flies carrying either *hSod1*^{WT} or *hSod1*^{A4V} are proportional to the strength of the arousing stimulus. This is the expected outcome from a sleeping organism. Normal arousal thresholds in these flies justifies that sleep in these flies is bona fide.

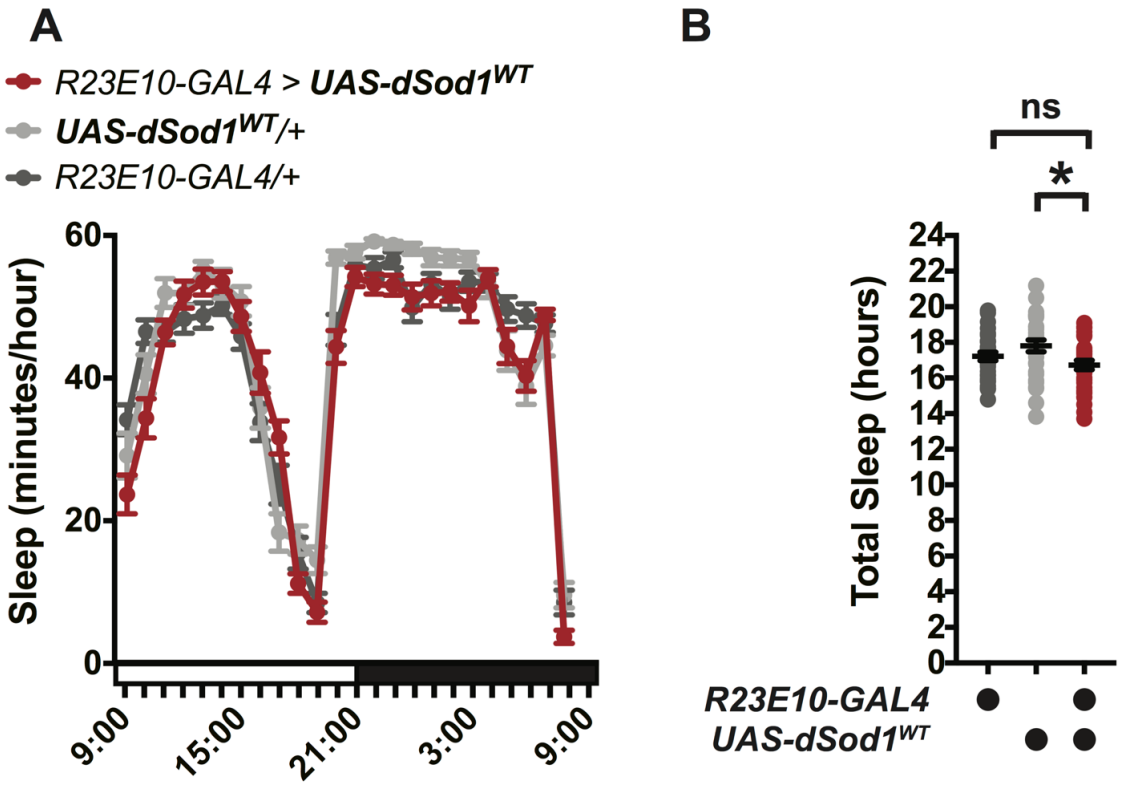

Figure 2.2.5 Expression of *dSod1*^{WT} in the dFB neurons.

Figure 2.2.5 Expression of *dSod1*^{WT} in the dFB neurons.

(A) *R23E10-GAL4* driven expression of wildtype *Drosophila* Sod1 significantly affects sleep (mean ± SEM, n = 29 – 32 per group). Two-way repeated measures ANOVA detected significant main effects for genotype ($F_{(2,90)}$ = 16.090, $\boldsymbol{p = 0.023}$, η^2 = 0.004) and time ($F_{(23,2070)}$ = 150.400, $\boldsymbol{p < 0.0001}$, η^2 = 0.656) as well as a significant genotype × time interaction ($F_{(46,2070)}$ = 3.076, $\boldsymbol{p < 0.0001}$, η^2 = 0.025).

(B) Total sleep time per day in flies expressing *dSod1*^{WT} in the dFB neurons did not differ significantly from both parental controls. One-way ANOVA detected significant differences ($F_{(2,90)}$ = 3.837, $\boldsymbol{p = 0.025}$, η^2 = 0.079), and post-hoc Holm-Šídák comparisons revealed that the experimental group was significantly different from the responder control ($t_{(90)}$ = 2.768, $\boldsymbol{p = 0.014}$, d = 0.497) but not the driver controls ($t_{(90)}$ = 1.262, $\boldsymbol{p = 0.210}$, d = 0.225).

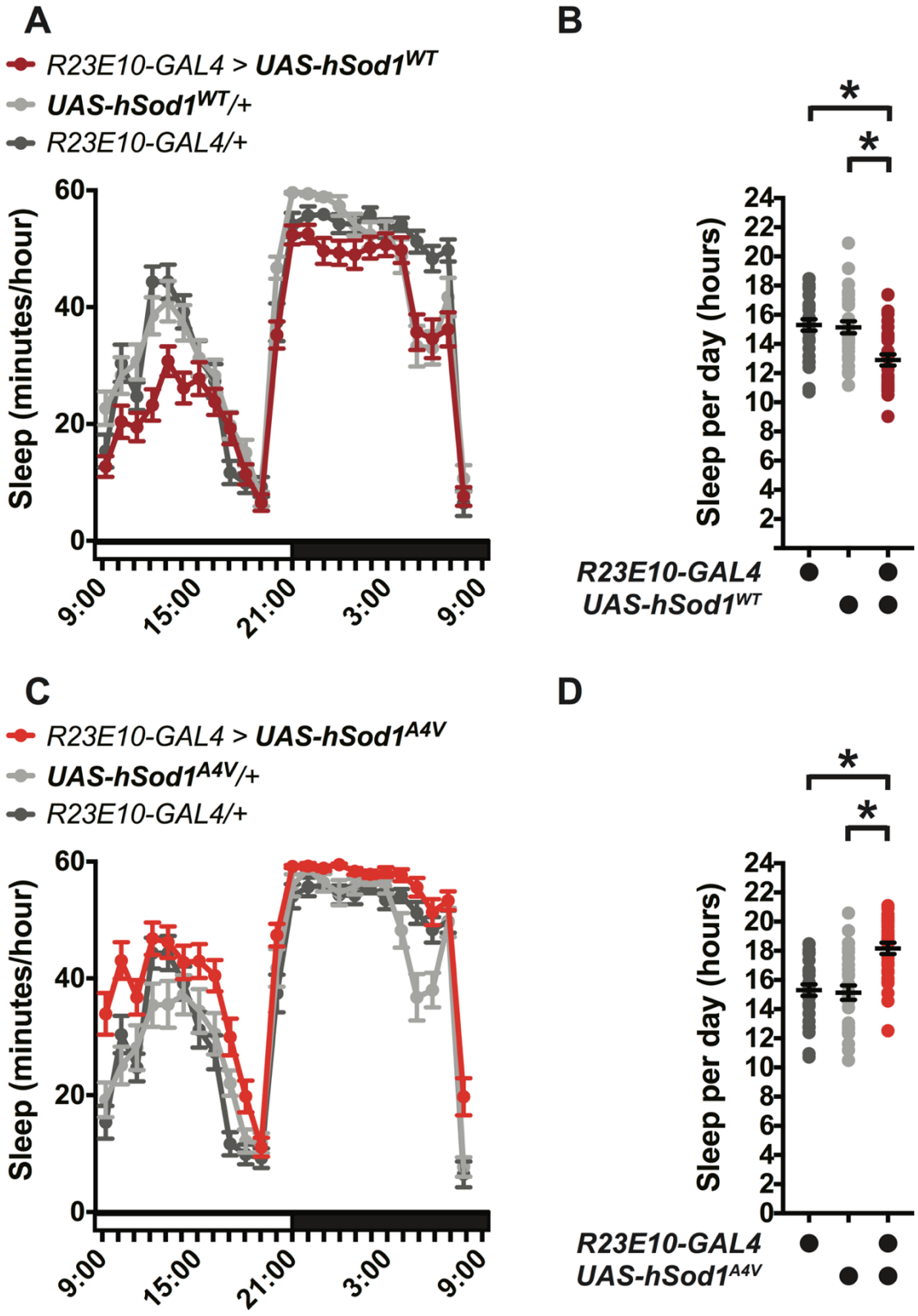

Figure 2.2.6 Sleep in flies overexpressing *hSod1^{WT}* or *hSod1^{A4V}* in the dFB neurons.

Figure 2.2.6 Sleep in flies overexpressing *hSod1^{WT}* or *hSod1^{A4V}* in the dFB neurons.

(A) *R23E10-GAL4* driven expression of wildtype human Sod1 decreases sleep (mean ± SEM, n = 32 per group). Two-way repeated measures ANOVA detected significant main effects for genotype ($F_{(2,92)} = 11.580$, $\boldsymbol{p < 0.0001}$, $\eta^2 = 0.017$) and time ($F_{(23,2116)} = 156.300$, $\boldsymbol{p < 0.0001}$, $\eta^2 = 0.558$) as well as a significant genotype × time interaction ($F_{(46,2116)} = 3.756$, $\boldsymbol{p < 0.0001}$, $\eta^2 = 0.027$).

(B) Total sleep time per day in flies expressing *hSod1^{WT}* in the dFB neurons differed significantly from both parental controls. One-way ANOVA detected significant differences ($F_{(2,92)} = 11.580$, $\boldsymbol{p < 0.0001}$, $\eta^2 = 0.201$), and post-hoc Holm-Šídák comparisons revealed that the experimental group was significantly different from both parental controls ($t_{(92)} \geq 4.025$, $\boldsymbol{p \leq 0.0001}$, $d \geq 0.712$).

(C) *R23E10-GAL4* driven expression of mutant human Sod1 increases sleep (mean ± SEM, n = 32 per group). Two-way repeated measures ANOVA detected significant main effects for genotype ($F_{(2,87)} = 16.090$, $\boldsymbol{p < 0.0001}$, $\eta^2 = 0.029$) and time ($F_{(23,2001)} = 150.400$, $\boldsymbol{p < 0.0001}$, $\eta^2 = 0.551$) as well as a significant genotype × time interaction ($F_{(46,2001)} = 3.076$, $\boldsymbol{p < 0.0001}$, $\eta^2 = 0.023$).

(D) Total sleep time per day in flies expressing *hSod1^{A4V}* in the dFB neurons differed significantly from both parental controls. One-way ANOVA detected significant differences ($F_{(2,87)} = 16.090$, $\boldsymbol{p < 0.0001}$, $\eta^2 = 0.270$), and post-hoc Holm-Šídák comparisons revealed that the experimental group was significantly different from both parental controls ($t_{(87)} \geq 4.802$, $\boldsymbol{p < 0.0001}$, $d \geq 0.870$).

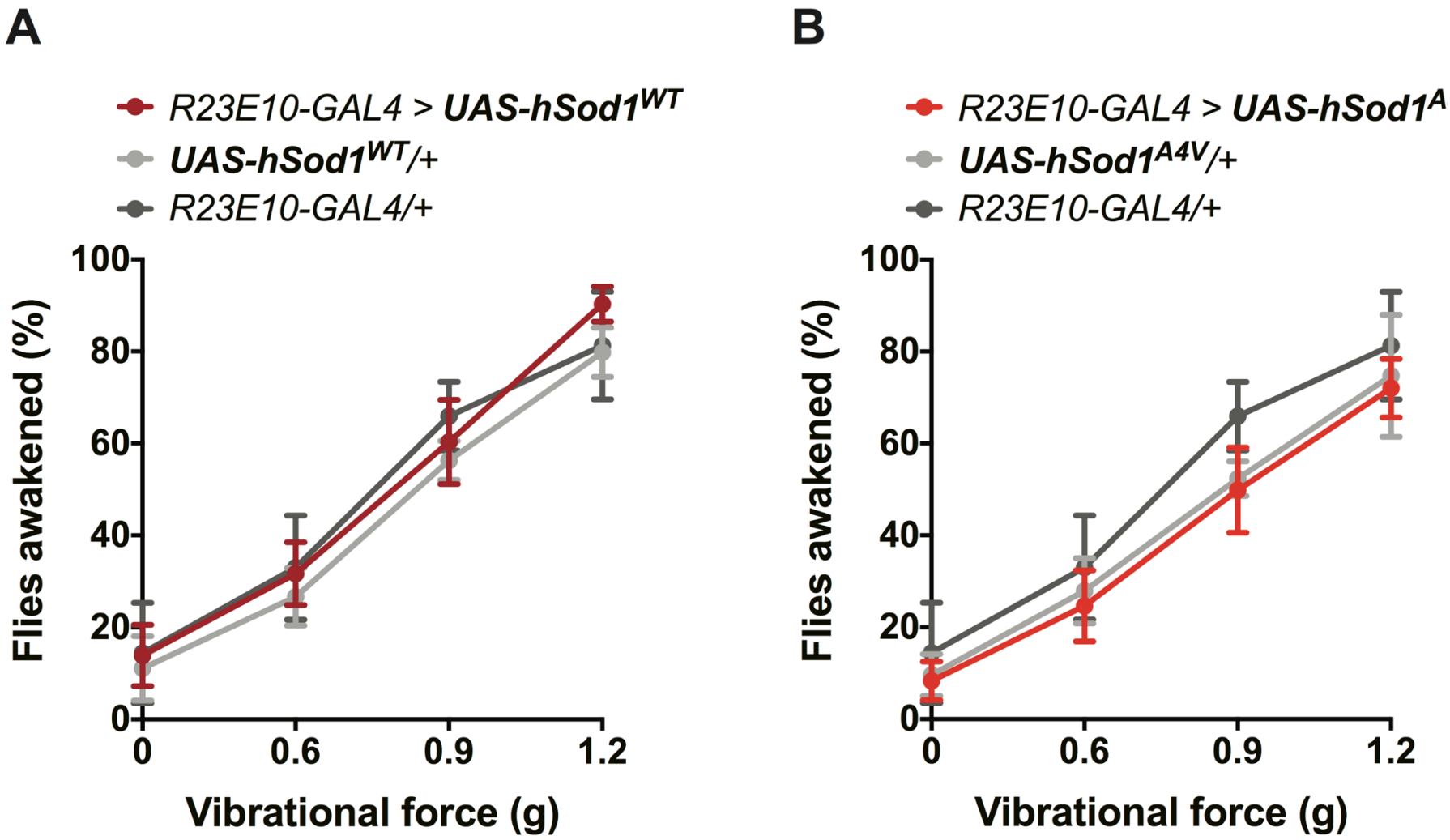

Figure 2.2.7 Arousal thresholds of flies overexpressing *hSod1*^{WT} or *hSod1*^{A4V} in the dFB neurons.

Figure 2.2.7 Arousal thresholds of flies overexpressing *hSod1*^{WT} or *hSod1*^{A4V} in the dFB neurons.

(A) *R23E10-GAL4* driven expression of wildtype human Sod1 does not affect arousal thresholds (mean ± SEM, n = 6 trials per group). Two-way repeated measures ANOVA detected a significant main effect for vibrational force ($F_{(3,60)}$ = 46.370, $\boldsymbol{p < 0.0001}$, η^2 = 0.691) but significant difference was detected neither for genotype ($F_{(2,60)}$ = 0.604, $\boldsymbol{p = 0.550}$, η^2 = 0.006) nor the genotype × force interaction ($F_{(6,60)}$ = 0.162, $\boldsymbol{p = 0.986}$, η^2 = 0.005).

(B) *R23E10-GAL4* driven expression of mutant Sod1 does not affect arousal thresholds (mean ± SEM, n = 6 trials per group). Two-way repeated measures ANOVA detected a significant main effect for vibrational force ($F_{(3,60)}$ = 33.130, $\boldsymbol{p < 0.0001}$, η^2 = 0.611) but significant difference was neither detected for genotype ($F_{(2,60)}$ = 1.424, $\boldsymbol{p = 0.249}$, η^2 = 0.018) nor the genotype × force interaction ($F_{(6,60)}$ = 0.080; $\boldsymbol{p = 0.998}$; η^2 = 0.003).

Fluctuations in ROS levels in other regions of the fly brain do not affect sleep.

Do dFB neurons have a unique role as transducers of ROS production into sleep? To address this, I modulated the resistance of different groups of neurons to oxidative stress, by using $hSod1^{WT}$ and $hSod1^{A4V}$. I tested the effect on sleep of altering ROS levels in various clock cells (PDF-positive neurons [LN_vs]; CRY-positive neurons [LN_vs, LN_ds, DN_1s])[129,130], mushroom body (MB) Kenyon cells, and olfactory projection neurons. None of these manipulations, which targeted neurons with established roles in sleep (clock and Kenyon cells) as well as neurons lacking such a role (projection neurons), altered sleep (**Figure 2.2.8**).

The results from the overexpression of $hSod1^{WT}$ or $hSod1^{A4V}$ in the above five brain regions (dFB, PDF-positive, CRY-positive, MB, and olfactory projection neurons) was pooled for an omnibus analysis (**Tables A45** and **A46**, respectively). Here, brain region was included as a factor in a two-way ANOVA. Despite the more conservative thresholds for statistical significance (due to the familywise error rate), overexpression of $hSod1^{WT}$ or $hSod1^{A4V}$ significantly affected sleep only in the dFB neurons. This aligns with the outcomes of region-specific analyses demonstrated above (**Figure 2.2.6**) and below (**Figure 2.2.8**)

This suggests that dFB neurons experience particularly large ROS fluctuations (**Figure 2.2.3**), express specialized machinery that allows them to transduce ROS signals into sleep, or both.

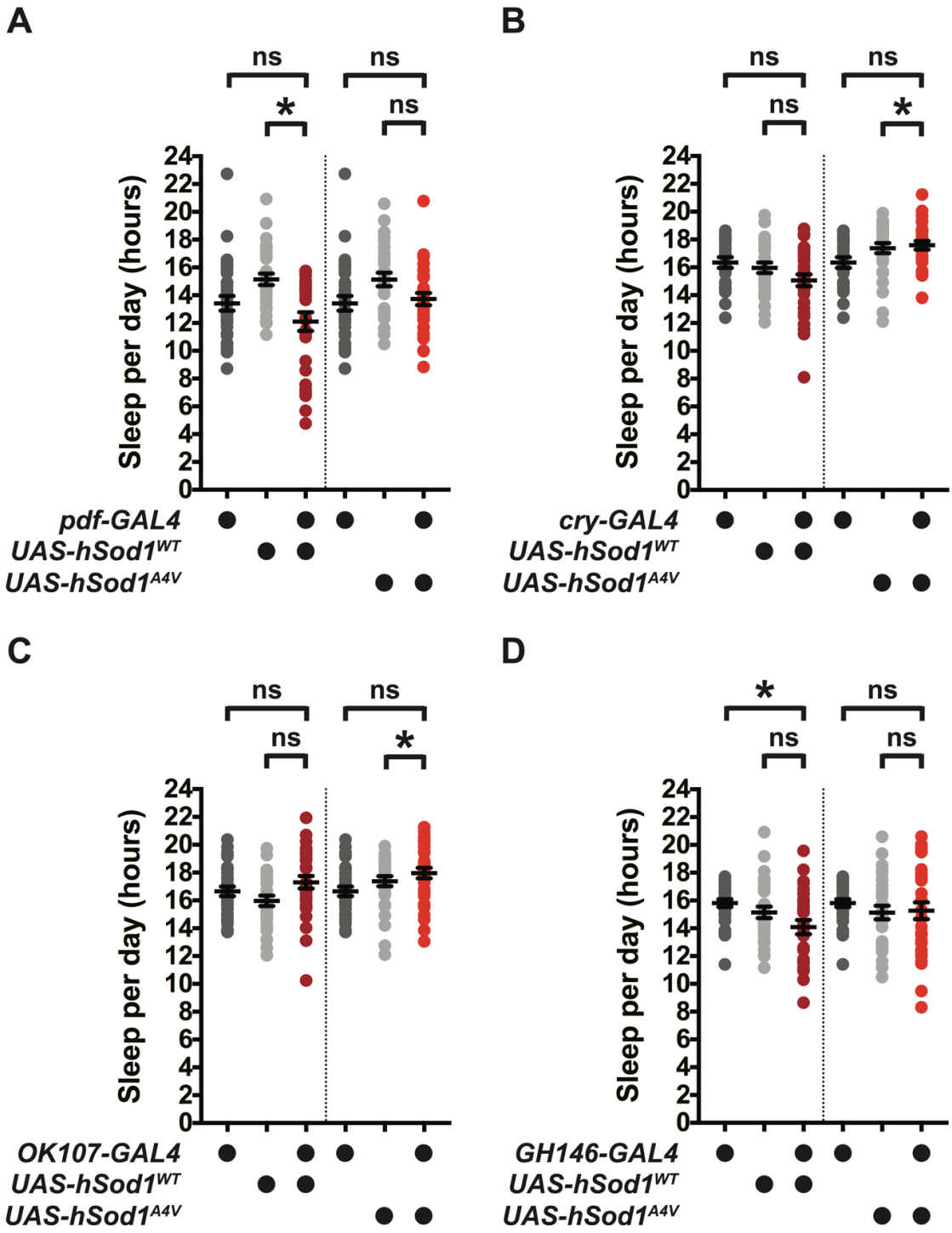

Figure 2.2.8 Sleep in flies following the overexpression of *hSod1*^{WT} or *hSod1*^{A4V} in different brain regions.

Figure 2.2.8 Sleep in flies following the overexpression of *hSod1^{WT}* or *hSod1^{A4V}* in different brain regions.

(A) Total sleep time per day in flies overexpressing *hSod1^{WT}* or *hSod1^{A4V}* (left and right of dotted line) in PDF-positive neurons (mean ± SEM, n = 28 – 32 per group). In the *hSod1^{WT}* dataset, Kruskal-Wallis test detected significant differences ($H = 11.220$, $\mathbf{p = 0.004}$). Post-hoc Dunn's comparisons revealed that the experimental group was significantly different from the responder control ($Z = 2.878$, $\mathbf{p = 0.004}$) but not the driver controls ($Z < 0.0001$, $\mathbf{p > 0.9999}$). In the *hSod1^{A4V}* dataset, one-way ANOVA detected significant differences ($F_{(2,88)} = 3.845$, $\mathbf{p = 0.035}$, $\eta^2 = 0.073$). Post-hoc Holm-Šídák comparisons did not reveal significant differences between the experimental control and either parental control ($t_{(88)} \leq 2.040$; $\mathbf{p \geq 0.087}$; $d \leq 0.372$).

(B) Total sleep time per day in flies overexpressing *hSod1^{WT}* or *hSod1^{A4V}* (left and right of dotted line) in CRY-positive neurons (mean ± SEM, n = 23 – 32 per group). In the *hSod1^{WT}* dataset, one-way ANOVA did not detected significant differences ($F_{(2,81)} = 2.713$, $\mathbf{p = 0.072}$, $\eta^2 = 0.063$). In the *hSod1^{A4V}* dataset, Kruskal-Wallis test detected significant differences ($H = 6.560$, $\mathbf{p = 0.036}$). Post-hoc Dunn's comparisons revealed that the experimental group was significantly different from the responder control ($Z = 1.995$, $\mathbf{p = 0.046}$) but not the driver control ($Z < 0.0001$, $\mathbf{p > 0.9999}$).

(C) Total sleep time per day in flies overexpressing *hSod1^{WT}* or *hSod1^{A4V}* (left and right of dotted line) in the mushroom body neurons (mean ± SEM, n = 23 – 32 per group). In the *hSod1^{WT}* dataset, one-way ANOVA did not detect significant differences ($F_{(2,86)} = 2.821$, $\mathbf{p = 0.065}$, $\eta^2 = 0.062$). In the *hSod1^{A4V}* dataset, Kruskal-Wallis test detected significant differences ($H = 7.204$, $\mathbf{p = 0.027}$). Post-hoc Dunn's comparisons revealed

that the experimental group was significantly different from the responder control (Z = 2.432, $\boldsymbol{p}$ **= 0.015**) but not the driver controls (Z = 0.532, $\boldsymbol{p}$ **= 0.595**).

(D) Total sleep time per day in flies overexpressing $hSod1^{WT}$ or $hSod1^{A4V}$ (left and right of dotted line) in the projection neurons (mean ± SEM, n = 28 – 32 per group). In the $hSod1^{WT}$ dataset, Kruskal-Wallis test detected significant differences (H = 7.342, $\boldsymbol{p}$ **= 0.026**). Post-hoc Dunn's comparisons revealed that the experimental group was significantly different from the driver control (Z = 2.457, $\boldsymbol{p}$ **= 0.014**) but not the responder control (Z = 0.986, $\boldsymbol{p}$ **= 0.324**). In the $hSod1^{A4V}$ dataset, Kruskal-Wallis test did not detect significant differences (H = 1.252, $\boldsymbol{p}$ **= 0.535**).

2.2.5 Hk mediates the sleep-promoting effect of ROS in dFB neurons.

Given that ROS accumulation in dFB neurons promotes sleep, and that Shaker currents in dFB neurons are upregulated during sleep, it seemed plausible that the redox sensing ability of the Shaker beta subunit Hk provides the mechanistic link between the cells' redox state and their electrical activity. If this notion is correct, suppressing *Hk* in dFB neurons via RNAi interference should not only decrease baseline sleep (**Figures 2.2.1** and **2.2.9** (**A** and **B**) but also occlude the effect of elevated ROS production caused by overexpressing $hSod1^{A4V}$.

***Hk* knock down in the dFB neurons nullifies the effects of modulating oxidative levels.**

As **Figures 2.2.10-A** and **B** show, co-expressing $hSod1^{WT}$ and Hk^{RNAi} in dFB neurons does not additively affect sleep when compared to the expression of either construct alone; the sleep reduction in flies expressing both $hSod1^{WT}$ and Hk^{RNAi} is comparable to that observed in flies expressing just Hk^{RNAi}. In contrast, co-expressing Hk^{RNAi} with $hSod1^{A4V}$ in dFB neurons counteracted the sleep-promoting effect of enhanced ROS generation in flies expressing *R23E10-GAL4* driven $hSod1^{A4V}$ (**Figures 2.2.10-C** and **D**). Collectively, these results suggest that Hk responds to changes in cellular redox levels.

However, *Hk* knockdown in dFB neurons was able only partially to negate the sleep promoting effect of $hSod1^{A4V}$. One potential explanation for this result is that the expression of not one but two UAS-driven transgenes dilutes the transcriptional activity of R23E10-GAL4.

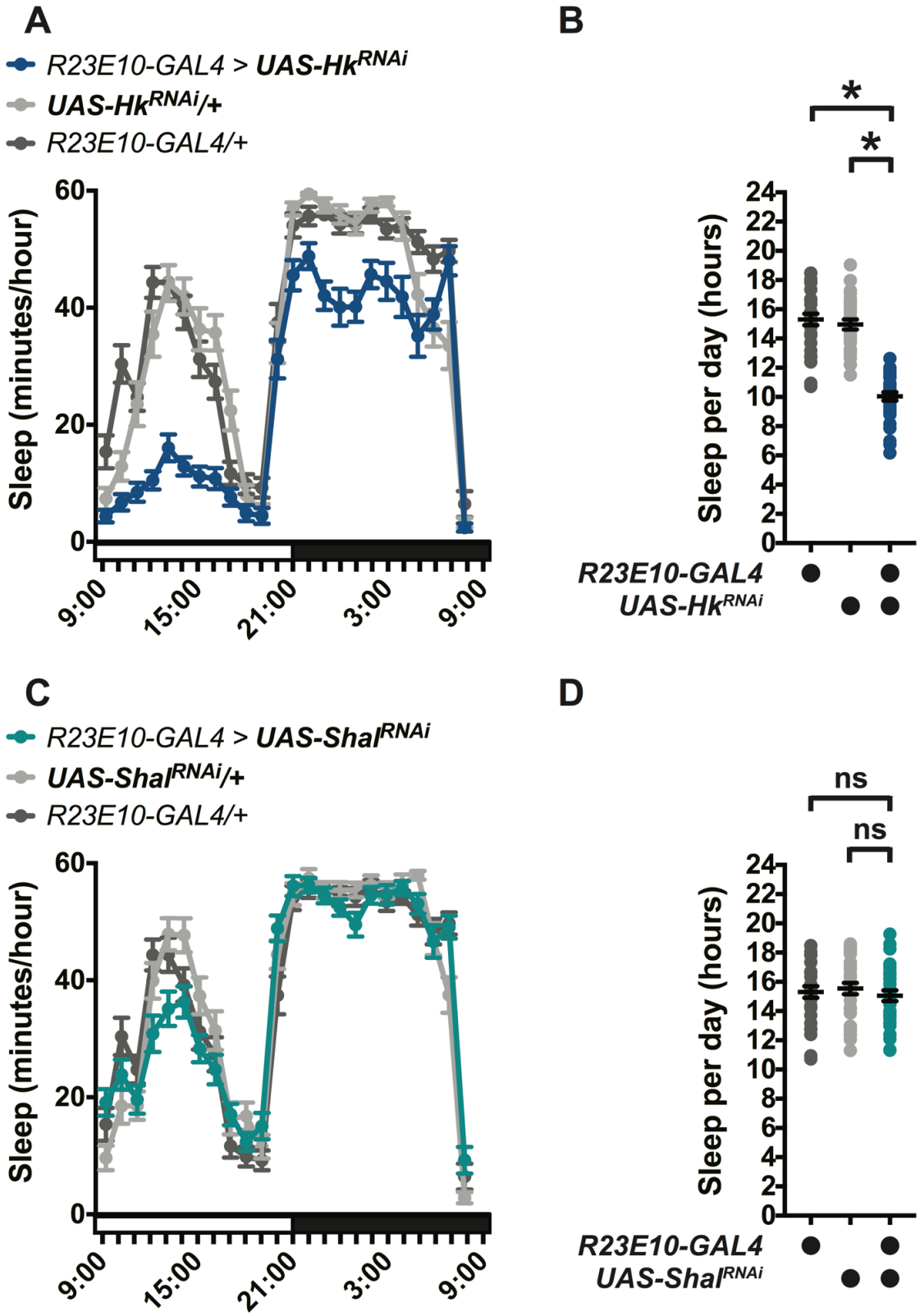

Figure 2.2.9 Sleep in flies expressing *Hk* or *Shal* RNAi in the dFB neurons.

Figure 2.2.9 Sleep in flies expressing *Hk* or *Shal* RNAi in the dFB neurons.

(A) *R23E10-GAL4* driven expression of Hk^{RNAi} decreases sleep (mean ± SEM, n = 29 – 32 per group). Two-way repeated measures ANOVA detected significant main effects for genotype ($F_{(2,92)}$ = 65.740, $\boldsymbol{p < 0.0001}$, η^2 = 0.066) and time ($F_{(23,2116)}$ = 173.600, $\boldsymbol{p < 0.0001}$, η^2 = 0.549) as well as a significant genotype × time interaction ($F_{(46,2116)}$ = 7.612, $\boldsymbol{p < 0.0001}$, η^2 = 0.048).

(B) Total sleep time per day in flies expressing Hk^{RNAi} in the dFB neurons differed significantly from both parental controls. One-way ANOVA detected significant differences ($F_{(2,89)}$ = 75.440, $\boldsymbol{p < 0.0001}$, η^2 = 0.629), and post-hoc Holm-Šídák comparisons revealed that the experimental group was significantly different from both parental controls ($t_{(89)} \geq 10.100$, $\boldsymbol{p < 0.0001}$, $d \geq 1.829$).

(C) *R23E10-GAL4* driven expression of $Shal^{RNAi}$ does not alter sleep (mean ± SEM, n = 31 – 32 per group). Two-way repeated measures ANOVA detected a significant main effect for time ($F_{(23,2116)}$ = 173.600, $\boldsymbol{p < 0.0001}$, η^2 = 0.549) as well as a significant genotype × time interaction ($F_{(46,2116)}$ = 7.612, $\boldsymbol{p < 0.0001}$, η^2 = 0.048) but did not detect a significant main effect for genotype ($F_{(2,92)}$ = 65.740, $\boldsymbol{p < 0.0001}$, η^2 = 0.066).

(D) Total sleep time per day in flies expressing $Shal^{RNAi}$ in the dFB neurons did not differ significantly from either parental control. One-way ANOVA did not detected significant differences ($F_{(2,90)}$ = 0.410, $\boldsymbol{p = 0.665}$, η^2 = 0.009).

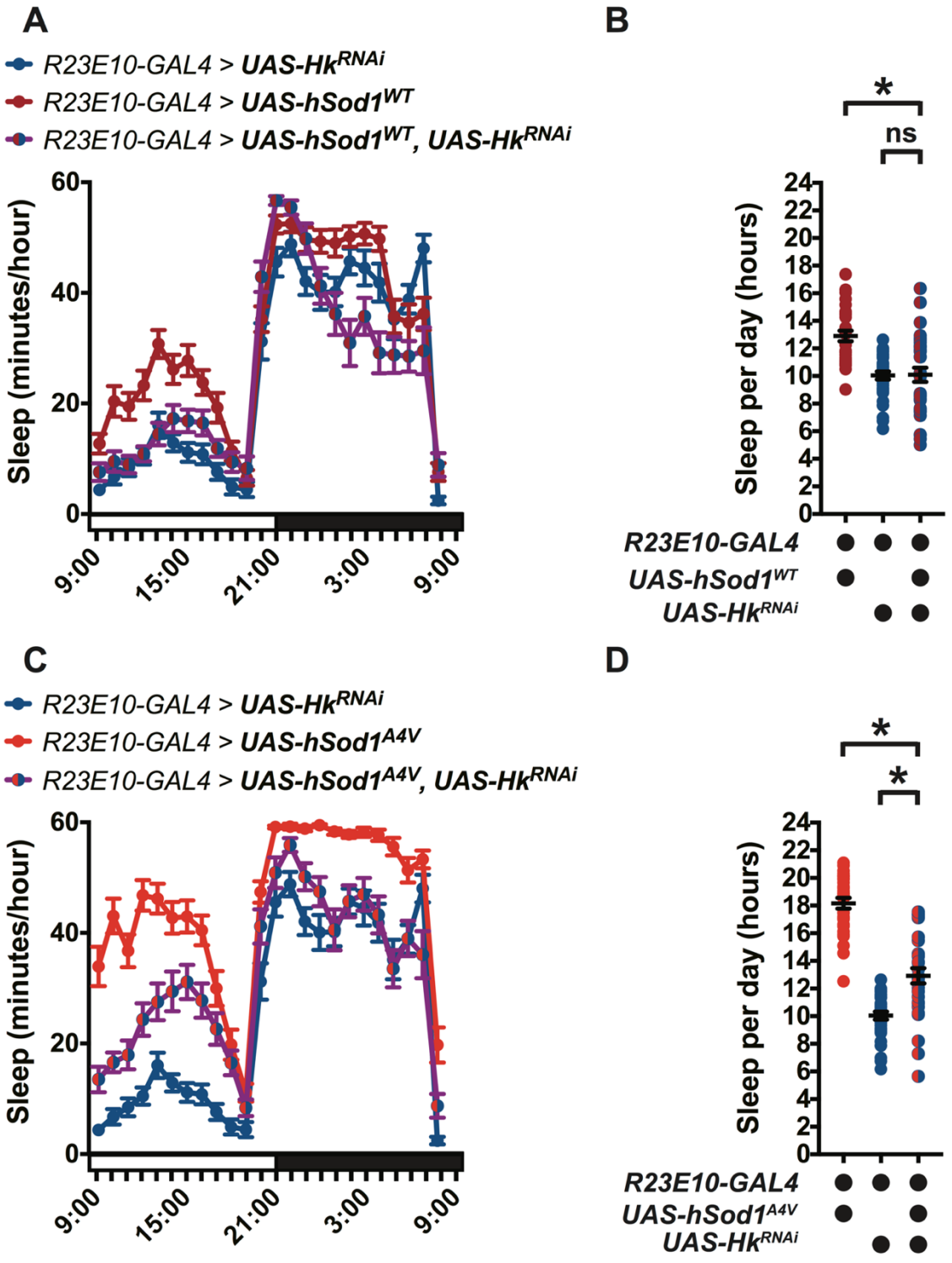

Figure 2.2.10 Sleep in flies co-expressing *Hk*^{RNAi} along with *hSod1*^{WT} or *hSod1*^{A4V} in the dFB neurons.

Figure 2.2.10 Sleep in flies co-expressing Hk^{RNAi} along with $hSod1^{WT}$ or $hSod1^{A4V}$ in the dFB neurons.

(A) *R23E10-GAL4* driven co-expression of Hk^{RNAi} and $hSod1^{WT}$ further decreases sleep compared to when the latter is expressed alone (mean ± SEM, n = 30 – 32 per group). Two-way repeated measures ANOVA detected significant main effects for genotype ($F_{(2,93)}$ = 16.400, $\boldsymbol{p < 0.0001}$, η^2 = 0.025) and time ($F_{(23,2139)}$ = 148.000, $\boldsymbol{p < 0.0001}$, η^2 = 0.532) as well as a significant genotype × time interaction ($F_{(46,2139)}$ = 5.338, $\boldsymbol{p < 0.0001}$, η^2 = 0.038).

(B) Total sleep time per day in flies co-expressing Hk^{RNAi} and $hSod1^{WT}$ in the dFB neurons. One-way ANOVA detected significant differences ($F_{(2,93)}$ = 16.400, $\boldsymbol{p < 0.0001}$, η^2 = 0.261). Post-hoc Holm-Šídák comparisons revealed that the experimental group was significantly different from the $hSod1^{WT}$ control ($t_{(93)}$ = 4.917, $\boldsymbol{p < 0.0001}$, d = 0.869) but not the Hk^{RNAi} control ($t_{(93)}$ = 0.086, $\boldsymbol{p = 0.932}$, d = 0.015).

(C) *R23E10-GAL4* driven expression of Hk^{RNAi} occludes the sleep promoting effects of $hSod1^{A4V}$ (mean ± SEM, n = 30 – 32 per group). Two-way repeated measures ANOVA detected significant main effects for genotype ($F_{(2,89)}$ = 98.860, $\boldsymbol{p < 0.0001}$, η^2 = 0.148) and time ($F_{(23,2047)}$ = 123.900, $\boldsymbol{p < 0.0001}$, η^2 = 0.433) as well as a significant genotype × time interaction ($F_{(46,2047)}$ = 5.553, $\boldsymbol{p < 0.0001}$, η^2 = 0.039).

(D) Total sleep time per day in flies co-expressing Hk^{RNAi} and $hSod1^{A4V}$ in the dFB neurons. Kruskal-Wallis test detected significant differences (H = 61.810, $\boldsymbol{p < 0.0001}$). Post-hoc Holm-Šídák comparisons revealed that the experimental group was significantly different from both the $hSod1^{A4V}$ and Hk^{RNAi} controls ($Z \geq 3.090$; $\boldsymbol{p \leq 0.002}$).

The sleep phenotypes arising from *hSod1^{WT}* or *hSod1^{A4V}* overexpression in dFB neurons depend on Hk.

To test whether the ectopic presence of any RNAi construct can mask the effect of expressing *hSod1^{WT}* or *hSod1^{A4V}*, I replaced *Hk^{RNAi}* with a hairpin construct directed against the voltage-gated potassium channel, Shal (*Shal^{RNAi}*). Knocking down *Shal* in dFB neurons does not affect sleep in (**Figures 2.2.8-C** and **D**)[24]. Co-expression of *hSod1^{WT}* with *Shal^{RNAi}* did not alter sleep in flies when compared to flies expressing each construct separately (**Figure 2.2.11-A**). Co-expressing *Shal^{RNAi}* with *hSod1^{A4V}* increased sleep, in a manner qualitatively similar to the increase seen in flies expressing *hSod1^{A4V}* alone (**Figure 2.2.11-B**). However, there is a significant difference in the magnitude of these sleep changes between flies co-expressing *hSod1^{A4V}* and *Shal^{RNAi}* versus those expressing *hSod1^{A4V}* alone. This difference most likely reflects the dilution of R23E10-GAL4 owing to the presence of multiple UAS transgenes, a notion corroborated below. Nevertheless, the evidence firmly implicates Hk in the dFB neurons' response to changes in cellular redox state.

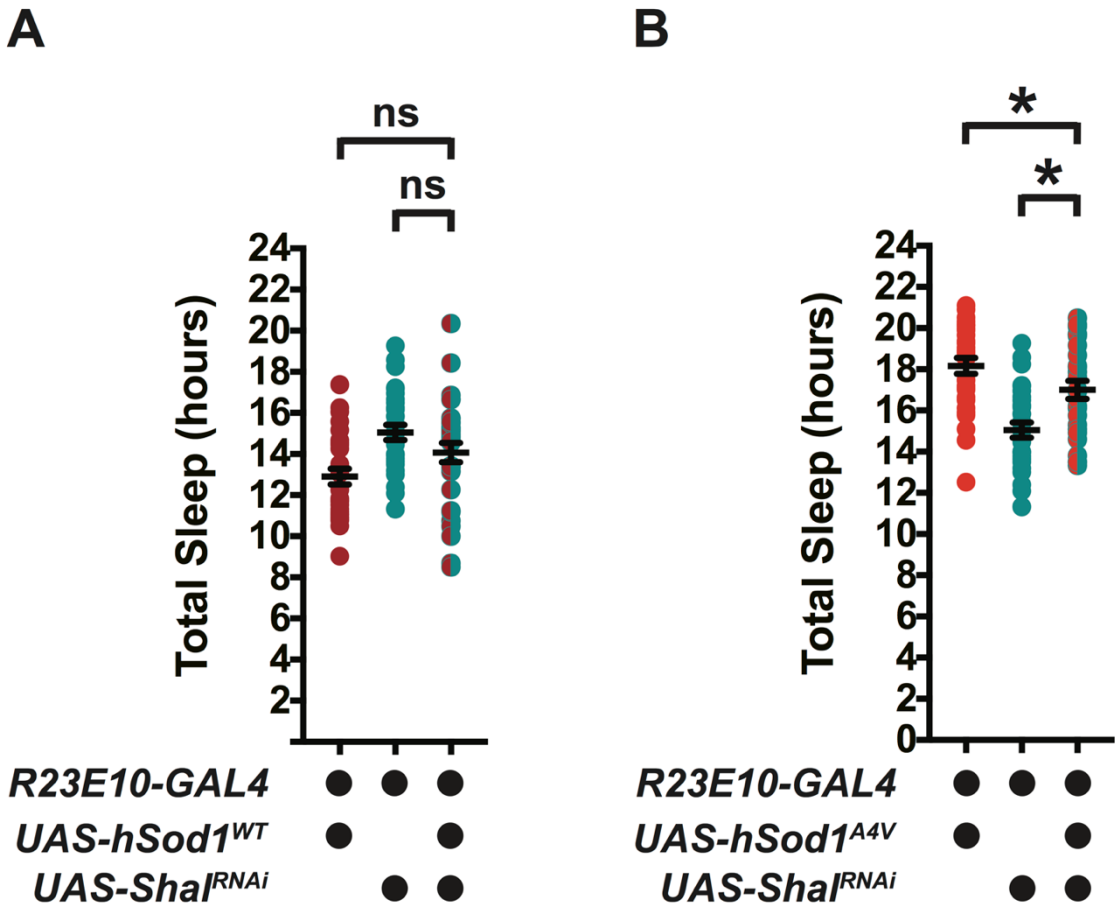

Figure 2.2.11 Sleep in flies co-expressing *Shal*^{RNAi} along with wild type or mutant Sod1 in the dFB neurons.

Figure 2.2.11 Sleep in flies co-expressing *Shal*^{RNAi} along with wild type or mutant Sod1 in the dFB neurons.

(A) Total sleep time per day in flies co-expressing *Shal*^{RNAi} and *hSod1*^{WT} in the dFB neurons. One-way ANOVA detected significant differences ($F_{(2,92)} = 6.893$, $\boldsymbol{p = 0.002}$, $\eta^2 = 0.130$). Post-hoc Holm-Šídák comparisons revealed that the experimental group did not significantly differ from either the *hSod1*^{WT} or *Hk*^{RNAi} control ($t_{(92)} \leq 2.036$, $\boldsymbol{p \geq 0.087}$, $d \leq 0.360$).

(B) Total sleep time per day in flies co-expressing *Shal*^{RNAi} and *hSod1*^{A4V} in the dFB neurons. One-way ANOVA detected significant differences ($F_{(2,85)} = 16.63$, $\boldsymbol{p < 0.0001}$, $\eta^2 = 0.281$). Post-hoc Holm-Šídák comparisons revealed that the experimental group was significantly different from both the *hSod1*^{WT} and *Hk*^{RNAi} controls ($t_{(85)} \geq 2.060$, $\boldsymbol{p \leq 0.042}$, $d \geq 0.386$).

The presence of UAS-transgenes dilutes the GAL4-driver's transcriptional efficiency.

To evaluate whether the level of R23E10-GAL4 limits the transcription of two responder constructs, I conducted a simultaneous knockdown of *Hk* and *Shal*. As predicted for a dilution model, this resulted in a decreased effect size for the Hk^{RNAi} when co-expressed with $Shal^{RNAi}$ (**Figure 2.2.12**). The simultaneous expression of multiple responder constructs from a common driver thus lowers the driver's efficacy, which explains the milder behavioural phenotypes observed in **Figure 2.2.12**. This is also generalizable to previous instances in **Figures 2.2.10** and **2.2.11** where a single GAL4 driver was coupled with two UAS transgenes.

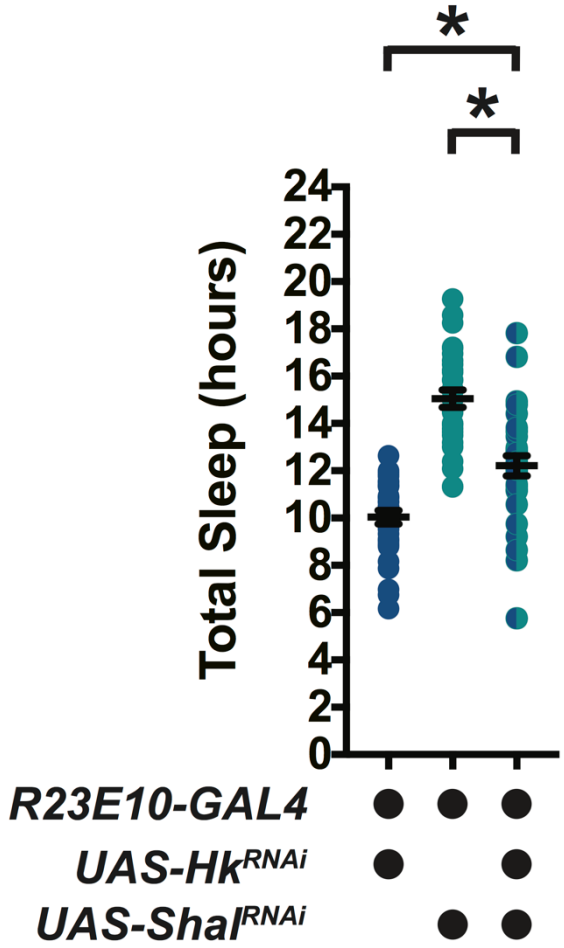

Figure 2.2.12 Sleep in flies co-expressing *Shal*^{RNAi} and *Hk*^{RNAi} along with wild type or mutant Sod1 in the dFB neurons.

Figure 2.2.12 Sleep in flies co-expressing *Shal*^{RNAi} and *Hk*^{RNAi} along with wild type or mutant Sod1 in the dFB neurons.

Total sleep time per day in flies co-expressing *Hk*^{RNAi} and *Shal*^{RNAi} in the dFB neurons. One-way ANOVA detected significant differences ($F_{(2,91)} = 48.24$, $\boldsymbol{p < 0.0001}$, $\eta^2 = 0.515$). Post-hoc Holm-Šídák comparisons revealed that the experimental group was significantly different from both the and *Hk*^{RNAi} and *Shal*^{RNAi} controls ($t_{(91)} \geq 4.247$; $\boldsymbol{p <}$ **0.0001**; $d \geq 0.757$).

Chapter 3: Discussion

3.1 Sleep homeostasis in the dorsal fan-shaped body: a recap.

In 2011, Donlea et al. discovered the unique sleep promoting role of the dorsal fan-shaped body neurons[34]. Since then, our understanding of how these neurons regulate sleep has grown. First, periods of electrical activity and quiescence of these neurons coincide with sleeping and waking states[24,25]. Moreover, it was shown that the fly's sleep history modifies the intrinsic electrical properties of the dFB neurons, and this underlies the homeostatic regulation of sleep[25]. This connection is well illustrated through flies carrying a mutation for *crossveinless-c* (*cv-c*), which encodes a Rho GAP[25]. These mutants sleep less and fail to recover from sleep deprivation[25]. Both of these phenotypes were shown to be due to reduced membrane excitability in the dFB neurons[25].

Second, arousal promoting dopaminergic neurons[131,132] inhibit the dFB neurons[24]. Dopamine release alters the biophysical makeup of these neurons by reducing A-type potassium currents carried by Shaker (Sh) while increasing leak potassium currents carried by Sandman (sand), a two-pore domain potassium channel[24]. Remarkably, this balance between two potassium currents is flipped during sleep (i.e. greater A-type K^+ currents and reduced leak K^+ currents)[24]. Periods of electrical activity and inactivity of dFB neurons thus triggers and maintains sleep and wakefulness in flies very much like an electric switch.

These findings form the foundation for my work. Focusing on dFB neurons, which are integral for homeostatic sleep regulation, I searched for intracellular signaling molecules that act as gears for this switch and, thus, reflect a fly's sleep history.

3.2 Sleep regulation via Rho GTPases.

3.2.1 A model for sleep regulation via Rho GTPases in the dFB neurons.

Although Cv-c must function in dFB neurons for proper sleep regulation, it was unclear whether this regulatory role depends on the protein's Rho GAP activity (GTPase activating protein). I have shown that this is indeed the case, and that Rac1 and Rho1 (the latter being the substrate for Cv-c) regulate sleep in a mutually antagonistic manner.

In my current model, Rac1 promotes sleep whereas its antagonist, Rho1, promotes arousal. The activities of Rac1 and Rho1 are cyclically modulated by guanine nucleotide exchange factors (GEFs) and GTPase activating proteins (GAPs); notably, Cv-c acts as a Rho GAP for Rho1 and curtails its activity. Downstream targets from Rac1 and Rho1 must, therefore, influence the excitability of the dFB neurons. Signals upstream to Rac1 and Rho1 may target these GTPases directly or affect their activity indirectly via GEFs or GAPs[95,98]. This mutual antagonism conveniently allows for signals of opposing valences to compete for control over the fly's behavioural state.

3.2.2. The wild type genetic background is unsuitable for behavioural assays of Rho GTPase dynamics.

Yet, why do overexpression experiments in the wild type genetic background produce puzzlingly isotropic results? A plausible explanation lies in the delicate cellular balance of Rho GTPases. In healthy cells, signaling through Rho GTPases depends more on their dynamic cycling rather than the independent action of a single Rho GTPase in its GTP bound ON state[95]. Disturbing this balance will create knock-on effects through the cycle, which explains why constitutively active and dominant negative Rho GTPase mutations frequently generate similar phenotypes[91,133-135]. This is very much consistent with the confusingly unidirectional decreases in sleep I observed in wild type flies overexpressing

constitutively active or dominant negative Rac1 (*Rac1*^{L89} and *Rac1*^{V12}, respectively) in dFB neurons.

In addition, further complications arise due to the mutual antagonism between Rac1 and Rho1 that I uncovered. Under physiological conditions, Rac1 and Rho1 compete by inactivating GEFs (e.g. activated Rac1 inhibits p115-RhoGEF[136] and PDZ-RhoGEF[137]) or activating GAPs (e.g. activated Rho1 activates ROCK, which, in turn, inhibits ArhGAP[138]) that regulate the antagonistic GTPase. Hence, the result is a dynamic compensatory system where perturbations in one Rho GTPase's activity are titrated by reciprocal modulation of its opposing partner. This is most evident from the neural development literature. During development, Rac1 and Rho1 modulate axon growth via actin polymerization and depolymerization, respectively[95-98]. The former is required to extend an exploring growth cone process while the latter helps to retract it[95,98]. Since both components are required, removing either one impairs axon outgrowth[95,98]. Moreover, disrupting the cycling between the ON and OFF states of each GTPase through constitutively active or dominant negative mutations also produces the same phenotype (i.e. failed axon outgrowth)[96,97]. These recurrent and delicate interactions render the wild type genetic background unfavourable for behavioural genetics assays.

3.2.3 Processes upstream and downstream to sleep regulatory Rho GTPases.

What are the signals that feed into and flow from this network of GTPases? One potential upstream signal may come from the dopaminergic innervation of dFB neurons[24]. Dopamine in these cells acts through the Dop1R2 receptor, a G protein-coupled receptor (GPCR) whose activation leads to neuronal inhibition by increasing and decreasing leak and A-type potassium currents, respectively[24]. Additionally, G proteins are also linked to the activation of GEFs and GAPs for Rho GTPases[139-141]. Dop1R2 signals through

$G_{i/o}$[24,142], which targets Rho1[143-147] and Rac1[148-150] in a tissue specific manner. Were Dop1R2 to inhibit dFB neuron activity via Rho GTPases, it would need to empower Rho1 activity. Direct activation of Rho1 or its GEF may fulfill this goal. Alternatively, Rho1 can be indirectly activated by lowering Rac1's suppressing influence on Rho1. Thus, Rho GTPases can flexibly connect upstream inputs to downstream targets.

Based on Cv-c's role in regulating dFB neuron excitability, ion channels must lie downstream of the Rho GTPases. The electrical activity of dFB neurons is reciprocally regulated through fast and slow potassium currents[24], and the ion channels underlying these currents (i.e. Sh and sand, respectively) may be (indirectly) regulated by GTPases. One possible mediator is phosphatidylinositol 4,5-biphosphate (PIP_2), a phospholipid created through the activity of phosphatidylinositol 4-phosphate 5-kinase (PIP5K)[151-153]. Rho GTPases and their immediate downstream substrates (e.g. ROCK, a downstream kinase activated by Rho1) can augment PIP5K activity to increase PIP2 production[154-156]. This inhibits fast A-type currents through voltage-gated K^+ channels such as Sh[154]. Since ROCK is known to increase PIP5K activity[156], this can feasibly reduce membrane excitability by curtailing A-type currents.

Another mode of regulating ion channels is by changing their density at the cell surface. Leak K^+ currents are frequently regulated by shuttling the two-pore K^+ ion channels to and from the membrane[157]. Specifically, sand in the dFB neurons is regulated through selective exocytosis upon dopaminergic stimulation[24]. Since Rho GTPases such as Rac1 are known to influence ion channel trafficking to and from the membrane[158-160], one can speculate their regulation of electrical excitability in the dFB neuronal membrane by shuttling sand. This may further be aided by PIP2[153,157]. Numerous precedents and potential mechanisms thus exist for Rho GTPase regulation of K^+ currents.

3.2.4 Future directions.

There are at least three avenues of research that ought to be pursued to further validate and understand the present model of sleep regulation via Rho GTPases.

First, Rac1 and Rho1 activity in the dFB neurons must be further verified. Due to genetic constraints, I was only able to test the expression of $Rac1^{L89}$ and $Rho1^{RNAi}$ in the *cv-c* mutant background. The picture that my results paint must be further elaborated by testing other Rac1 and Rho1 mutations. Specifically, constitutively active Rac1 ($Rac1^{V12}$) and dominant negative Rho1 ($Rho1^{N19}$) must be examined. If Rac1 were sleep promoting, the *cv-c* mutation, which I predict to constitutively activate Rho1, should be counteracted by a constitutively active Rac1, and this should restore sleep. These experiments are technically challenging, for all the required genes and alleles lie on the same chromosome, and thus, sequential recombination must be completed to generate the required genotype. This is not only time consuming, but the success rate is very low. Nonetheless, these experiments ought to be pursued in the future to properly validate the current model.

Second, it is imperative to explore the electrophysiological changes that result from genetic manipulations of the Rho GTPases. For instance, it is essential to test whether knocking down Rho1 in the *cv-c* mutants rescues the excitability of dFB neurons as one would predict. Moreover, based on our current model of the electrical switch in the dFB neurons, it is reasonable to hypothesize that the *cv-c* mutant phenotype may originate from the failure to withdraw sand from the membrane[24,25]. This can be evaluated through voltage clamp studies where the detection of an enhanced leak K^+ current would support this hypothesis. Voltage clamp analyses will also clarify the K^+ current (i.e. A-type or leak) affected by the manipulations of individual Rho GTPases. Thus, these experiments will clarify the connection between Rho GTPases and changes in the membrane biophysics.

Third, for a comprehensive model, it will be necessary to identify all the GEFs and GAPs that regulate Rac1 and Rho1. Currently, Cv-c is the only GAP known to regulate sleep; we do not know what GEF acts upon Rho1, and we know neither the GEF nor the GAP acting on Rac1. Characterizing these modifying enzymes will be instrumental to create a complete picture of the sleep regulatory Rho GTPase machinery in the dFB neurons. Additionally, the identification of downstream targets of Rac1 and Rho1 will connect their activities to electrical changes at the plasma membrane. Acquiring this information will require extensive behavioural genetic screens and the follow-up testing of select candidate genes in the *cv-c* mutant background.

3.3 Sleep regulation via neuronal redox states.

3.3.1 A model for sleep regulation via redox modulation in the dFB neurons.

Redox sensing by Hyperkinetic (Hk), a beta subunit of the Sh K^+ channel complex, regulates sleep. I hypothesized that Hk's redox sensing capability is necessary for sleep regulation in the dFB neurons. My results support this prediction, and they also indicate that the production of reactive oxygen species (ROS) promotes sleep by acting through Hk.

Accordingly, these results suggest a model of sleep regulation based on the metabolic (redox) state of dFB neurons. When flies are awake, dFB neurons are electrically silent and the demand for energy in the form of ATP accordingly low. Mitochondrial nicotinamide adenine dinucleotide (NADH) levels are expected to be high under these conditions and ATP production and respiration low—conditions that favour the production of ROS by the electron transport chain, especially complex I[161]. The subsequent oxidation of the Hk-bound nicotinamide adenine dinucleotide, in all likelihood NADPH[108,162], increases A-type currents in dFB neurons and facilitates sustained electrical activity, thereby triggering sleep. The model thus positions the mitochondrion at an intriguing intersection between cellular metabolism and sleep.

3.3.2 Sources of mitochondrial ROS production.

The mitochondria is the main source of intracellular ROS[57]. Where in the mitochondria does such ROS originate? To answer this, we must first understand the electron transport chain (ETC). One of the textbook functions of the mitochondria is cellular respiration: the conversion of chemical energy in nutrients to readily usable packets of energy in the form of adenosine triphosphate (ATP). Cellular energy metabolism can be broken down into three groups of processes: glycolysis, the Krebs cycle (also known as the citric acid

cycle), and oxidative phosphorylation[163]. Glucose is broken down into pyruvate during glycolysis. Pyruvate enters the mitochondrial Krebs cycle where its oxidation to CO_2 is used to reduce (i.e. transfer electrons to) nicotinamide adenine dinucleotide (NAD) and flavin adenine dinucleotide (FAD), which are converted into NADH and $FADH_2$, respectively. These nucleotide-based compounds are reducing agents that deliver electrons to the ETC for oxidative phosphorylation.

The ETC is comprised of four large protein complexes (I – IV) located in the inner mitochondrial membrane. Complex I begins the process by oxidizing (i.e. removing electrons from) NADH and shuttling electrons through complexes III and IV. Complex II does the same for $FADH_2$ and transfers the extracted electrons through complexes III and IV. Electron transfer through complexes I, III, and IV is coupled to the pumping of protons (H^+) into the intermembrane space, creating an electrochemical gradient across the inner mitochondrial membrane termed the proton motive force ($\Delta\psi$). $\Delta\psi$ drives ATP production through ATP synthase, an H^+-driven turbine that couples the flow of H^+ down its gradient to the phosphorylation of ADP. Thus, oxidative phosphorylation is a multi-step process that connects the transport of electrons from NADH and $FADH_2$ with the generation of the $\Delta\psi$ and ultimately ATP synthesis.

It is these electrons shuttling through the ETC that potentially give rise to ROS. When a cell actively respires, $\Delta\psi$ is small and electron flow through the ETC is unperturbed. Nonetheless, there are small amounts of electrons that leak, and these are transferred to O_2 to create superoxide ions (O_2^-), a ROS[161]. This occurs at complexes I and III, which release O_2^- into the matrix and intermembrane space, respectively[161]. Mitochondria have diverse defense mechanisms against ROS, one of which involves superoxide dismutase (Sod1 [or copper-zinc Sod] in the intermembrane space and Sod2

[or manganese Sod] in the matrix)[57]. These enzymes convert O_2^- into H_2O_2, which is released by the mitochondria into the cytoplasm[57].

Oxidative challenges arise when the cell does not actively respire. This leads to ROS production along two routes. If there is little oxidative phosphorylation, NADH accumulates in the matrix, and a backlog of unused electrons at complex I leads to ROS production[161]. Reduced ATP synthesis leads to a failure to dissipate the $\Delta\psi$. This elevated $\Delta\psi$ alters the course of electron flow[161]. Coenzyme Q (CoQ), which normally collects electrons from complex I en route to complex III, reverses its course and instead returns the electrons to complex I through a process aptly called reverse electron transport (RET)[161]. During RET, complex I catalyzes the O_2's oxidation of $CoQH_2$ (reduced CoQ), creating O_2^-. This is the single greatest source of ROS production in the mitochondria[161].

In summary, mitochondrial ROS production and cell respiration are inversely related. This fits the model I propose for sleep regulation via ROS, as dFB neurons are electrically active during sleep and quiescent during waking. Action potentials are some of the most energetically expensive cellular processes[46-48]. Such a high expenditure stems from the recruitment of energy-heavy devices such as the Na^+-K^+ pump, which is necessary for Na^+ extrusion[46]. Hence, spiking neurons exhibit a higher energy demand than those that are silent[46]. In the dFB neurons, ROS would be expected to accumulate when the flies are awake, which is when dFB neurons are electrically and metabolically inactive. Increased ROS would then trigger sleep, during which ATP production is accelerated and ROS production curtailed.

3.3.3 Oxidative regulation of membrane biophysics.

How does H_2O_2, the product of mitochondrial oxidation released into the cytoplasm, affect the membrane excitability of dFB neurons? Specifically, how does Hk respond to

increased cellular oxidation? Structurally Hk is an aldo-keto reductase (AKR)[84,110,164]. The most conserved feature of an AKR is its NADPH (nicotinamide adenine dinucleotide phosphate) binding pocket, and its ability to use NADPH in the reduction of aldehydes and ketones[108,164]. While bound to NADPH, the AKR further binds to this carbonyl compound, which it reduces through a hydride transfer from NADPH[108]. The resulting alcohol is released from the active site along with $NADP^{+}$[108]. Thus, NADPH oxidation confers the AKR with two chemically functional states. This makes AKRs useful binary switches that regulate cellular function based on redox levels.

Hk is a fully functional AKR, and it uses this catalytic ability to couple its redox monitoring function to its modulation of fast A-type K^+ conductance through the Sh K^+ channel complex[164]. Sh-based A-type currents are essential for shortening the relative refractory period of an action potential. The depolarized membrane potential acts as an inertial force that resists sequential spiking, and fast K^+ currents restore the resting membrane potential. Thus, enhanced A-type currents facilitate high frequency spiking activity. Hk provides an inactivation gate for Sh[108,110,164]. Hk attaches to the N terminus of the Sh alpha subunit and accelerates a mode of fast inactivation[107,164]. In its NADPH-bound state, Hk's N-type inactivation quickly curtails A-type K^+ currents[84,108,110]. Fast inactivation is disabled when the NADPH is oxidized and the resulting $NADP^+$ released[108,165]. This amplifies and potentiates A-type currents. For spiking neurons, this will optimize the relative refractory period and subsequently support high frequency firing rates.

High electrical activity in dFB neurons trigger sleep in flies, and this involves increases in A-type K^+ currents. Accordingly, higher cellular oxidation can potentiate electrical output by disinhibiting Hk's built-in inactivation mechanism.

Then, how do mitochondrial ROS affect Hk? ROS generated in the mitochondria

enter the cytoplasm as H_2O_2. It is currently unknown how H_2O_2 interacts with Hk *in vivo*. However, Hk's catalytic activity as an AKR suggests some speculative mechanisms. For a substrate to be reduced by Hk, it must possess a carbonyl group. One common reaction involving cytosolic H_2O_2 is lipid peroxidation, and the resulting product is frequently an aldehyde, such as 4-oxo-2-nonenal[166,167]. Prolonged exposures of linoleic acid, a common membrane fatty acid, to high cytoplasmic H_2O_2 drive its peroxidation to 4-oxo-2-nonenal, whose redox potential is sufficient to oxidize the NADPH bound to Hk[108,165]. Similarly, oxidized 1-palmitoyl-2-arachidonoyl-3-phosphotidyl choline (PAPC), another product of lipid peroxidation, leads to the oxidation of the NADPH bound to Hk[168] by producing 1-palmitoyl-2-oxovaleroyl-3-phosphatidylcholine (POVPC), which has one of the highest specific binding affinities for Hk[165].

3.3.4 Future directions.

To consolidate the present model, five further experimental avenues need to be pursued.

First, it will be important to establish cellular respiration, or the lack of it, as the sleep-relevant source of ROS. This could be accomplished by measuring changes in sleep after forcing RET in the mitochondria. There are two requirements for RET to occur: the $\Delta\psi$ must be high, and electrons must flow towards complex I[161]. The former can be accomplished by suppressing the expression of uncoupling proteins in the inner mitochondrial membrane. Under normal conditions, uncoupling proteins dissipate the $\Delta\psi$ by providing a pore for H^+ to flow into the matrix[169]. Thus, removing them from the inner mitochondrial membrane should lead to a greater $\Delta\psi$, which will promote ROS production by RET. Additionally, reverse electron flow can be forced by hindering the regular flow of electrons to complex III[161]. This can be achieved by knocking down specific components of the ETC. For instance, CoQ normally transports electrons from complex I to complex III[163]. Complex I binds to CoQ in its fully oxidized form

(ubiquinone), which collects electrons derived from NADH and shuttles them to complex III[161]. Mutating the ubiquinone binding pocket in complex I should disconnect complex I from the default electron flow in the ETC while leaving its enzymatic functions intact. This would drive RET and increase ROS production. Genetically manipulating the composition of the ETC will be critical to substantiate the connection between cell respiration and ROS production in the dFB mitochondria.

Second, it is important to demonstrate that oxidation changes the electrical activity of the dFB neurons. This can be tested by recording from these neurons while in the presence of wild type and mutant Sod1. For any differences in electrical activity, it will also be informative to dissect the ionic currents contributing to this difference. This can be achieved through a voltage clamp experiment (similar to that conducted by Pimentel et al.[24]) to identify changes in individual ionic currents, particularly those related to K^+. The behavioural data pinpointing Hk as the locus of ROS regulation will be further strengthened if electrophysiological analyses also demonstrate elevations in the A-type current following oxidation.

Third, it will be intriguing to test whether the dFB neurons are the sole connection between cellular metabolism and sleep. In the previous chapter, I illustrated that the dFB neurons were the only cells that changed the flies' sleep as a function of constitutive increases or decreases in cellular oxidation. The failure to see similar, let alone any, change in four other clusters of neurons suggests that perhaps the dFB neurons are unique in their ability to sense and respond to subtle changes in redox state. This can be properly examined by using an intersectional genetic strategy to manipulate ROS levels in every neuron in the fly brain except the dFB. This will involve the use of the LexA/LexAop system in addition to the GAL4/UAS system. *R23E10-LexA* will drive the expression of the GAL4 suppressor, GAL80, in dFB neurons. Simultaneously in the same fly, *elav-*

GAL4 will drive the panneuronal expression of $hSod1^{WT}$ or $hSod1^{A4V}$. If the dFB neurons are uniquely redox sensitive, changing redox levels in every other neuron except in the dFB should not alter sleep. Unique redox sensitivity in the dFB neurons, if validated, will have important implications regarding their homeostatic regulation of sleep.

Finally, such a result needs to be followed up through an in-depth characterization of the underlying molecular machinery. This is perhaps best accomplished through deep sequencing techniques such as RNAseq. Translating ribosome affinity purification (TRAP) allows the extraction of actively translated mRNA from discrete cell populations[170]. This is accomplished by the targeted expression of GFP::RpL10A, a GFP tagged ribosomal construct, which can be immunoprecipitated[170]. By driving the expression of this engineered ribosome in the dFB neurons, it will be possible to purify actively translated mRNA, and this can be used for a transcriptomic analysis of the dFB neurons. By comparing transcriptomic changes in rested flies versus sleep deprived flies, one can identify whether certain mitochondrial or metabolic genes or up- or downregulated as a consequence of sleep deprivation. This will be a step towards a more comprehensive understanding of the signaling cascade that connects metabolism to sleep.

Chapter 4: Materials and Methods

4.1 Drosophila strains.

All fly stocks were nurtured on standard media of sucrose, yeast, molasses, and agar and kept on a 12-hour light/12-hour dark schedule. Most fly stocks were obtained from in-house stock collections at the CNCB, the Bloomington *Drosophila* Stock Center (BDSC), or the Vienna *Drosophila* Resource Center (VDRC). The *cv-c* rescue constructs were generated as described below, and the *Hk* rescue constructs were gifts from Todd C. Holmes (University of California, Irvine).

Table 4.1 Mutant stocks

Fly stock	Source
cv-c^{MB03717}	BDSC #24085
cv-c^{C524}	CNCB stock collection
Hk^{1}	BDSC #3562

Table 4.2 GAL4 driver stocks

Fly stock	Source
R23E10-GAL4	BDSC #49032
GAL80^{TS}*:R23E10-GAL4*	CNCB stock collection
pdf-GAL4	CNCB stock collection
cry-GAL4	CNCB stock collection
OK107-GAL4	CNCB stock collection
GH146-GAL4	CNCB stock collection

Table 4.3 UAS responder stocks: overexpression constructs

Fly stock	Source
UAS-cv-c^{WT}	Constructed *de novo* in-house
UAS-cv-c^{R601Q}	Constructed *de novo* in-house
UAS-cv-c$^{WT-CTHA}$	Constructed *de novo* in-house
UAS-cv-c$^{R601Q-CTHA}$	Constructed *de novo* in-house
UAS-Cdc42^{V12}	BDSC #4854
UAS-Rac1^{L89}	BDSC #5129
UAS-Cdc42^{F89}	BDSC #6286
UAS-Cdc42^{V12}	BDSC #6287
UAS-Cdc42^{N17}	BDSC #6288
UAS-Rac1^{L89}	BDSC #6290
UAS-Rac1^{V12}	BDSC #6291
UAS-Rac1^{N17}	BDSC #6292
UAS-Rac1^{WT}	BDSC #6293
UAS-Cdc42^{WT}	BDSC #28873
UAS-Rac1^{WT}	BDSC #28874
UAS-Rho1^{N19}	BDSC #7328
UAS-Rho1$^{V14, E40L}$	BDSC #7332
UAS-Rho1^{V14}	BDSC #7330
UAS-Rho1^{WT-sph}	BDSC #7334
UAS-Rac2^{WT}	BDSC #26650
UAS-FLAG-Rho1^{D100N}	BDSC #9391
UAS-Hk^{WT}	Gift from Todd C. Holmes
UAS-Hk^{K289M}	Gift from Todd C. Holmes
UAS-MitoTimer	BDSC #57323
UAS-dSod1^{WT}	BDSC #33605
UAS-hSod1^{WT}	BDSC #33606
UAS-hSod1^{A4V}	BDSC #33607

Table 4.4 UAS responder stocks: RNAi constructs

Fly stock	Source
UAS-cv-c^{RNAi}	CNCB stock collection
UAS-Rac2^{RNAi}	VDRC #28923GD
UAS-Rac2^{RNAi}	VDRC #50349GD
UAS-Rac1^{RNAi}	VDRC #49246GD
UAS-Rac1^{RNAi}	VDRC #49247GD
UAS-Cdc42^{RNAi}	VDRC #100794KK
UAS-Rho1^{RNAi}	VDRC #109420KK
UAS-Rho1^{RNAi}	VDRC #12734GD
UAS-RhoBtB^{RNAi}	VDRC #100815KK
UAS-RhoL^{RNAi}	VDRC #102461KK
UAS-RhoU^{RNAi}	VDRC #103533KK
UAS-RhoU^{RNAi}	VDRC #108227KK
UAS-Mtl^{RNAi}	VDRC #102528KK
UAS-Mtl^{RNAi}	VDRC #108427KK
UAS-Sh^{RNAi}	VDRC #104474KK
UAS-Hk^{RNAi}	VDRC #101402KK
UAS-qvr^{RNAi}	VDRC #104533KK
UAS-Shab^{RNAi}	VDRC #102218KK
UAS-Shal^{RNAi}	VDRC #103363KK
UAS-Shaw^{RNAi}	VDRC #110589KK
UAS-slo^{RNAi}	VDRC #104421KK
UAS-SK^{RNAi}	VDRC #103985KK
UAS-Ih^{RNAi}	VDRC #110274KK
UAS-sei^{RNAi}	VDRC #104698KK
UAS-CngB^{RNAi}	VDRC #100882KK
UAS-Cngl^{RNAi}	VDRC #102411KK
UAS-Irk1^{RNAi}	VDRC #107389KK
UAS-Irk2^{RNAi}	VDRC #108140KK

4.2 Molecular biology.

The rescue constructs, *UAS-cv-c*^{WT}, *UAS-cv-c*^{R601Q}, *UAS-cv-c*$^{WT\text{-}CTHA}$, and *UAS-cv-c*$^{R601Q\text{-}CTHA}$ were created from a full cDNA sequence for *cv-c* (RE02250; *Drosophila* Genomics Resource Center). The R601Q mutation was generated using the Q5® site-directed mutagenesis kit (New England BioLabs®, Inc.). Wild type and mutant constructs were PCR amplified to introduce NotI and Acc65I sites at their 5' and 3' termini, respectively. Sequences encoding triple-HA epitope tags were also added to the 3' end using this technique. The excised fragments were inserted into the destination vector, pJFRC-MUH[75]. Using the *mini-white* allele in the vector as a marker, the final constructs were injected into p{CaryP}attp40 larvae for introduction into the attp40 landing site on the second chromosome through ΦC31 integration (BestGene, Inc.)[171].

4.3 Confocal microscopy.

Brains were dissected in PBS (1.86 mM NaH_2PO_4, 8.41 mM Na_2HPO_4, 175 mM NaCl) and fixed for 30 – 45 min in 4 % paraformaldehyde in PBS at 4 ˚C. Dissected brains were immunostained in sequential incubations with primary antibodies for 48 hours (1:1000 rat anti-HA high affinity, Roche) and subsequently incubated in secondary antibodies for 24 hours (1:1000 goat anti-rat, conjugated to Alexa Fluor® 633, Life Technologies). The brains were permeabilized through the addition of 0.1% Triton X-100 in the incubating solution. All specimens were washed three times for 10 min each with PBS following each stage and were consequently mounted in Vectashield (Vector Labs) and imaged using a Leica TCS SP5 confocal microscope.

4.4 Behavioural analyses.

4.4.1 Sleep measurements using *Drosophila* Activity Monitors.

Female flies (n = 16 – 32 per group, age: 4 – 7 days) were individually placed into narrow, 6 mm long glass tubes. Female flies have lower (and thus, less saturated) daytime sleep than male flies[172], which facilitates the discernment of differences in sleep that can stem from differing experimental conditions. This is especially useful for detecting increases in sleep. The glass tubes were inserted into Trikinetics *Drosophila* Activity Monitors (DAM), in which an infrared beam transects the tubes to measure activity based on beam breaks. These monitors were placed in incubators (Panasonic MIR-254-PE) with a 12-hour light/12-hour dark schedule. As is customary in the field, sleep was operationally defined as a state where the interval between beam breaks was 5 minutes or longer[173]. This threshold is based on the observation that flies that have been behaviourally quiescent for 5 minutes or longer showed dramatically decreased behavioural responses to stimuli (both simple and complex)[19,172,173]. Flies were assumed dead in the absence of a beam break for over 1400 minutes and excluded from the analysis.

4.4.2 Sleep deprivation using SNAP.

Female flies (age: 4 – 7 days) were loaded into Trikinetics DAMs, and then set into the sleep nullifying apparatus (SNAP)[118]. This mechanical system holds up to 6 activity monitors and tilts them asymmetrically from -60° to +60° at which point they are restored to their original position through the action of a torsion spring[118]. Accordingly, this restorative force displaces the flies (in tubes placed in the monitors) during the recoiling, downward motion. This mechanical disturbance was repeated at a frequency of 10 times per minute. Flies used for MitoTimer measurements were sleep deprived for 24 hours.

4.4.3 Arousal threshold measurements.

Female flies (n = 16 – 32 per group, age: 4 – 7 days) were loaded into Trikinetics DAMs that were attached to shaftless vibrating motors (310-113; Precision Motors), and arousal thresholds were measured by applying mechanical stimulation through these motors[25,128]. The vibrating motion serves as arousing tactile and proprioceptive stimulation[128]. The efficacy of arousal increases as a function of the intensity of the stimulus[128]. The stimulation intensity was controlled by changing the voltage, and flies were exposed to stimuli ranging from 0 to 1.2 g. Each stimulation episode was 15 s long, and flies were stimulated at the start of every hour from 9AM to 4PM; during this period the arousal threshold was highest during the day[128]. Arousal thresholds were quantified as the percentage of sleeping flies (behaviourally quiescent in the preceding 5 min) that were awakened (displayed locomotion) following the stimulatory episode. Each stimulation intensity was repeated 6 times, and arousability was recorded only for flies that were sleeping immediately prior to stimulus presentation. Based on previous studies, the efficacy to arouse the fly increases proportionally to the intensity of the stimulus[25,128]. Since other physical restrictions to locomotion should not produce such a graded arousal response[127], this approach was adopted to evaluate whether the increases in sleep that I detected in some of my experiments are genuine.

4.5 Functional imaging of redox state.

Flies expressing MitoTimer were imaged at two time windows during the day: 8AM – 11AM and 4PM – 6PM. Sleep deprived flies were systematically imaged in the evening (sleep deprivation was continued up until the flies were prepared for imaging), and control (non-deprived) flies were imaged during both periods. For each imaging session, flies were fixed by eicosane (Sigma Aldrich®) to a custom-printed imaging chamber. The cuticle and trachea overlying the dorsal fan-shaped body (dFB) or mushroom body (MB) were surgically removed to create a small window, and the exposed brain was superfused with carbogenated solution (95% O_2, 5% CO_2) containing 5 mM TES, 103 mM NaCl, 3 mM KCl, 1.5 mM $CaCl_2$, 4 mM $MgCl_2$, 26 mM $NaHCO_3$, 1 mM NaH_2PO_4, 8 mM trehalose and 10 mM glucose, pH 7.3.

Fly brains were imaged *in vivo* using two-photon microscopy. Fluorescence was excited with 140-fs light pulses centered at 910 nm (Chameleon Ultra II, Coherent). The excitation laser was attenuated via a Pockels cell (Conoptics 302RM) and coupled to a Movable Objective Microscope (Sutter Instruments) equipped with a Zeiss 20×, 1.0 NA W-Plan-Apochromat objective. Emitted photons were dissociated from excitation light by a series of dichromatic mirrors and dielectric and colored glass filters and detected by GaAsP photomultiplier tubes (Hamamatsu Photonics H10770PA- 40 SEL). Photomultiplier currents were amplified (Laser Components HCA-4M-500K-C) and passed through a custom-designed integrator circuit to maximize the signal-to-noise ratio. The microscope was controlled through MPScope 2.0 via a PCI-6110 DAQ board (National Instruments). Green and red fluorescence was simultaneously collected through FF01-525/45 (BrightLine®) and ET605/70 filters (Chroma®), respectively. Images were acquired as z-stacks for each region of interest in each hemisphere. For the dFB, images were collected from the axons, dendrites, and soma. For the MB, images were collected from the calyx, horizontal lobes, and vertical lobes.

Images were analyzed using a Matlab algorithm developed by Laker et al.[116]. The

MitoTimer signals were analyzed ratiometrically; positive pixels were thresholded at a value 1.5× the mean grey value of the background pixels for each channel. Saturated pixels (grey level 255) were filtered from the analysis. The red to green ratio was calculated as a mean ratio value from the remaining positive pixels. All images were analyzed blind to experimental group allocation.

4.6 Statistical analyses.

Data were analyzed in Prism 7 (GraphPad). Group means were compared by one-way (parametric and non-parametric) or two-way analyses of variance (ANOVA). A repeated-measures design was used wherever appropriate. The assumptions of normality or sphericity were evaluated through the Shapiro-Wilk and Brown-Forsythe tests, respectively. The assumption of homogeneity of variance was tested using Bartlett's test. When all assumptions were satisfied, parametric analyses were used, followed by planned pairwise post-hoc analyses using Holm-Šídák's multiple comparisons test. When any one of the above assumptions was violated, non-parametric analyses (Kruskal Wallis test) were used, followed by Dunn's multiple comparisons test.

Bibliography

1. Galen. *De Plenitudine*. **72,** (L. Reichert, 2001).
2. Hulskamp, M. A. A. Sleep and Dreams in Ancient Medical Diagnosis and Prognosis. (2008).
3. Epidemics VI. *The Classical Review* **33,** 187–188 (1983).
4. Galen. *On Sense Perception*. (S. Karger, 1970).
5. Galen. *Galeni De Temperamentis Libri III*. (B. G. Teubner, 1904).
6. Cirelli, C. & Tononi, G. Is sleep essential? *PLoS Biol.* **6,** e216 (2008).
7. Campbell, S. S. & Tobler, I. Animal sleep: a review of sleep duration across phylogeny. *Neurosci Biobehav Rev* **8,** 269–300 (1984).
8. Siegel, J. M. Do all animals sleep? *Trends in Neurosciences* **31,** 208–213 (2008).
9. Borbély, A. A. A two process model of sleep regulation. *Hum Neurobiol* **1,** 195–204 (1982).
10. Rosenwasser, A. M. & Turek, F. W. in *Principles and Practice of Sleep Medicine* 351–361.e6 (Elsevier, 2017). doi:10.1016/B978-0-323-24288-2.00034-9
11. Konopka, R. J. & Benzer, S. Clock mutants of Drosophila melanogaster. *PNAS* **68,** 2112–2116 (1971).
12. Takahashi, J. S., Hong, H.-K., Ko, C. H. & McDearmon, E. L. The genetics of mammalian circadian order and disorder: implications for physiology and disease. *Nat. Rev. Genet.* **9,** 764–775 (2008).
13. Allada, R. & Chung, B. Y. Circadian organization of behavior and physiology in Drosophila. *Annu. Rev. Physiol.* **72,** 605–624 (2010).
14. Yu, W., Zheng, H., Houl, J. H., Dauwalder, B. & Hardin, P. E. PER-dependent rhythms in CLK phosphorylation and E-box binding regulate circadian transcription. *Genes Dev.* **20,** 723–733 (2006).
15. Emery, P., So, W. V., Kaneko, M., Hall, J. C. & Rosbash, M. CRY, a Drosophila clock and light-regulated cryptochrome, is a major contributor to circadian rhythm resetting and photosensitivity. *Cell* **95,** 669–679 (1998).
16. Dubruille, R. & Emery, P. A plastic clock: how circadian rhythms respond to environmental cues in Drosophila. *Mol. Neurobiol.* **38,** 129–145 (2008).
17. Achermann, P. & Borbély, A. A. in *Principles and Practice of Sleep Medicine* 377–387.e6 (Elsevier, 2017). doi:10.1016/B978-0-323-24288-2.00036-2
18. Banks, S., Dorrian, J., Basner, M. & Dinges, D. F. in *Principles and Practice of Sleep Medicine* 49–55.e4 (Elsevier, 2017). doi:10.1016/B978-0-323-24288-2.00005-2
19. Shaw, P. J., Cirelli, C., Greenspan, R. J. & Tononi, G. Correlates of sleep and waking in Drosophila melanogaster. *Science (New York, NY)* **287,** 1834–1837 (2000).
20. Koh, K. *et al.* Identification of SLEEPLESS, a sleep-promoting factor. *Science (New York, NY)* **321,** 372–376 (2008).
21. Bushey, D., Tononi, G. & Cirelli, C. The Drosophila fragile X mental retardation gene regulates sleep need. *J. Neurosci.* **29,** 1948–1961 (2009).
22. Bushey, D., Tononi, G. & Cirelli, C. Sleep and synaptic homeostasis: structural evidence in Drosophila. *Science (New York, NY)* **332,** 1576–1581 (2011).
23. Ishimoto, H. & Kitamoto, T. The steroid molting hormone Ecdysone regulates

sleep in adult Drosophila melanogaster. *Genetics* **185,** 269–281 (2010).
24. Pimentel, D. *et al.* Operation of a homeostatic sleep switch. *Nature* **536,** 333–337 (2016).
25. Donlea, J. M., Pimentel, D. & Miesenböck, G. Neuronal machinery of sleep homeostasis in Drosophila. *Neuron* **81,** 860–872 (2014).
26. Gilestro, G. F., Tononi, G. & Cirelli, C. Widespread changes in synaptic markers as a function of sleep and wakefulness in Drosophila. *Science (New York, NY)* **324,** 109–112 (2009).
27. Yang, G. *et al.* Sleep promotes branch-specific formation of dendritic spines after learning. *Science (New York, NY)* **344,** 1173–1178 (2014).
28. de Vivo, L. *et al.* Ultrastructural evidence for synaptic scaling across the wake/sleep cycle. *Science (New York, NY)* **355,** 507–510 (2017).
29. Xie, L. *et al.* Sleep drives metabolite clearance from the adult brain. *Science (New York, NY)* **342,** 373–377 (2013).
30. Rasch, B. & Born, J. About sleep's role in memory. *Physiol. Rev.* **93,** 681–766 (2013).
31. McGaugh, J. L. Memory--a century of consolidation. *Science (New York, NY)* **287,** 248–251 (2000).
32. Peigneux, P., Fogel, S. & Smith, C. in *Principles and Practice of Sleep Medicine* 229–238.e6 (Elsevier, 2017). doi:10.1016/B978-0-323-24288-2.00022-2
33. Orban, P. *et al.* Sleep after spatial learning promotes covert reorganization of brain activity. *PNAS* **103,** 7124–7129 (2006).
34. Donlea, J. M., Thimgan, M. S., Suzuki, Y., Gottschalk, L. & Shaw, P. J. Inducing sleep by remote control facilitates memory consolidation in Drosophila. *Science (New York, NY)* **332,** 1571–1576 (2011).
35. Wilson, M. A. & McNaughton, B. L. Reactivation of hippocampal ensemble memories during sleep. *Science (New York, NY)* **265,** 676–679 (1994).
36. Wilson, M. A. & McNaughton, B. L. Dynamics of the hippocampal ensemble code for space. *Science (New York, NY)* **261,** 1055–1058 (1993).
37. Shen, J., Kudrimoti, H. S., McNaughton, B. L. & Barnes, C. A. Reactivation of neuronal ensembles in hippocampal dentate gyrus during sleep after spatial experience. *J Sleep Res* **7 Suppl 1,** 6–16 (1998).
38. Tononi, G. & Cirelli, C. Sleep and the price of plasticity: from synaptic and cellular homeostasis to memory consolidation and integration. *Neuron* **81,** 12–34 (2014).
39. Barlow, H. B. The twelfth Bartlett memorial lecture: the role of single neurons in the psychology of perception. *Q J Exp Psychol A* **37,** 121–145 (1985).
40. Hebb, D. O. *The Organization of Behaviour*. (John Wiley & Sons, Inc., 1949).
41. Tononi, G. & Cirelli, C. Sleep and synaptic homeostasis: a hypothesis. *Brain Res. Bull.* **62,** 143–150 (2003).
42. Tononi, G. & Cirelli, C. Sleep function and synaptic homeostasis. *Sleep Med Rev* **10,** 49–62 (2006).
43. Frank, M. G. Erasing synapses in sleep: is it time to be SHY? *Neural Plast.* **2012,** 264378–15 (2012).
44. Donlea, J. M., Ramanan, N. & Shaw, P. J. Use-dependent plasticity in clock neurons regulates sleep need in Drosophila. *Science (New York, NY)* **324,** 105–108 (2009).
45. Liu, S., Liu, Q., Tabuchi, M. & Wu, M. N. Sleep Drive Is Encoded by Neural Plastic Changes in a Dedicated Circuit. *Cell* **165,** 1347–1360 (2016).

46. Attwell, D. & Laughlin, S. B. An energy budget for signaling in the grey matter of the brain. *J. Cereb. Blood Flow Metab.* **21,** 1133–1145 (2001).
47. Alle, H., Roth, A. & Geiger, J. R. P. Energy-efficient action potentials in hippocampal mossy fibers. *Science (New York, NY)* **325,** 1405–1408 (2009).
48. Harris, J. J., Jolivet, R. & Attwell, D. Synaptic energy use and supply. *Neuron* **75,** 762–777 (2012).
49. Bear, M. F., Connors, B. W. & Paradiso, M. A. *Neuroscience*. (Lippincott Williams & Wilkins, 2007).
50. Safiulina, D. & Kaasik, A. Energetic and dynamic: how mitochondria meet neuronal energy demands. *PLoS Biol.* **11,** e1001755 (2013).
51. Wang, Y., Wang, R. & Xu, X. Neural Energy Supply-Consumption Properties Based on Hodgkin-Huxley Model. *Neural Plast.* **2017,** 6207141–11 (2017).
52. Cirelli, C., Gutierrez, C. M. & Tononi, G. Extensive and divergent effects of sleep and wakefulness on brain gene expression. *Neuron* **41,** 35–43 (2004).
53. Zimmerman, J. E. *et al.* Multiple mechanisms limit the duration of wakefulness in Drosophila brain. *Physiol. Genomics* **27,** 337–350 (2006).
54. Mackiewicz, M. *et al.* Macromolecule biosynthesis: a key function of sleep. *Physiol. Genomics* **31,** 441–457 (2007).
55. Seugnet, L. *et al.* Identifying sleep regulatory genes using a Drosophila model of insomnia. *J. Neurosci.* **29,** 7148–7157 (2009).
56. Mackiewicz, M., Naidoo, N., Zimmerman, J. E. & Pack, A. I. Molecular mechanisms of sleep and wakefulness. *Ann. N. Y. Acad. Sci.* **1129,** 335–349 (2008).
57. Halliwell, B. & Gutteridge, J. M. *Free radicals in biology and medicine*. (Oxford University Press, Inc., 2007).
58. Shaw, P. J., Tononi, G., Greenspan, R. J. & Robinson, D. F. Stress response genes protect against lethal effects of sleep deprivation in Drosophila. *Nature* **417,** 287–291 (2002).
59. Terao, A. *et al.* Differential increase in the expression of heat shock protein family members during sleep deprivation and during sleep. *Neuroscience* **116,** 187–200 (2003).
60. Kaufman, R. J. Orchestrating the unfolded protein response in health and disease. *J. Clin. Invest.* **110,** 1389–1398 (2002).
61. Handy, D. E. & Loscalzo, J. Redox regulation of mitochondrial function. *Antioxid. Redox Signal.* **16,** 1323–1367 (2012).
62. Kimura, M., Kapás, L. & Krueger, J. M. Oxidized glutathione promotes sleep in rabbits. *Brain Res. Bull.* **45,** 545–548 (1998).
63. Ikeda, M. *et al.* Brain oxidation is an initial process in sleep induction. *Neuroscience* **130,** 1029–1040 (2005).
64. Williams, M. J. *et al.* Recurrent Sleep Fragmentation Induces Insulin and Neuroprotective Mechanisms in Middle-Aged Flies. *Front Aging Neurosci* **8,** 180 (2016).
65. Villafuerte, G. *et al.* Sleep deprivation and oxidative stress in animal models: a systematic review. *Oxid Med Cell Longev* **2015,** 234952–15 (2015).
66. Hendricks, J. C. *et al.* Rest in Drosophila is a sleep-like state. *Neuron* **25,** 129–138 (2000).
67. Cirelli, C. *et al.* Reduced sleep in Drosophila Shaker mutants. *Nature* **434,** 1087–1092 (2005).
68. Seugnet, L., Boero, J., Gottschalk, L., Duntley, S. P. & Shaw, P. J. Identification of a biomarker for sleep drive in flies and humans. *PNAS* **103,**

19913–19918 (2006).
69. Seugnet, L., Suzuki, Y., Donlea, J. M., Gottschalk, L. & Shaw, P. J. Sleep deprivation during early-adult development results in long-lasting learning deficits in adult Drosophila. *Sleep* **34,** 137–146 (2011).
70. Bellen, H. J., Tong, C. & Tsuda, H. 100 years of Drosophila research and its impact on vertebrate neuroscience: a history lesson for the future. *Nat. Rev. Neurosci.* **11,** 514–522 (2010).
71. Sehgal, A., Price, J. L., Man, B. & Young, M. W. Loss of circadian behavioral rhythms and per RNA oscillations in the Drosophila mutant timeless. *Science (New York, NY)* **263,** 1603–1606 (1994).
72. Bushey, D., Huber, R., Tononi, G. & Cirelli, C. Drosophila Hyperkinetic mutants have reduced sleep and impaired memory. *J. Neurosci.* **27,** 5384–5393 (2007).
73. Brand, A. H. & Perrimon, N. Targeted gene expression as a means of altering cell fates and generating dominant phenotypes. *Development (Cambridge, England)* **118,** 401–415 (1993).
74. Sepp, K. J. & Auld, V. J. Conversion of lacZ enhancer trap lines to GAL4 lines using targeted transposition in Drosophila melanogaster. *Genetics* **151,** 1093–1101 (1999).
75. Pfeiffer, B. D. *et al.* Tools for neuroanatomy and neurogenetics in Drosophila. *Proc. Natl. Acad. Sci. U.S.A.* **105,** 9715–9720 (2008).
76. Pfeiffer, B. D. *et al.* Refinement of tools for targeted gene expression in Drosophila. *Genetics* **186,** 735–755 (2010).
77. Jenett, A. *et al.* A GAL4-driver line resource for Drosophila neurobiology. *Cell Rep* **2,** 991–1001 (2012).
78. Adams, M. D. *et al.* The genome sequence of Drosophila melanogaster. *Science (New York, NY)* **287,** 2185–2195 (2000).
79. Venken, K. J. T., Simpson, J. H. & Bellen, H. J. Genetic manipulation of genes and cells in the nervous system of the fruit fly. *Neuron* **72,** 202–230 (2011).
80. Hanesch, U., Fischbach, K. F. & Heisenberg, M. Neuronal architecture of the central complex in Drosophila melanogaster. *Cell Tissue Res.* **257,** 343–366 (1989).
81. Young, J. M. & Armstrong, J. D. Structure of the adult central complex in Drosophila: organization of distinct neuronal subsets. *J. Comp. Neurol.* **518,** 1500–1524 (2010).
82. Young, J. M. & Armstrong, J. D. Building the central complex in Drosophila: the generation and development of distinct neural subsets. *J. Comp. Neurol.* **518,** 1525–1541 (2010).
83. Lima, S. Q. & Miesenböck, G. Remote control of behavior through genetically targeted photostimulation of neurons. *Cell* **121,** 141–152 (2005).
84. Chouinard, S. W., Wilson, G. F., Schlimgen, A. K. & Ganetzky, B. A potassium channel beta subunit related to the aldo-keto reductase superfamily is encoded by the Drosophila hyperkinetic locus. *PNAS* **92,** 6763–6767 (1995).
85. Denholm, B. *et al.* crossveinless-c is a RhoGAP required for actin reorganisation during morphogenesis. *Development (Cambridge, England)* **132,** 2389–2400 (2005).
86. Barras, D. & Widmann, C. GAP-independent functions of DLC1 in metastasis. *Cancer Metastasis Rev.* **33,** 87–100 (2014).
87. Nakano-Kobayashi, A., Tai, Y., Nadif Kasri, N. & Van Aelst, L. The X-linked mental retardation protein OPHN1 interacts with Homer1b/c to control spine

endocytic zone positioning and expression of synaptic potentiation. *J. Neurosci.* **34,** 8665–8671 (2014).
88. de Madrid, B. H., Greenberg, L. & Hatini, V. RhoGAP68F controls transport of adhesion proteins in Rab4 endosomes to modulate epithelial morphogenesis of Drosophila leg discs. *Dev. Biol.* **399,** 283–295 (2015).
89. Sato, D., Sugimura, K., Satoh, D. & Uemura, T. Crossveinless-c, the Drosophila homolog of tumor suppressor DLC1, regulates directional elongation of dendritic branches via down-regulating Rho1 activity. *Genes Cells* **15,** 485–500 (2010).
90. Bernards, A. GAPs galore! A survey of putative Ras superfamily GTPase activating proteins in man and Drosophila. *Biochim. Biophys. Acta* **1603,** 47–82 (2003).
91. Luo, L., Liao, Y. J., Jan, L. Y. & Jan, Y. N. Distinct morphogenetic functions of similar small GTPases: Drosophila Drac1 is involved in axonal outgrowth and myoblast fusion. *Genes Dev.* **8,** 1787–1802 (1994).
92. Ng, J. *et al.* Rac GTPases control axon growth, guidance and branching. *Nature* **416,** 442–447 (2002).
93. Ng, J. & Luo, L. Rho GTPases regulate axon growth through convergent and divergent signaling pathways. *Neuron* **44,** 779–793 (2004).
94. Bellen, H. J. *et al.* The BDGP gene disruption project: single transposon insertions associated with 40% of Drosophila genes. *Genetics* **167,** 761–781 (2004).
95. Luo, L. Rho GTPases in neuronal morphogenesis. *Nat. Rev. Neurosci.* **1,** 173–180 (2000).
96. Sander, E. E., Klooster, ten, J. P., van Delft, S., van der Kammen, R. A. & Collard, J. G. Rac downregulates Rho activity: reciprocal balance between both GTPases determines cellular morphology and migratory behavior. *J. Cell Biol.* **147,** 1009–1022 (1999).
97. Iden, S. & Collard, J. G. Crosstalk between small GTPases and polarity proteins in cell polarization. *Nat. Rev. Mol. Cell Biol.* **9,** 846–859 (2008).
98. Guilluy, C., Garcia-Mata, R. & Burridge, K. Rho protein crosstalk: another social network? *Trends Cell Biol.* **21,** 718–726 (2011).
99. Wu, M., Robinson, J. E. & Joiner, W. J. SLEEPLESS is a bifunctional regulator of excitability and cholinergic synaptic transmission. *Curr. Biol.* **24,** 621–629 (2014).
100. MacKinnon, R. & Yellen, G. Mutations affecting TEA blockade and ion permeation in voltage-activated K+ channels. *Science (New York, NY)* **250,** 276–279 (1990).
101. Perozo, E., MacKinnon, R., Bezanilla, F. & Stefani, E. Gating currents from a nonconducting mutant reveal open-closed conformations in Shaker K+ channels. *Neuron* **11,** 353–358 (1993).
102. Heginbotham, L., Lu, Z., Abramson, T. & MacKinnon, R. Mutations in the K+ channel signature sequence. *Biophys. J.* **66,** 1061–1067 (1994).
103. Hidalgo, P. & MacKinnon, R. Revealing the architecture of a K+ channel pore through mutant cycles with a peptide inhibitor. *Science (New York, NY)* **268,** 307–310 (1995).
104. Zhou, M., Morais-Cabral, J. H., Mann, S. & MacKinnon, R. Potassium channel receptor site for the inactivation gate and quaternary amine inhibitors. *Nature* **411,** 657–661 (2001).
105. Gulbis, J. M., Zhou, M., Mann, S. & MacKinnon, R. Structure of the

cytoplasmic beta subunit-T1 assembly of voltage-dependent K+ channels. *Science (New York, NY)* **289,** 123–127 (2000).
106. Long, S. B., Campbell, E. B. & Mackinnon, R. Crystal structure of a mammalian voltage-dependent Shaker family K+ channel. *Science (New York, NY)* **309,** 897–903 (2005).
107. Gulbis, J. M., Mann, S. & MacKinnon, R. Structure of a voltage-dependent K+ channel beta subunit. *Cell* **97,** 943–952 (1999).
108. Weng, J., Cao, Y., Moss, N. & Zhou, M. Modulation of voltage-dependent Shaker family potassium channels by an aldo-keto reductase. *J. Biol. Chem.* **281,** 15194–15200 (2006).
109. Scott, V. E. *et al.* Primary structure of a beta subunit of alpha-dendrotoxin-sensitive K+ channels from bovine brain. *PNAS* **91,** 1637–1641 (1994).
110. Pan, Y., Weng, J., Cao, Y., Bhosle, R. C. & Zhou, M. Functional coupling between the Kv1.1 channel and aldoketoreductase Kvbeta1. *J. Biol. Chem.* **283,** 8634–8642 (2008).
111. Ueda, A. & Wu, C.-F. Effects of hyperkinetic, a beta subunit of Shaker voltage-dependent K+ channels, on the oxidation state of presynaptic nerve terminals. *J. Neurogenet.* **22,** 1–13 (2008).
112. Trout, W. E. & Kaplan, W. D. A relation between longevity, metabolic rate, and activity in shaker mutants of Drosophila melanogaster. *Exp. Gerontol.* **5,** 83–92 (1970).
113. Budnik, V., Zhong, Y. & Wu, C.-F. Morphological plasticity of motor axons in Drosophila mutants with altered excitability. *J Neurosci* **10,** 3754–3768 (1990).
114. Schlimgen, A. K. The genetic and molecular characterization of Hk, a gene affecting neuronal excitability in Drosophila melanogaster. (1991).
115. Wang, J. W. & Wu, C.-F. In vivo functional role of the Drosophila hyperkinetic beta subunit in gating and inactivation of Shaker K+ channels. *Biophys. J.* **71,** 3167–3176 (1996).
116. Laker, R. C. *et al.* A novel MitoTimer reporter gene for mitochondrial content, structure, stress, and damage in vivo. *J. Biol. Chem.* **289,** 12005–12015 (2014).
117. Terskikh, A. *et al.* 'Fluorescent timer': protein that changes color with time. *Science (New York, NY)* **290,** 1585–1588 (2000).
118. Seugnet, L., Suzuki, Y., Vine, L., Gottschalk, L. & Shaw, P. J. D1 receptor activation in the mushroom bodies rescues sleep-loss-induced learning impairments in Drosophila. *Curr. Biol.* **18,** 1110–1117 (2008).
119. Heisenberg, M. Mushroom body memoir: from maps to models. *Nat. Rev. Neurosci.* **4,** 266–275 (2003).
120. Pitman, J. L., McGill, J. J., Keegan, K. P. & Allada, R. A dynamic role for the mushroom bodies in promoting sleep in Drosophila. *Nature* **441,** 753–756 (2006).
121. Parkes, T. L. *et al.* Extension of Drosophila lifespan by overexpression of human SOD1 in motorneurons. *Nat. Genet.* **19,** 171–174 (1998).
122. Mockett, R. J., Radyuk, S. N., Benes, J. J., Orr, W. C. & Sohal, R. S. Phenotypic effects of familial amyotrophic lateral sclerosis mutant Sod alleles in transgenic Drosophila. *PNAS* **100,** 301–306 (2003).
123. Martin, I., Jones, M. A. & Grotewiel, M. Manipulation of Sod1 expression ubiquitously, but not in the nervous system or muscle, impacts age-related parameters in Drosophila. *FEBS Lett.* **583,** 2308–2314 (2009).
124. Mockett, R. J., Sohal, B. H. & Sohal, R. S. Expression of multiple copies of mitochondrially targeted catalase or genomic Mn superoxide dismutase

transgenes does not extend the life span of Drosophila melanogaster. *Free Radic. Biol. Med.* **49,** 2028–2031 (2010).
125. Hitchler, M. J. & Domann, F. E. Regulation of CuZnSOD and its redox signaling potential: implications for amyotrophic lateral sclerosis. *Antioxid. Redox Signal.* **20,** 1590–1598 (2014).
126. Yim, H. S., Kang, J. H., Chock, P. B., Stadtman, E. R. & Yim, M. B. A familial amyotrophic lateral sclerosis-associated A4V Cu, Zn-superoxide dismutase mutant has a lower Km for hydrogen peroxide. Correlation between clinical severity and the Km value. *J. Biol. Chem.* **272,** 8861–8863 (1997).
127. Yim, M. B., Yim, H. S., Chock, P. B. & Stadtman, E. R. Enhanced free radical generation of FALS-associated Cu,Zn-SOD mutants. *Neurotox Res* **1,** 91–97 (1999).
128. van Alphen, B., Yap, M. H. W., Kirszenblat, L., Kottler, B. & van Swinderen, B. A dynamic deep sleep stage in Drosophila. *J Neurosci* **33,** 6917–6927 (2013).
129. Benito, J., Houl, J. H., Roman, G. W. & Hardin, P. E. The blue-light photoreceptor CRYPTOCHROME is expressed in a subset of circadian oscillator neurons in the Drosophila CNS. *J. Biol. Rhythms* **23,** 296–307 (2008).
130. Nitabach, M. N. & Taghert, P. H. Organization of the Drosophila circadian control circuit. *Curr. Biol.* **18,** R84–93 (2008).
131. Ueno, T. *et al.* Identification of a dopamine pathway that regulates sleep and arousal in Drosophila. *Nat. Neurosci.* **15,** 1516–1523 (2012).
132. Liu, Q., Liu, S., Kodama, L., Driscoll, M. R. & Wu, M. N. Two dopaminergic neurons signal to the dorsal fan-shaped body to promote wakefulness in Drosophila. *Curr. Biol.* **22,** 2114–2123 (2012).
133. Zipkin, I. D., Kindt, R. M. & Kenyon, C. J. Role of a new Rho family member in cell migration and axon guidance in C. elegans. *Cell* **90,** 883–894 (1997).
134. Kuhn, T. B., Brown, M. D. & Bamburg, J. R. Rac1-dependent actin filament organization in growth cones is necessary for beta1-integrin-mediated advance but not for growth on poly-D-lysine. *J. Neurobiol.* **37,** 524–540 (1998).
135. Ruchhoeft, M. L., Ohnuma, S., McNeill, L., Holt, C. E. & Harris, W. A. The neuronal architecture of Xenopus retinal ganglion cells is sculpted by rho-family GTPases in vivo. *J. Neurosci.* **19,** 8454–8463 (1999).
136. Nimnual, A. S., Taylor, L. J. & Bar-Sagi, D. Redox-dependent downregulation of Rho by Rac. *Nat. Cell Biol.* **5,** 236–241 (2003).
137. Rosenfeldt, H., Castellone, M. D., Randazzo, P. A. & Gutkind, J. S. Rac inhibits thrombin-induced Rho activation: evidence of a Pak-dependent GTPase crosstalk. *J Mol Signal* **1,** 8 (2006).
138. Sanz-Moreno, V. *et al.* Rac activation and inactivation control plasticity of tumor cell movement. *Cell* **135,** 510–523 (2008).
139. Siderovski, D. P. & Willard, F. S. The GAPs, GEFs, and GDIs of heterotrimeric G-protein alpha subunits. *Int. J. Biol. Sci.* **1,** 51–66 (2005).
140. Siehler, S. Regulation of RhoGEF proteins by G12/13-coupled receptors. *Br. J. Pharmacol.* **158,** 41–49 (2009).
141. Yu, F.-X., Mo, J.-S. & Guan, K.-L. Upstream regulators of the Hippo pathway. *Cell Cycle* **11,** 4097–4098 (2012).
142. Reale, V., Hannan, F., Hall, L. M. & Evans, P. D. Agonist-specific coupling of a cloned Drosophila melanogaster D1-like dopamine receptor to multiple second messenger pathways by synthetic agonists. *J Neurosci* **17,** 6545–6553 (1997).

143. Vitale, N., Gensse, M., Chasserot-Golaz, S., Aunis, D. & Bader, M. F. Trimeric G proteins control regulated exocytosis in bovine chromaffin cells: sequential involvement of Go associated with secretory granules and Gi3 bound to the plasma membrane. *Eur. J. Neurosci.* **8,** 1275–1285 (1996).
144. Gasman, S., Chasserot-Golaz, S., Popoff, M. R., Aunis, D. & Bader, M. F. Trimeric G proteins control exocytosis in chromaffin cells. Go regulates the peripheral actin network and catecholamine secretion by a mechanism involving the small GTP-binding protein Rho. *J. Biol. Chem.* **272,** 20564–20571 (1997).
145. Gasman, S., Chasserot-Golaz, S., Hubert, P., Aunis, D. & Bader, M. F. Identification of a potential effector pathway for the trimeric Go protein associated with secretory granules. Go stimulates a granule-bound phosphatidylinositol 4-kinase by activating RhoA in chromaffin cells. *J. Biol. Chem.* **273,** 16913–16920 (1998).
146. Murthy, K. S., Zhou, H., Huang, J. & Pentyala, S. N. Activation of PLC-delta1 by Gi/o-coupled receptor agonists. *Am. J. Physiol., Cell Physiol.* **287,** C1679–87 (2004).
147. Evron, T. *et al.* G Protein and β-arrestin signaling bias at the ghrelin receptor. *J. Biol. Chem.* **289,** 33442–33455 (2014).
148. He, J. C. *et al.* The G alpha(o/i)-coupled cannabinoid receptor-mediated neurite outgrowth involves Rap regulation of Src and Stat3. *J. Biol. Chem.* **280,** 33426–33434 (2005).
149. Nakata, H. & Kozasa, T. Functional characterization of Galphao signaling through G protein-regulated inducer of neurite outgrowth 1. *Mol. Pharmacol.* **67,** 695–702 (2005).
150. Bromberg, K. D., Iyengar, R. & He, J. C. Regulation of neurite outgrowth by G(i/o) signaling pathways. *Front. Biosci.* **13,** 4544–4557 (2008).
151. Roth, M. G. Phosphoinositides in constitutive membrane traffic. *Physiol. Rev.* **84,** 699–730 (2004).
152. Di Paolo, G. & De Camilli, P. Phosphoinositides in cell regulation and membrane dynamics. *Nature* **443,** 651–657 (2006).
153. Logothetis, D. E. *et al.* Phosphoinositide control of membrane protein function: a frontier led by studies on ion channels. *Annu. Rev. Physiol.* **77,** 81–104 (2015).
154. Oliver, D. *et al.* Functional conversion between A-type and delayed rectifier K+ channels by membrane lipids. *Science (New York, NY)* **304,** 265–270 (2004).
155. Weernink, P. A. O. *et al.* Activation of type I phosphatidylinositol 4-phosphate 5-kinase isoforms by the Rho GTPases, RhoA, Rac1, and Cdc42. *J. Biol. Chem.* **279,** 7840–7849 (2004).
156. Stirling, L., Williams, M. R. & Morielli, A. D. Dual roles for RHOA/RHO-kinase in the regulated trafficking of a voltage-sensitive potassium channel. *Mol. Biol. Cell* **20,** 2991–3002 (2009).
157. O'Kelly, I. Endocytosis as a mode to regulate functional expression of two-pore domain potassium (K_2p) channels. *Pflugers Arch.* **467,** 1133–1142 (2015).
158. Jones, S. V. P. Role of the small GTPase Rho in modulation of the inwardly rectifying potassium channel Kir2.1. *Mol. Pharmacol.* **64,** 987–993 (2003).
159. Bezzerides, V. J., Ramsey, I. S., Kotecha, S., Greka, A. & Clapham, D. E. Rapid vesicular translocation and insertion of TRP channels. *Nat. Cell Biol.* **6,** 709–720 (2004).
160. Boyer, S. B., Slesinger, P. A. & Jones, S. V. P. Regulation of Kir2.1 channels

by the Rho-GTPase, Rac1. *J. Cell. Physiol.* **218,** 385–393 (2009).
161. Murphy, M. P. How mitochondria produce reactive oxygen species. *Biochem. J.* **417,** 1–13 (2009).
162. Jez, J. M., Bennett, M. J., Schlegel, B. P., Lewis, M. & Penning, T. M. Comparative anatomy of the aldo-keto reductase superfamily. *Biochem. J.* **326 (Pt 3),** 625–636 (1997).
163. Berg, J. M., Tymoczko, J. L. & Stryer, L. *Biochemistry*. (W H Freeman, 2002).
164. Pan, Y., Weng, J., Levin, E. J. & Zhou, M. Oxidation of NADPH on Kvbeta1 inhibits ball-and-chain type inactivation by restraining the chain. *Proc. Natl. Acad. Sci. U.S.A.* **108,** 5885–5890 (2011).
165. Tipparaju, S. M., Barski, O. A., Srivastava, S. & Bhatnagar, A. Catalytic mechanism and substrate specificity of the beta-subunit of the voltage-gated potassium channel. *Biochemistry* **47,** 8840–8854 (2008).
166. Rindgen, D., Nakajima, M., Wehrli, S., Xu, K. & Blair, I. A. Covalent modifications to 2'-deoxyguanosine by 4-oxo-2-nonenal, a novel product of lipid peroxidation. *Chem. Res. Toxicol.* **12,** 1195–1204 (1999).
167. Lee, S. H. & Blair, I. A. Characterization of 4-oxo-2-nonenal as a novel product of lipid peroxidation. *Chem. Res. Toxicol.* **13,** 698–702 (2000).
168. Xie, Z., Barski, O. A., Cai, J., Bhatnagar, A. & Tipparaju, S. M. Catalytic reduction of carbonyl groups in oxidized PAPC by Kvβ2 (AKR6). *Chem. Biol. Interact.* **191,** 255–260 (2011).
169. Wolkow, C. A. & Iser, W. B. Uncoupling protein homologs may provide a link between mitochondria, metabolism and lifespan. *Ageing Res. Rev.* **5,** 196–208 (2006).
170. Thomas, A. *et al.* A versatile method for cell-specific profiling of translated mRNAs in Drosophila. *PLoS ONE* **7,** e40276 (2012).
171. Groth, A. C., Fish, M., Nusse, R. & Calos, M. P. Construction of transgenic Drosophila by using the site-specific integrase from phage phiC31. *Genetics* **166,** 1775–1782 (2004).
172. Andretic, R. & Shaw, P. J. Essentials of sleep recordings in Drosophila: moving beyond sleep time. *Meth. Enzymol.* **393,** 759–772 (2005).
173. Huber, R. *et al.* Sleep homeostasis in Drosophila melanogaster. *Sleep* **27,** 628–639 (2004).

Appendix

Table A1. Statistical tests for Figure 2.1.2-A

Sleep per hour (*two-way repeated measures ANOVA*):
Between group (*genotype*) → $F_{(2,43)} = 9.309$; $\boldsymbol{p = 0.0004}$; $\eta^2 = 0.043$
Within group (*time*) → $F_{(23,989)} = 64.590$; $\boldsymbol{p < 0.0001}$; $\eta^2 = 0.499$
Interaction (*genotype × time*) → $F_{(46,989)} = 1.895$; $\boldsymbol{p = 0.0004}$; $\eta^2 = 0.029$

Table A2. Statistical tests for Figure 2.1.2-B

Sleep per day (*one-way ANOVA*): $F_{(2,43)} = 3.886$; $\boldsymbol{p = 0.028}$; $\eta^2 = 0.153$	
R23E10-GAL4 > UAS-cv-c^{WT} **vs.** *UAS-cv-c^{WT}/+*	$t_{(43)} = 1.643$; $\boldsymbol{p = 0.108}$; $d = 0.424$
R23E10-GAL4 > UAS-cv-c^{WT} **vs.** *R23E10-GAL4/+*	$t_{(43)} = 2.781$; $\boldsymbol{p = 0.016}$; $d = 0.718$

Table A3. Statistical tests for Figure 2.1.2-C

Sleep per hour (*two-way repeated measures ANOVA*):
Between group (*genotype*) → $F_{(2,41)} = 71.270$; $\boldsymbol{p < 0.0001}$; $\eta^2 = 0.228$
Within group (*time*) → $F_{(23,943)} = 57.940$; $\boldsymbol{p < 0.0001}$; $\eta^2 = 0.382$
Interaction (*genotype × time*) → $F_{(46,943)} = 3.907$; $\boldsymbol{p < 0.0001}$; $\eta^2 = 0.052$

Table A4. Statistical tests for Figure 2.1.2-D

Sleep per day (*one-way ANOVA*): $F_{(2,41)} = 38.040$; $\boldsymbol{p < 0.0001}$; $\eta^2 = 0.650$	
R23E10-GAL4 > UAS-cv-c^{R601Q} **vs.** *UAS-cv-c^{R601Q}/+*	$t_{(41)} = 8.446$; $\boldsymbol{p < 0.0001}$; $d = 2.257$
R23E10-GAL4 > UAS-cv-c^{R601Q} **vs.** *R23E10-GAL4/+*	$t_{(41)} = 6.615$; $\boldsymbol{p < 0.0001}$; $d = 1.768$

Table A5. Statistical tests for Figure 2.1.3-A

Sleep per hour (*two-way repeated measures ANOVA*):
Between group (*genotype*) → $F_{(3,85)} = 37.000$; $\boldsymbol{p < 0.0001}$; $\eta^2 = 0.136$
Within group (*time*) → $F_{(23,1955)} = 129.200$; $\boldsymbol{p < 0.0001}$; $\eta^2 = 0.384$
Interaction (*genotype × time*) → $F_{(69,1955)} = 13.580$; $\boldsymbol{p < 0.0001}$; $\eta^2 = 0.121$

Table A6. Statistical tests for Figure 2.1.3-B

Sleep per day (*Kruskal-Wallis test*): $H = 34.530$; $\boldsymbol{p < 0.0001}$	
UAS-cv-c^{WT}/+: *R23E10-GAL4, cv-c^{MB03717}/cv-c^{C524}* **vs.** *UAS-cv-c^{WT}/+: cv-c^{MB03717}/cv-c^{C524}*	$Z = 3.891$; $\boldsymbol{p = 0.0001}$
UAS-cv-c^{WT}/+: *R23E10-GAL4, cv-c^{MB03717}/cv-c^{C524}* **vs.** *R23E10-GAL4, cv-c^{MB03717}/cv-c^{C524}*	$Z > 3.891$; $\boldsymbol{p < 0.0001}$

Table A7. Statistical tests for Figure 2.1.3-C

Total day activity (*Kruskal-Wallis test*): $H = 29.050$; $\boldsymbol{p < 0.0001}$	
UAS-cv-c^{WT}/+: *R23E10-GAL4, cv-c^{MB03717}/cv-c^{C524}* **vs.** *UAS-cv-c^{WT}/+: cv-c^{MB03717}/cv-c^{C524}*	$Z = 3.432$; $\boldsymbol{p = 0.0006}$
UAS-cv-c^{WT}/+: *R23E10-GAL4, cv-c^{MB03717}/cv-c^{C524}* **vs.** *R23E10-GAL4, cv-c^{MB03717}/cv-c^{C524}*	$Z > 3.891$; $\boldsymbol{p < 0.0001}$
Total night activity (*Kruskal-Wallis test*): $H = 14.32$; $\boldsymbol{p = 0.0008}$	
UAS-cv-c^{WT}/+: *R23E10-GAL4, cv-c^{MB03717}/cv-c^{C524}* **vs.** *UAS-cv-c^{WT}/+: cv-c^{MB03717}/cv-c^{C524}*	$Z = 1.774$; $\boldsymbol{p = 0.076}$
UAS-cv-c^{WT}/+: *R23E10-GAL4, cv-c^{MB03717}/cv-c^{C524}* **vs.** *R23E10-GAL4, cv-c^{MB03717}/cv-c^{C524}*	$Z = 3.616$; $\boldsymbol{p = 0.0003}$

Table A8. Statistical tests for Figure 2.1.4-A

Sleep per hour (*two-way repeated measures ANOVA*): Between group (*genotype*) → $F_{(3,92)} = 26.060$; $\boldsymbol{p < 0.0001}$; $\eta^2 = 0.073$ Within group (*time*) → $F_{(23,2116)} = 201.100$; $\boldsymbol{p < 0.0001}$; $\eta^2 = 0.504$ Interaction (*genotype × time*) → $F_{(69,2116)} = 7.750$; $\boldsymbol{p < 0.0001}$; $\eta^2 = 0.058$

Table A9. Statistical tests for Figure 2.1.4-B

Sleep per day (*Kruskal-Wallis Test*): $H = 26.020$; $\boldsymbol{p < 0.0001}$	
UAS-cv-c^{R601Q}/+: *R23E10-GAL4, cv-c^{MB03717}/cv-c^{C524}* **vs.** *UAS-cv-c^{R601Q}/+: cv-c^{MB03717}/cv-c^{C524}*	$Z = 0.423$; $\boldsymbol{p = 0.672}$
UAS-cv-c^{R601Q}/+: *R23E10-GAL4, cv-c^{MB03717}/cv-c^{C524}* **vs.** *R23E10-GAL4, cv-c^{MB03717}/cv-c^{C524}*	$Z = 3.719$; $\boldsymbol{p = 0.0002}$

Table A10. Statistical tests for Figure 2.1.4-C

Total day activity (*one-way ANOVA*): $F_{(2,77)} = 7.139$; $\boldsymbol{p = 0.0014}$; $\eta^2 = 0.156$	
UAS-cv-c^{R601Q}/+: *R23E10-GAL4, cv-c^{MB03717}/cv-c^{C524}* **vs.** *UAS-cv-c^{R601Q}/+: cv-c^{MB03717}/cv-c^{C524}*	$t_{(77)} = 2.653$; $\boldsymbol{p = 0.019}$; $d = 0.469$
UAS-cv-c^{R601Q}/+: *R23E10-GAL4, cv-c^{MB03717}/cv-c^{C524}* **vs.** *R23E10-GAL4, cv-c^{MB03717}/cv-c^{C524}*	$t_{(77)} = 1.373$; $\boldsymbol{p = 0.174}$; $d = 0.280$
Total night activity (*Kruskal-Wallis Test*): $H = 1.618$; $\boldsymbol{p = 0.445}$	
UAS-cv-c^{R601Q}/+: *R23E10-GAL4, cv-c^{MB03717}/cv-c^{C524}* **vs.** *UAS-cv-c^{R601Q}/+: cv-c^{MB03717}/cv-c^{C524}*	post hoc analyses are not applicable
UAS-cv-c^{R601Q}/+: *R23E10-GAL4, cv-c^{MB03717}/cv-c^{C524}* **vs.** *R23E10-GAL4, cv-c^{MB03717}/cv-c^{C524}*	

Table A11. Statistical tests for Figure 2.1.5

Sleep per day (*one-way ANOVA*): $F_{(34,525)} = 16.450$; $\mathbf{p < 0.0001}$; $\eta^2 = 0.516$		
	Experimental **vs.** *Reporter Control*	*Experimental* **vs.** *Driver Control*
UAS-Cdc42^{WT} (28873)	$t_{(525)} = 1.160$; $\mathbf{p = 0.959}$; $d = 0.290$	$t_{(525)} = 0.043$; $\mathbf{p > 0.999}$; $d = 0.011$
UAS-Cdc42^{V12} (4854)	$t_{(525)} = 0.637$; $\mathbf{p = 0.995}$; $d = 0.159$	$t_{(525)} = 1.522$; $\mathbf{p = 0.833}$; $d = 0.381$
UAS-Cdc42^{F89} (6286)	$t_{(525)} = 0.060$; $\mathbf{p > 0.999}$; $d = 0.015$	$t_{(525)} = 2.780$; $\mathbf{p = 0.097}$; $d = 0.695$
UAS-Cdc42^{N17} (6288)	$t_{(525)} = 3.611$; $\mathbf{p = 0.007}$; $d = 0.903$	$t_{(525)} = 2.965$; $\mathbf{p = 0.058}$; $d = 0.741$
UAS-Rho1^{WT}-sph (7334)	$t_{(525)} = 0.006$; $\mathbf{p > 0.999}$; $d = 0.001$	$t_{(525)} = 6.923$; $\mathbf{p < 0.0001}$; $d = 1.731$
UAS-Rho1^{V14} (7330)	$t_{(525)} = 0.548$; $\mathbf{p = 0.995}$; $d = 0.137$	$t_{(525)} = 1.792$; $\mathbf{p = 0.684}$; $d = 0.448$
UAS-Rho1$^{V14, E40L}$ (7332)	$t_{(525)} = 0.083$; $\mathbf{p > 0.999}$; $d = 0.021$	$t_{(525)} = 3.366$; $\mathbf{p = 0.017}$; $d = 0.842$
UAS-Rho^{N19} (7328)	$t_{(525)} = 1.192$; $\mathbf{p = 0.959}$; $d = 0.298$	$t_{(525)} = 1.637$; $\mathbf{p = 0.779}$; $d = 0.409$
UAS-FLAG-Rho1^{D100N} (9391)	$t_{(525)} = 0.693$; $\mathbf{p = 0.995}$; $d = 0.173$	$t_{(525)} = 3.286$; $\mathbf{p = 0.022}$; $d = 0.822$
UAS-Rac1^{WT} (6293)	$t_{(525)} = 2.731$; $\mathbf{p = 0.105}$; $d = 0.683$	$t_{(525)} = 0.467$; $\mathbf{p = 0.995}$; $d = 0.117$
UAS-Rac1^{WT} (28874)	$t_{(525)} = 1.929$; $\mathbf{p = 0.591}$; $d = 0.482$	$t_{(525)} = 0.825$; $\mathbf{p = 0.991}$; $d = 0.206$
UAS-Rac1^{V12} (6291)	$t_{(525)} = 6.721$; $\mathbf{p < 0.0001}$; $d = 1.680$	$t_{(525)} = 5.626$; $\mathbf{p < 0.0001}$; $d = 1.407$
UAS-Rac1^{L89} (5129)	$t_{(525)} = 3.717$; $\mathbf{p = 0.005}$; $d = 0.929$	$t_{(525)} = 4.245$; $\mathbf{p = 0.001}$; $d = 1.061$
UAS-Rac1^{L89} (6290)	$t_{(525)} = 5.383$; $\mathbf{p < 0.0001}$; $d = 1.346$	$t_{(525)} = 4.340$; $\mathbf{p = 0.0004}$; $d = 1.085$
UAS-Rac1^{N17} (6292)	$t_{(525)} = 5.827$; $\mathbf{p < 0.0001}$; $d = 1.457$	$t_{(525)} = 6.142$; $\mathbf{p < 0.0001}$; $d = 1.536$
UAS-Rac2^{WT} (26650)	$t_{(525)} = 0.959$; $\mathbf{p = 0.984}$; $d = 0.240$	$t_{(525)} = 5.188$; $\mathbf{p < 0.0001}$; $d = 1.297$

Table A12. Statistical tests for Figure 2.1.6

Sleep per day (*one-way ANOVA*): $F_{(28,1310)} = 12.820$; $\boldsymbol{p < 0.0001}$; $\eta^2 = 0.215$		
	Experimental **vs.** *Reporter Control*	*Experimental* **vs.** *Driver Control*
UAS-cv-c^{RNAi} (105435KK)	$t_{(1310)} = 6.576$; $\boldsymbol{p < 0.0001}$; $d = 0.959$	$t_{(1310)} = 4.993$; $\boldsymbol{p < 0.0001}$; $d = 0.617$
UAS-Cdc42^{RNAi} (100794KK)	$t_{(1310)} = 2.458$; $\boldsymbol{p = 0.145}$; $d = 0.355$	$t_{(1310)} = 2.268$; $\boldsymbol{p = 0.198}$; $d = 0.280$
UAS-Rho1^{RNAi} (12734GD)	$t_{(1310)} = 1.926$; $\boldsymbol{p = 0.360}$; $d = 0.482$	$t_{(1310)} = 2.586$; $\boldsymbol{p = 0.112}$; $d = 0.368$
UAS-Rho1^{RNAi} (109420KK)	$t_{(1310)} = 1.746$; $\boldsymbol{p = 0.433}$; $d = 0.252$	$t_{(1310)} = 1.725$; $\boldsymbol{p = 0.433}$; $d = 0.213$
UAS-Rac1^{RNAi} (49246GD)	$t_{(1310)} = 6.376$; $\boldsymbol{p < 0.0001}$; $d = 0.950$	$t_{(1310)} = 4.323$; $\boldsymbol{p = 0.0003}$; $d = 0.540$
UAS-Rac1^{RNAi} (49247GD)	$t_{(1310)} = 3.738$; $\boldsymbol{p = 0.003}$; $d = 0.666$	$t_{(1310)} = 4.218$; $\boldsymbol{p = 0.001}$; $d = 0.559$
UAS-Rac2^{RNAi} (28926GD)	$t_{(1310)} = 8.261$; $\boldsymbol{p < 0.0001}$; $d = 1.033$	$t_{(1310)} = 4.651$; $\boldsymbol{p < 0.0001}$; $d = 0.543$
UAS-Rac2^{RNAi} (50349GD)	$t_{(1310)} = 3.169$; $\boldsymbol{p = 0.020}$; $d = 0.457$	$t_{(1310)} = 0.992$; $\boldsymbol{p = 0.540}$; $d = 0.123$
UAS-RhoBtB^{RNAi} (100815KK)	$t_{(1310)} = 5.830$; $\boldsymbol{p < 0.0001}$; $d = 0.855$	$t_{(1310)} = 4.058$; $\boldsymbol{p = 0.001}$; $d = 0.501$
UAS-RhoL^{RNAi} (102461KK)	$t_{(1310)} = 4.570$; $\boldsymbol{p = 0.0001}$; $d = 0.685$	$t_{(1310)} = 2.297$; $\boldsymbol{p = 0.198}$; $d = 0.292$
UAS-RhoU^{RNAi} (103533KK)	$t_{(1310)} = 3.962$; $\boldsymbol{p = 0.001}$; $d = 0.581$	$t_{(1310)} = 1.642$; $\boldsymbol{p = 0.433}$; $d = 0.204$
UAS-RhoU^{RNAi} (1008227KK)	$t_{(1310)} = 4.315$; $\boldsymbol{p = 0.0003}$; $d = 0.623$	$t_{(1310)} = 4.671$; $\boldsymbol{p < 0.0001}$; $d = 0.577$
UAS-Mtl^{RNAi} (102528KK)	$t_{(1310)} = 3.447$; $\boldsymbol{p = 0.008}$; $d = 0.503$	$t_{(1310)} = 1.764$; $\boldsymbol{p = 0.433}$; $d = 0.219$
UAS-Mtl^{RNAi} (108427KK)	$t_{(1310)} = 1.379$; $\boldsymbol{p = 0.433}$; $d = 0.199$	$t_{(1310)} = 0.160$; $\boldsymbol{p = 0.873}$; $d = 0.020$

Table A13. Statistical tests for Figure 2.1.7

Sleep per day ratio, 18°C/31°C (*one-way ANOVA*): $F_{(18,529)} = 27.140$; $\boldsymbol{p < 0.0001}$; $\eta^2 = 0.480$		
	Experimental **vs.** *Reporter Control*	*Experimental* **vs.** *Driver Control*
UAS-Cdc42^{V12} (4854)	$t_{(529)} = 1.525$; $\boldsymbol{p = 0.495}$; $d = 0.281$	$t_{(529)} = 0.854$; $\boldsymbol{p = 0.632}$; $d = 0.160$
UAS-Cdc42^{N17} (6288)	$t_{(529)} = 3.090$; $\boldsymbol{p = 0.016}$; $d = 0.589$	$t_{(529)} = 6.052$; $\boldsymbol{p < 0.0001}$; $d = 1.134$
UAS-Rho1^{RNAi} (109420KK)	$t_{(529)} = 2.518$; $\boldsymbol{p = 0.071}$; $d = 0.449$	$t_{(529)} = 1.226$; $\boldsymbol{p = 0.631}$; $d = 0.226$
UAS-Rho1^{V14} (7330)	$t_{(529)} = 6.414$; $\boldsymbol{p < 0.0001}$; $d = 1.234$	$t_{(529)} = 10.140$; $\boldsymbol{p < 0.0001}$; $d = 1.989$
UAS-Rho^{N19} (7328)	$t_{(529)} = 3.829$; $\boldsymbol{p = 0.002}$; $d = 0.682$	$t_{(529)} = 3.100$; $\boldsymbol{p = 0.016}$; $d = 0.576$
UAS-Rac1^{RNAi} (48247GD)	$t_{(529)} = 3.761$; $\boldsymbol{p = 0.002}$; $d = 0.687$	$t_{(529)} = 4.246$; $\boldsymbol{p = 0.0003}$; $d = 0.788$
UAS-Rac1^{V12} (6291)	$t_{(529)} = 7.617$; $\boldsymbol{p < 0.0001}$; $d = 1.427$	$t_{(529)} = 3.685$; $\boldsymbol{p = 0.003}$; $d = 0.709$
UAS-Rac1^{L89} (6290)	$t_{(529)} = 4.794$; $\boldsymbol{p < 0.0001}$; $d = 0.931$	$t_{(529)} = 3.363$; $\boldsymbol{p = 0.007}$; $d = 0.666$
UAS-Rac1^{N17} (6292)	$t_{(529)} = 0.314$; $\boldsymbol{p = 0.754}$; $d = 0.059$	$t_{(529)} = 1.135$; $\boldsymbol{p = 0.631}$; $d = 0.213$

Table A14. Statistical tests for Figure 2.1.9-A

Sleep per day (*one-way ANOVA*): $F_{(2,82)} = 68.100$; $\boldsymbol{p < 0.0001}$; $\eta^2 = 0.624$	
UAS-Rho1^{RNAi}*/+:* *R23E10-GAL4, cv-c*^{MB03717}*/cv-c*^{C524} **vs.** *UAS-Rho1*^{RNAi}*/+: cv-c*^{MB03717}*/cv-c*^{C524}	$t_{(82)} = 6.192$; $\boldsymbol{p < 0.0001}$; $d = 1.203$
UAS-Rho1^{RNAi}*/+:* *R23E10-GAL4, cv-c*^{MB03717}*/cv-c*^{C524} **vs.** *R23E10-GAL4, cv-c*^{MB03717}*/cv-c*^{C524}	$t_{(82)} = 11.610$; $\boldsymbol{p < 0.0001}$; $d = 2.052$

Table A15. Statistical tests for Figure 2.1.9-B

Sleep per day (*Kruskal-Wallis Test*): $H = 13.610$; $\boldsymbol{p = 0.001}$	
UAS-Rac1^{L89}*/+:* *R23E10-GAL4, cv-c*^{MB03717}*/cv-c*^{C524} **vs.** *UAS-Rac1*^{L89}*/+: cv-c*^{MB03717}*/cv-c*^{C524}	$Z = 2.342$; $\boldsymbol{p = 0.019}$
UAS-Rac1^{L89}*/+:* *R23E10-GAL4, cv-c*^{MB03717}*/cv-c*^{C524} **vs.** *R23E10-GAL4, cv-c*^{MB03717}*/cv-c*^{C524}	$Z = 3.432$; $\boldsymbol{p = 0.0006}$

Table A16. Statistical tests for Figure 2.1.10-A

Sleep per day (*one-way ANOVA*): $F_{(2,82)} = 6.563$; $\boldsymbol{p = 0.002}$; $\eta^2 = 0.126$	
UAS-Cdc42^{V12}/+: *R23E10-GAL4, cv-c^{MB03717}/cv-c^{C524}* **vs.** *UAS-Cdc42^{V12}/+: cv-c^{MB03717}/cv-c^{C524}*	$t_{(82)} = 3.001$; $\boldsymbol{p = 0.007}$; $d = 0.539$
UAS-Cdc42^{V12}/+: *R23E10-GAL4, cv-c^{MB03717}/cv-c^{C524}* **vs.** *R23E10-GAL4, cv-c^{MB03717}/cv-c^{C524}*	$t_{(82)} = 0.292$; $\boldsymbol{p = 0.771}$; $d = 0.052$

Table A17. Statistical tests for Figure 2.1.10-B

Sleep per day (*one-way ANOVA*): $F_{(2,87)} = 6.081$; $\boldsymbol{p = 0.003}$; $\eta^2 = 0.123$	
UAS-Cdc42^{N17}/+: *R23E10-GAL4, cv-c^{MB03717}/cv-c^{C524}* **vs.** *UAS-Cdc42^{N17}/+: cv-c^{MB03717}/cv-c^{C524}*	$t_{(87)} = 2.253$; $\boldsymbol{p = 0.053}$; $d = 0.418$
UAS-Cdc42^{N17}/+: *R23E10-GAL4, cv-c^{MB03717}/cv-c^{C524}* **vs.** *R23E10-GAL4, cv-c^{MB03717}/cv-c^{C524}*	$t_{(87)} = 1.182$; $\boldsymbol{p = 0.240}$; $d = 0.212$

Table A18. Statistical tests for Figure 2.2.1

Sleep per day (*one-way ANOVA*): $F_{(28,884)} = 13.480$; $\boldsymbol{p < 0.0001}$; $\eta^2 = 0.299$		
	Experimental **vs.** *Reporter Control*	*Experimental* **vs.** *Driver Control*
UAS-Sh^{RNAi} (104474KK)	$t_{(884)} = 6.516$; $\boldsymbol{p < 0.0001}$; $d = 1.512$	$t_{(884)} = 5.339$; $\boldsymbol{p < 0.0001}$; $d = 0.959$
UAS-Hk^{RNAi} (101402KK)	$t_{(884)} = 4.991$; $\boldsymbol{p < 0.0001}$; $d = 0.882$	$t_{(884)} = 4.273$; $\boldsymbol{p = 0.001}$; $d = 0.767$
UAS-qvr^{RNAi} (104533KK)	$t_{(884)} = 5.741$; $\boldsymbol{p < 0.0001}$; $d = 1.031$	$t_{(884)} = 3.444$; $\boldsymbol{p = 0.001}$; $d = 0.629$
UAS-Shab^{RNAi} (102218KK)	$t_{(884)} = 4.151$; $\boldsymbol{p = 0.001}$; $d = 0.746$	$t_{(884)} = 3.961$; $\boldsymbol{p = 0.002}$; $d = 0.717$
UAS-Shal^{RNAi} (103363KK)	$t_{(884)} = 1.902$; $\boldsymbol{p = 0.501}$; $d = 0.336$	$t_{(884)} = 0.484$; $\boldsymbol{p = 0.936}$; $d = 0.087$
UAS-Shaw^{RNAi} (110589KK)	$t_{(884)} = 0.754$; $\boldsymbol{p = 0.936}$; $d = 0.133$	$t_{(884)} = 1.901$; $\boldsymbol{p = 0.501}$; $d = 0.341$
UAS-slo^{RNAi} (104421KK)	$t_{(884)} = 1.369$; $\boldsymbol{p = 0.732}$; $d = 0.246$	$t_{(884)} = 1.714$; $\boldsymbol{p = 0.517}$; $d = 0.310$
UAS-SK^{RNAi} (103985KK)	$t_{(884)} = 3.478$; $\boldsymbol{p = 0.011}$; $d = 0.615$	$t_{(884)} = 1.891$; $\boldsymbol{p = 0.501}$; $d = 0.340$
UAS-Ih^{RNAi} (110274KK)	$t_{(884)} = 1.951$; $\boldsymbol{p = 0.501}$; $d = 0.348$	$t_{(884)} = 2.528$; $\boldsymbol{p = 0.181}$; $d = 0.458$
UAS-sei^{RNAi} (104698KK)	$t_{(884)} = 1.976$; $\boldsymbol{p = 0.501}$; $d = 0.352$	$t_{(884)} = 0.829$; $\boldsymbol{p = 0.936}$; $d = 0.149$
UAS-CngB^{RNAi} (100882KK)	$t_{(884)} = 3.466$; $\boldsymbol{p = 0.011}$; $d = 0.613$	$t_{(884)} = 0.357$; $\boldsymbol{p = 0.936}$; $d = 0.064$
UAS-Cngl^{RNAi} (102411KK)	$t_{(884)} = 2.022$; $\boldsymbol{p = 0.486}$; $d = 0.366$	$t_{(884)} = 0.901$; $\boldsymbol{p = 0.936}$; $d = 0.166$
UAS-Irk1^{RNAi} (107389KK)	$t_{(884)} = 3.181$; $\boldsymbol{p = 0.027}$; $d = 0.567$	$t_{(884)} = 2.476$; $\boldsymbol{p = 0.195}$; $d = 0.445$
UAS-Irk2^{RNAi} (108140KK)	$t_{(884)} = 1.976$; $\boldsymbol{p = 0.501}$; $d = 0.352$	$t_{(884)} = 0.829$; $\boldsymbol{p = 0.936}$; $d = 0.149$

Table A19. Statistical tests for Figure 2.2.2-A

Sleep per hour (*two-way repeated measures ANOVA*):
Between group (*genotype*) → $F_{(2,75)} = 17.200$; $\boldsymbol{p < 0.0001}$; $\eta^2 = 0.050$
Within group (*time*) → $F_{(23,1725)} = 111.800$; $\boldsymbol{p < 0.0001}$; $\eta^2 = 0.447$
Interaction (*genotype × time*) → $F_{(46,1725)} = 7.910$; $\boldsymbol{p < 0.0001}$; $\eta^2 = 0.063$

Table A20. Statistical tests for Figure 2.2.2-B

Sleep per day (*one-way ANOVA*): $F_{(2,91)} = 16.550$; $\boldsymbol{p < 0.0001}$; $\eta^2 = 0.2668$	
Hk^1:UAS-Hk^{WT}/+:R23E10-GAL4/+ **vs.** *UAS-Hk^{WT}/+:R23E10-GAL4/+*	$t_{(91)} = 4.720$; $\boldsymbol{p < 0.0001}$; $d = 0.848$
Hk^1:UAS-Hk^{WT}/+:R23E10-GAL4/+ **vs.** *Hk^1/+:+:R23E10-GAL4/+*	$t_{(91)} = 5.221$; $\boldsymbol{p < 0.0001}$; $d = 0.930$

Table A21. Statistical tests for Figure 2.2.2-C

Sleep per hour (*two-way repeated measures ANOVA*):
Between group (*genotype*) → $F_{(2,76)} = 15.320$; $\boldsymbol{p < 0.0001}$; $\eta^2 = 0.073$
Within group (*time*) → $F_{(23,1748)} = 97.490$; $\boldsymbol{p < 0.0001}$; $\eta^2 = 0.360$
Interaction (*genotype × time*) → $F_{(46,1748)} = 12.300$; $\boldsymbol{p < 0.0001}$; $\eta^2 = 0.091$

Table A22. Statistical tests for Figure 2.2.2-D

Sleep per day (*one-way ANOVA*): $F_{(2,92)} = 0.101$; $\boldsymbol{p = 0.904}$; $\eta^2 = 0.002$	
Hk^1:UAS-Hk^{K289M}/+:R23E10-GAL4/+ **vs.** *UAS-Hk^{K289M}/+:R23E10-GAL4/+*	post hoc analyses are not applicable
Hk^1:UAS-Hk^{K289M}/+:R23E10-GAL4/+ **vs.** *Hk^1/+:+:R23E10-GAL4/+*	

Table A23. Statistical tests for Figure 2.2.3-B

DFB dendrite red/green ratio (*Kruskal-Wallis Test*): $H = 18.490$; $\mathbf{p < 0.0001}$	
Sleep deprived **vs.** *Control: 8AM – 11AM*	$Z = 3.891$; $\mathbf{p < 0.0001}$
Sleep deprived **vs.** *Control: 4PM – 6PM*	$Z = 2.346$; $\mathbf{p = 0.019}$
Control: 8AM – 11AM **vs.** *Control: 4PM – 6PM*	$Z < 0.0001$; $\mathbf{p > 0.9999}$

Table A24. Statistical tests for Figure 2.2.3-C

Sleep per hour (*two-way repeated measures ANOVA*):
Between group (*genotype*) → $F_{(2,91)} = 7.951$; $\mathbf{p = 0.0007}$; $\eta^2 = 0.011$
Within group (*time*) → $F_{(23,2093)} = 198.200$; $\mathbf{p < 0.0001}$; $\eta^2 = 0.602$
Interaction (*genotype × time*) → $F_{(46,2093)} = 7.712$; $\mathbf{p < 0.0001}$; $\eta^2 = 0.047$

Table A25. Statistical tests for Figure 2.2.3-D

Sleep per day (*one-way ANOVA*): $F_{(2,91)} = 7.951$; $\mathbf{p = 0.0007}$; $\eta^2 = 0.1488$	
R23E10-GAL4 > UAS-MitoTimer **vs.** *UAS-MitoTimer/+*	$t_{(91)} = 3.875$; $\mathbf{p = 0.0004}$; $d = 0.696$
R23E10-GAL4 > UAS-MitoTimer **vs.** *R23E10-GAL4/+*	$t_{(91)} = 2.768$; $\mathbf{p = 0.007}$; $d = 0.493$

Table A26. Statistical tests for Figure 2.2.4-A

DFB axon red/green ratio (*one-way ANOVA*): $F_{(2,25)} = 2.763$; $\boldsymbol{p = 0.082}$; $\eta^2 = 0.181$	
Sleep deprived **vs.** *Control: 8AM – 11AM*	post hoc analyses are not applicable
Sleep deprived **vs.** *Control: 4PM – 6PM*	
Control: 8AM – 11AM **vs.** *Control: 4PM – 6PM*	

Table A27. Statistical tests for Figure 2.2.4-B

DFB soma red/green ratio (*Kruskal-Wallis Test*): $H = 4.923$; $\boldsymbol{p = 0.085}$	
Sleep deprived **vs.** *Control: 8AM – 11AM*	post hoc analyses are not applicable
Sleep deprived **vs.** *Control: 4PM – 6PM*	
Control: 8AM – 11AM **vs.** *Control: 4PM – 6PM*	

Table A28. Statistical tests for Figures 2.2.3-B, 2.2.4-A, and -B

Red/green ratio (*two-way ANOVA*): Factor 1 (*dFB compartment*) → $F_{(2,130)} = 18.060$; $\boldsymbol{p < 0.0001}$; $\eta^2 = 0.180$ Factor 2 (*deprivation*) → $F_{(2,130)} = 12.200$; $\boldsymbol{p < 0.0001}$; $\eta^2 = 0.122$ Interaction (*dFB compartment × deprivation*) → $F_{(4,130)} = 1.682$; $\boldsymbol{p = 0.158}$; $\eta^2 = 0.034$	
Axon (*8AM – 11AM* **vs.** *Deprived*)	$t_{(130)} = 1.871$; $\boldsymbol{p = 0.316}$; $d = 0.564$
Axon (*4PM – 6PM* **vs.** *Deprived*)	$t_{(130)} = 1.887$; $\boldsymbol{p = 0.316}$; $d = 0.647$
Axon (*4PM – 6PM* **vs.** *8AM – 11AM*)	$t_{(130)} = 0.316$; $\boldsymbol{p = 0.753}$; $d = 0.108$
Dendrite (*8AM – 11AM* **vs.** *Deprived*)	$t_{(130)} = 4.863$; $\boldsymbol{p < 0.0001}$; $d = 1.049$
Dendrite (*4PM – 6PM* **vs.** *Deprived*)	$t_{(130)} = 2.863$; $\boldsymbol{p = 0.04}$; $d = 0.705$
Dendrite (*4PM – 6PM* **vs.** *8AM – 11AM*)	$t_{(130)} = 1.247$; $\boldsymbol{p = 0.535}$; $d = 0.302$
Soma (*8AM – 11AM* **vs.** *Deprived*)	$t_{(130)} = 1.366$; $\boldsymbol{p = 0.535}$; $d = 0.291$
Soma (*4PM – 6PM* **vs.** *Deprived*)	$t_{(130)} = 2.107$; $\boldsymbol{p = 0.232}$; $d = 0.511$
Soma (*4PM – 6PM* **vs.** *8AM – 11AM*)	$t_{(130)} = 0.959$; $\boldsymbol{p = 0.564}$; $d = 0.233$

Table A29. Statistical tests for Figure 2.2.4-C

MB calyx red/green ratio (*Welch's t test*): *Sleep deprived* **vs.** *Control: 8AM – 11AM*	$t_{(30.41)} = 1.582$; $\boldsymbol{p = 0.124}$; d = 0.363

Table A30. Statistical tests for Figure 2.2.4-D

MB HL red/green ratio (*Mann-Whitney test*): *Sleep deprived* **vs.** *Control: 8AM – 11AM*	$U = 127$; $\boldsymbol{p = 0.126}$

Table A31. Statistical tests for Figure 2.2.4-E

MB VL red/green ratio (*Mann-Whitney test*): *Sleep deprived* **vs.** *Control: 8AM – 11AM*	U= 120; $\boldsymbol{p = 0.082}$

Table A32. Statistical tests for Figures 2.2.4-C, -D, and -E

Red/green ratio (*two-way ANOVA*): Factor 1 (*MB compartment*) → $F_{(2,108)} = 26.570$; $\boldsymbol{p < 0.0001}$; $\eta^2 = 0.314$ Factor 2 (*deprivation*) → $F_{(1,108)} = 7.809$; $\boldsymbol{p = 0.006}$; $\eta^2 = 0.046$ Interaction (*MB compartment × deprivation*) → $F_{(2,130)} = 0.137$; $\boldsymbol{p = 0.872}$; $\eta^2 = 0.002$	
Calyx (*8AM – 11AM* **vs.** *Deprived*)	$t_{(108)} = 1.188$; $\boldsymbol{p = 0.237}$; $d = 0.273$
HL (*8AM – 11AM* **vs.** *Deprived*)	$t_{(108)} = 1.865$; $\boldsymbol{p = 0.183}$; $d = 0.428$
VL (*8AM – 11AM* **vs.** *Deprived*)	$t_{(108)} = 1.788$; $\boldsymbol{p = 0.183}$; $d = 0.410$

Table A33. Statistical tests for Figure 2.2.5-A

Sleep per hour (*two-way repeated measures ANOVA*): Between group (*genotype*) → $F_{(2,90)} = 16.090$; $\boldsymbol{p = 0.023}$; $\eta^2 = 0.004$ Within group (*time*) → $F_{(23,2070)} = 150.400$; $\boldsymbol{p < 0.0001}$; $\eta^2 = 0.656$ Interaction (*genotype × time*) → $F_{(46,2070)} = 3.076$; $\boldsymbol{p < 0.0001}$; $\eta^2 = 0.025$

Table A34. Statistical tests for Figure 2.2.5-B

Sleep per day (*one way ANOVA*): $F_{(2,90)} = 3.837$; $\boldsymbol{p = 0.025}$; $\eta^2 = 0.079$	
R23E10-GAL4 > UAS-dSod1^{WT} **vs.** *UAS-dSod1^{WT}/+*	$t_{(90)} = 2.768$; $\boldsymbol{p = 0.014}$; $d = 0.497$
R23E10-GAL4 > UAS-dSod1^{WT} **vs.** *R23E10-GAL4/+*	$t_{(90)} = 1.262$; $\boldsymbol{p = 0.210}$; $d = 0.225$

Table A35. Statistical tests for Figure 2.2.6-A

Sleep per hour (*two-way repeated measures ANOVA*):
Between group (*genotype*) → $F_{(2,92)} = 11.580$; $\boldsymbol{p < 0.0001}$; $\eta^2 = 0.017$
Within group (*time*) → $F_{(23,2116)} = 156.300$; $\boldsymbol{p < 0.0001}$; $\eta^2 = 0.558$
Interaction (*genotype × time*) → $F_{(46,2116)} = 3.756$; $\boldsymbol{p < 0.0001}$; $\eta^2 = 0.027$

Table A36. Statistical tests for Figure 2.2.6-B

Sleep per day (*one way ANOVA*): $F_{(2,92)} = 11.580$; $\boldsymbol{p < 0.0001}$; $\eta^2 = 0.201$	
R23E10-GAL4 > UAS-hSod1^{WT} **vs.** *UAS-hSod1*^{WT}*/+*	$t_{(92)} = 4.025$; $\boldsymbol{p = 0.0001}$; $d = 0.712$
R23E10-GAL4 > UAS-hSod1^{WT} **vs.** *R23E10-GAL4/+*	$t_{(92)} = 4.288$; $\boldsymbol{p < 0.0001}$; $d = 0.764$

Table A37. Statistical tests for Figure 2.2.6-C

Sleep per hour (*two-way repeated measures ANOVA*):
Between group (*genotype*) → $F_{(2,87)} = 16.090$; $\boldsymbol{p < 0.0001}$; $\eta^2 = 0.029$
Within group (*time*) → $F_{(23,2001)} = 150.400$; $\boldsymbol{p < 0.0001}$; $\eta^2 = 0.551$
Interaction (*genotype × time*) → $F_{(46,2001)} = 3.076$; $\boldsymbol{p < 0.0001}$; $\eta^2 = 0.023$

Table A38. Statistical tests for Figure 2.2.6-D

Sleep per day (*one way ANOVA*): $F_{(2,87)} = 16.090$; $\boldsymbol{p < 0.0001}$; $\eta^2 = 0.270$	
R23E10-GAL4 > UAS-hSod1^{A4V} **vs.** *UAS-hSod1*^{A4V}*/+*	$t_{(87)} = 5.016$; $\boldsymbol{p < 0.0001}$; $d = 0.924$
R23E10-GAL4 > UAS-hSod1^{A4V} **vs.** *R23E10-GAL4/+*	$t_{(87)} = 4.802$; $\boldsymbol{p < 0.0001}$; $d = 0.870$

Table A39. Statistical tests for Figure 2.2.7-A

Flies awakened (*two-way ANOVA*): Between group (*genotype*) → $F_{(2,60)} = 0.604$; $\mathbf{p = 0.550}$; $\eta^2 = 0.006$ Within group (*vibrational force*) → $F_{(3,60)} = 46.370$; $\mathbf{p < 0.0001}$; $\eta^2 = 0.691$ Interaction (*genotype × vibrational force*) → $F_{(6,60)} = 0.162$; $\mathbf{p = 0.986}$; $\eta^2 = 0.005$	
R23E10-GAL4 > UAS-hSod1^{WT} (*0g* **vs.** *0.6g*)	$t_{(60)} = 1.572$; $\mathbf{p = 0.914}$; $d = 0.642$
R23E10-GAL4 > UAS-hSod1^{WT} (*0g* **vs.** *0.9g*)	$t_{(60)} = 4.107$; $\mathbf{p = 0.005}$; $d = 1.677$
R23E10-GAL4 > UAS-hSod1^{WT} (*0g* **vs.** *1.2g*)	$t_{(60)} = 6.754$; $\mathbf{p < 0.0001}$; $d = 2.757$
R23E10-GAL4 > UAS-hSod1^{WT} (*0.6g* **vs.** *0.9g*)	$t_{(60)} = 2.535$; $\mathbf{p = 0.361}$; $d = 1.035$
R23E10-GAL4 > UAS-hSod1^{WT} (*0.6g* **vs.** *1.2g*)	$t_{(60)} = 5.183$; $\mathbf{p = 0.0002}$; $d = 2.116$
R23E10-GAL4 > UAS-hSod1^{WT} (*0.9g* **vs.** *1.2g*)	$t_{(60)} = 2.648$; $\mathbf{p = 0.2976}$; $d = 1.081$
UAS-hSod1^{WT}/+ (*0g* **vs.** *0.6g*)	$t_{(60)} = 1.377$; $\mathbf{p = 0.961}$; $d = 0.562$
UAS-hSod1^{WT}/+ (*0g* **vs.** *0.9g*)	$t_{(60)} = 3.997$; $\mathbf{p = 0.008}$; $d = 1.632$
UAS-hSod1^{WT}/+ (*0g* **vs.** *1.2g*)	$t_{(60)} = 6.075$; $\mathbf{p < 0.0001}$; $d = 2.480$
UAS-hSod1^{WT}/+ (*0.6g* **vs.** *0.9g*)	$t_{(60)} = 2.620$; $\mathbf{p = 0.309}$; $d = 1.070$
UAS-hSod1^{WT}/+ (*0.6g* **vs.** *1.2g*)	$t_{(60)} = 4.698$; $\mathbf{p = 0.0008}$; $d = 1.918$
UAS-hSod1^{WT}/+ (*0.9g* **vs.** *1.2g*)	$t_{(60)} = 2.078$; $\mathbf{p = 0.686}$; $d = 0.848$
R23E10-GAL4/+ (*0g* **vs.** *0.6g*)	$t_{(60)} = 1.639$; $\mathbf{p = 0.895}$; $d = 0.669$
R23E10-GAL4/+ (*0g* **vs.** *0.9g*)	$t_{(60)} = 4.553$; $\mathbf{p = 0.001}$; $d = 1.859$
R23E10-GAL4/+ (*0g* **vs.** *1.2g*)	$t_{(60)} = 5.908$; $\mathbf{p < 0.0001}$; $d = 2.412$
R23E10-GAL4/+ (*0.6g* **vs.** *0.9g*)	$t_{(60)} = 2.914$; $\mathbf{p = 0.161}$; $d = 1.190$
R23E10-GAL4/+ (*0.6g* **vs.** *1.2g*)	$t_{(60)} = 4.269$; $\mathbf{p = 0.003}$; $d = 1.743$
R23E10-GAL4/+ (*0.9g* **vs.** *1.2g*)	$t_{(60)} = 1.355$; $\mathbf{p = 0.961}$; $d = 0.553$
0g: *R23E10-GAL4 > UAS-hSod1^{WT}* **vs.** *0g*: *UAS-hSod1^{WT}/+*	$t_{(60)} = 0.246$; $\mathbf{p = 0.999}$; $d = 0.100$
0g: *R23E10-GAL4 > UAS-hSod1^{WT}* **vs.** *0g*: *R23E10-GAL4/+*	$t_{(60)} = 0.049$; $\mathbf{p = 0.999}$; $d = 0.020$
0.6g: *R23E10-GAL4 > UAS-hSod1^{WT}* **vs.** *0.6g*: *UAS-hSod1^{WT}/+*	$t_{(60)} = 0.441$; $\mathbf{p = 0.999}$; $d = 0.180$
0.6g: *R23E10-GAL4 > UAS-hSod1^{WT}* **vs.** *0.6g*: *R23E10-GAL4/+*	$t_{(60)} = 0.116$; $\mathbf{p = 0.999}$; $d = 0.048$
0.9g: *R23E10-GAL4 > UAS-hSod1^{WT}* **vs.** *0.9g*: *UAS-hSod1^{WT}/+*	$t_{(60)} = 0.356$; $\mathbf{p = 0.999}$; $d = 0.145$
0.9g: *R23E10-GAL4 > UAS-hSod1^{WT}* **vs.** *0.9g*: *R23E10-GAL4/+*	$t_{(60)} = 0.496$; $\mathbf{p = 0.999}$; $d = 0.202$
1.2g: *R23E10-GAL4 > UAS-hSod1^{WT}* **vs.** *1.2g*: *UAS-hSod1^{WT}/+*	$t_{(60)} = 0.925$; $\mathbf{p = 0.995}$; $d = 0.378$
1.2g: *R23E10-GAL4 > UAS-hSod1^{WT}* **vs.** *1.2g*: *R23E10-GAL4/+*	$t_{(60)} = 0.797$; $\mathbf{p = 0.996}$; $d = 0.325$

Table A40. Statistical tests for Figure 2.2.7-B

Flies awakened (*two-way ANOVA*): Between group (*genotype*) → $F_{(2,60)} = 1.424$; $\boldsymbol{p = 0.249}$; $\eta^2 = 0.018$ Within group (*vibrational force*) → $F_{(3,60)} = 33.130$; $\boldsymbol{p < 0.0001}$; $\eta^2 = 0.611$ Interaction (*genotype × vibrational force*) → $F_{(6,60)} = 0.080$; $\boldsymbol{p = 0.998}$; $\eta^2 = 0.003$	
R23E10-GAL4 > UAS-hSod1^{A4V} (*0g* **vs.** *0.6g*)	$t_{(60)} = 1.325$; $\boldsymbol{p = 0.982}$; $d = 0.541$
R23E10-GAL4 > UAS-hSod1^{A4V} (*0g* **vs.** *0.9g*)	$t_{(60)} = 3.373$; $\boldsymbol{p = 0.056}$; $d = 1.377$
R23E10-GAL4 > UAS-hSod1^{A4V} (*0g* **vs.** *1.2g*)	$t_{(60)} = 5.176$; $\boldsymbol{p = 0.0002}$; $d = 2.113$
R23E10-GAL4 > UAS-hSod1^{A4V} (*0.6g* **vs.** *0.9g*)	$t_{(60)} = 2.048$; $\boldsymbol{p = 0.781}$; $d = 0.836$
R23E10-GAL4 > UAS-hSod1^{A4V} (*0.6g* **vs.** *1.2g*)	$t_{(60)} = 3.852$; $\boldsymbol{p = 0.014}$; $d = 1.573$
R23E10-GAL4 > UAS-hSod1^{A4V} (*0.9g* **vs.** *1.2g*)	$t_{(60)} = 1.804$; $\boldsymbol{p = 0.883}$; $d = 0.736$
UAS-hSod1^{A4V} /+ (*0g* **vs.** *0.6g*)	$t_{(60)} = 1.492$; $\boldsymbol{p = 0.961}$; $d = 0.609$
UAS-hSod1^{A4V} /+ (*0g* **vs.** *0.9g*)	$t_{(60)} = 3.475$; $\boldsymbol{p = 0.043}$; $d = 1.419$
UAS-hSod1^{A4V} /+ (*0g* **vs.** *1.2g*)	$t_{(60)} = 5.297$; $\boldsymbol{p = 0.0001}$; $d = 2.162$
UAS-hSod1^{A4V} /+ (*0.6g* **vs.** *0.9g*)	$t_{(60)} = 1.983$; $\boldsymbol{p = 0.798}$; $d = 0.810$
UAS-hSod1^{A4V} /+ (*0.6g* **vs.** *1.2g*)	$t_{(60)} = 3.804$; $\boldsymbol{p = 0.016}$; $d = 1.553$
UAS-hSod1^{A4V} /+ (*0.9g* **vs.** *1.2g*)	$t_{(60)} = 1.822$; $\boldsymbol{p = 0.882}$; $d = 0.744$
R23E10-GAL4/+ (*0g* **vs.** *0.6g*)	$t_{(60)} = 1.507$; $\boldsymbol{p = 0.961}$; $d = 0.615$
R23E10-GAL4/+ (*0g* **vs.** *0.9g*)	$t_{(60)} = 4.186$; $\boldsymbol{p = 0.005}$; $d = 1.709$
R23E10-GAL4/+ (*0g* **vs.** *1.2g*)	$t_{(60)} = 5.432$; $\boldsymbol{p < 0.0001}$; $d = 2.218$
R23E10-GAL4/+ (*0.6g* **vs.** *0.9g*)	$t_{(60)} = 2.679$; $\boldsymbol{p = 0.298}$ $d = 1.094$
R23E10-GAL4/+ (*0.6g* **vs.** *1.2g*)	$t_{(60)} = 3.925$; $\boldsymbol{p = 0.012}$; $d = 1.602$
R23E10-GAL4/+ (*0.9g* **vs.** *1.2g*)	$t_{(60)} = 1.246$; $\boldsymbol{p = 0.985}$; $d = 0.509$
0g: *R23E10-GAL4 > UAS-hSod1^{A4V}* **vs.** *0g*: *UAS-hSod1^{A4V} /+*	$t_{(60)} = 0.102$; $\boldsymbol{p = 0.999}$; $d = 0.042$
0g: *R23E10-GAL4 > UAS-hSod1^{A4V}* **vs.** *0g*: *R23E10-GAL4/+*	$t_{(60)} = 0.497$; $\boldsymbol{p = 0.999}$; $d = 0.203$
0.6g: *R23E10-GAL4 > UAS-hSod1^{A4V}* **vs.** *0.6g*: *UAS-hSod1^{A4V} /+*	$t_{(60)} = 0.269$; $\boldsymbol{p = 0.999}$; $d = 0.110$
0.6g: *R23E10-GAL4 > UAS-hSod1^{A4V}* **vs.** *0.6g*: *R23E10-GAL4/+*	$t_{(60)} = 0.679$; $\boldsymbol{p = 0.999}$; $d = 0.277$
0.9g: *R23E10-GAL4 > UAS-hSod1^{A4V}* **vs.** *0.9g*: *UAS-hSod1^{A4V} /+*	$t_{(60)} = 0.204$; $\boldsymbol{p = 0.999}$; $d = 0.083$
0.9g: *R23E10-GAL4 > UAS-hSod1^{A4V}* **vs.** *0.9g*: *R23E10-GAL4/+*	$t_{(60)} = 1.310$; $\boldsymbol{p = 0.982}$; $d = 0.535$
1.2g: *R23E10-GAL4 > UAS- hSod1^{A4V}* **vs.** *1.2g*: *UAS- hSod1^{A4V} /+*	$t_{(60)} = 0.222$; $\boldsymbol{p = 0.999}$; $d = 0.091$
1.2g: *R23E10-GAL4 > UAS- hSod1^{A4V}* **vs.** *1.2g*: *R23E10-GAL4/+*	$t_{(60)} = 0.753$; $\boldsymbol{p = 0.999}$; $d = 0.307$

Table A41. Statistical tests for Figure 2.2.8-A

Sleep per day (*Kruskal-Wallis test*): $H = 11.220$; $\mathbf{p = 0.004}$	
pdf-GAL4 > UAS-hSod1^{WT} **vs.** *UAS-hSod1^{WT}/+*	$Z = 2.878$; $\mathbf{p = 0.004}$
pdf-GAL4 > UAS-hSod1^{WT} **vs.** *pdf-GAL4/+*	$Z < 0.0001$; $\mathbf{p > 0.9999}$
Sleep per day (*one way ANOVA*): $F_{(2,88)} = 3.845$; $\mathbf{p = 0.035}$; $\eta^2 = 0.073$	
pdf-GAL4 > UAS-hSod1^{A4V} **vs.** *UAS-hSod1^{A4V}/+*	$t_{(88)} = 2.040$; $\mathbf{p = 0.087}$; $d = 0.372$
pdf-GAL4 > UAS-hSod1^{A4V} **vs.** *R23E10-GAL4/+*	$t_{(88)} = 0.649$; $\mathbf{p = 0.649}$; $d = 0.082$

Table A42. Statistical tests for Figure 2.2.8-B

Sleep per day (*one way ANOVA*): $F_{(2,81)} = 2.713$; $\mathbf{p = 0.072}$; $\eta^2 = 0.063$	
cry-GAL4 > UAS-hSod1^{WT} **vs.** *UAS-hSod1^{WT}/+*	post hoc analyses are not applicable
cry-GAL4 > UAS-hSod1^{WT} **vs.** *cry-GAL4/+*	
Sleep per day (*Kruskal-Wallis test*): $H = 6.560$; $\mathbf{p = 0.036}$	
cry-GAL4 > UAS-hSod1^{A4V} **vs.** *UAS-hSod1^{A4V}/+*	$Z = 1.995$; $\mathbf{p = 0.046}$
cry-GAL4 > UAS-hSod1^{A4V} **vs.** *cry-GAL4/+*	$Z < 0.0001$; $\mathbf{p > 0.9999}$

Table A43. Statistical tests for Figure 2.2.8-C

Sleep per day (*one way ANOVA*): $F_{(2,86)} = 2.821$; $\boldsymbol{p = 0.065}$; $\eta^2 = 0.062$	
OK107-GAL4 > UAS-hSod1^{WT} **vs.** *UAS-hSod1^{WT}/+*	post hoc analyses are not applicable
OK107-GAL4 > UAS-hSod1^{WT} **vs.** *OK107-GAL4/+*	
Sleep per day (*one way ANOVA*): $H = 7.204$; $\boldsymbol{p = 0.027}$	
OK107-GAL4 > UAS-hSod1^{A4V} **vs.** *UAS-hSod1^{A4V}/+*	$Z = 2.432$; $\boldsymbol{p = 0.015}$
OK107-GAL4 > UAS-hSod1^{A4V} **vs.** *OK107-GAL4/+*	$Z = 0.532$; $\boldsymbol{p = 0.595}$

Table A44. Statistical tests for Figure 2.2.8-D

Sleep per day (*Kruskal-Wallis test*): $H = 7.342$; $\boldsymbol{p = 0.026}$	
GH146-GAL4 > UAS-hSod1^{WT} **vs.** *UAS-hSod1^{WT}/+*	$Z = 0.986$; $\boldsymbol{p = 0.324}$
GH146-GAL4 > UAS-hSod1^{WT} **vs.** *GH146-GAL4/+*	$Z = 2.457$; $\boldsymbol{p = 0.014}$
Sleep per day (*Kruskal-Wallis test*): $H = 1.252$; $\boldsymbol{p = 0.535}$	
GH146-GAL4 > UAS-hSod1^{WT} **vs.** *UAS-hSod1^{WT}/+*	post hoc analyses are not applicable
GH146-GAL4 > UAS-hSod1^{WT} **vs.** *GH146-GAL4/+*	

Table A45. Statistical tests for Figures 2.2.6-B and 2.2.8

Sleep per day (*two-way ANOVA*): *UAS-hSod1^{WT}* Factor 1 (*genotype*) → $F_{(2,432)} = 4.587$; $\boldsymbol{p < 0.0001}$; $\eta^2 = 0.044$ Factor 2 (*brain region*) → $F_{(4,432)} = 22.820$; $\boldsymbol{p < 0.0001}$; $\eta^2 = 0.157$ Interaction (*genotype × brain region*) → $F_{(8,432)} = 12.790$; $\boldsymbol{p < 0.0001}$; $\eta^2 = 0.063$	
R23E10-GAL4 (*responder control* **vs.** *driven*)	$t_{(432)} = 3.794$; $\boldsymbol{p = 0.001}$; $d = 0.671$
R23E10-GAL4 (*driver control* **vs.** *driven*)	$t_{(432)} = 4.042$; $\boldsymbol{p = 0.001}$; $d = 0.720$
pdf-GAL4 (*responder control* **vs.** *driven*)	$t_{(432)} = 4.983$; $\boldsymbol{p < 0.0001}$; $d = 0.910$
pdf-GAL4 (*driver control* **vs.** *driven*)	$t_{(432)} = 2.139$; $\boldsymbol{p = 0.171}$; $d = 0.394$
cry-GAL4 (*responder control* **vs.** *driven*)	$t_{(432)} = 1.490$; $\boldsymbol{p = 0.255}$; $d = 0.270$
cry-GAL4 (*driver control* **vs.** *driven*)	$t_{(432)} = 1.982$; $\boldsymbol{p = 0.179}$; $d = 0.378$
OK107-GAL4 (*responder control* **vs.** *driven*)	$t_{(432)} = 2.166$; $\boldsymbol{p = 0.171}$; $d = 0.399$
OK107-GAL4 (*driver control* **vs.** *driven*)	$t_{(432)} = 1.067$; $\boldsymbol{p = 0.287}$; $d = 0.195$
GH146-GAL4 (*responder control* **vs.** *driven*)	$t_{(432)} = 1.732$; $\boldsymbol{p = 0.232}$; $d = 0.316$
GH146-GAL4 (*driver control* **vs.** *driven*)	$t_{(432)} = 2.742$; $\boldsymbol{p = 0.044}$; $d = 0.518$

Table A46. Statistical tests for Figures 2.2.6-D and 2.2.8

Sleep per day (*two-way ANOVA*): *UAS-hSod1^{A4V}* Factor 1 (*genotype*) → $F_{(2,428)} = 7.281$; $\boldsymbol{p = 0.0008}$; $\eta^2 = 0.024$ Factor 2 (*brain region*) → $F_{(4,428)} = 28.860$; $\boldsymbol{p < 0.0001}$; $\eta^2 = 0.193$ Interaction (*genotype × brain region*) → $F_{(8,428)} = 4.64$; $\boldsymbol{p < 0.0001}$; $\eta^2 = 0.062$	
R23E10-GAL4 (*responder control* **vs.** *driven*)	$t_{(428)} = 5.002$; $\boldsymbol{p < 0.0001}$; $d = 0.921$
R23E10-GAL4 (*driver control* **vs.** *driven*)	$t_{(428)} = 4.789$; $\boldsymbol{p < 0.0001}$; $d = 0.867$
pdf-GAL4 (*responder control* **vs.** *driven*)	$t_{(428)} = 2.336$; $\boldsymbol{p = 0.149}$; $d = 0.426$
pdf-GAL4 (*driver control* **vs.** *driven*)	$t_{(428)} = 0.522$; $\boldsymbol{p = 0.937}$; $d = 0.094$
cry-GAL4 (*responder control* **vs.** *driven*)	$t_{(428)} = 0.347$; $\boldsymbol{p = 0.937}$; $d = 0.064$
cry-GAL4 (*driver control* **vs.** *driven*)	$t_{(428)} = 1.925$; $\boldsymbol{p = 0.288}$; $d = 0.374$
OK107-GAL4 (*responder control* **vs.** *driven*)	$t_{(428)} = 0.981$; $\boldsymbol{p = 0.862}$; $d = 0.178$
OK107-GAL4 (*driver control* **vs.** *driven*)	$t_{(428)} = 2.218$; $\boldsymbol{p = 0.175}$; $d = 0.398$
GH146-GAL4 (*responder control* **vs.** *driven*)	$t_{(428)} = 0.222$; $\boldsymbol{p = 0.937}$; $d = 0.040$
GH146-GAL4 (*driver control* **vs.** *driven*)	$t_{(428)} = 0.914$; $\boldsymbol{p = 0.862}$; $d = 0.167$

Table A47. Statistical tests for Figure 2.2.9-A

Sleep per hour (*two-way repeated measures ANOVA*):
Between group (*genotype*) → $F_{(2,92)} = 65.740$; $\boldsymbol{p < 0.0001}$; $\eta^2 = 0.066$
Within group (*time*) → $F_{(23,2116)} = 173.600$; $\boldsymbol{p < 0.0001}$; $\eta^2 = 0.549$
Interaction (*genotype × time*) → $F_{(46,2116)} = 7.612$; $\boldsymbol{p < 0.0001}$; $\eta^2 = 0.048$

Table A48. Statistical tests for Figure 2.2.9-B

Sleep per day (*one way ANOVA*): $F_{(2,89)} = 75.440$; $\boldsymbol{p < 0.0001}$; $\eta^2 = 0.629$	
R23E10-GAL4 > UAS-Hk^{RNAi} **vs.** *UAS-Hk^{RNAi} /+*	$t_{(89)} = 10.100$; $\boldsymbol{p < 0.0001}$; $d = 1.829$
R23E10-GAL4 > UAS-Hk^{RNAi} **vs.** *R23E10-GAL4/+*	$t_{(89)} = 11.000$; $\boldsymbol{p < 0.0001}$; $d = 1.960$

Table A49. Statistical tests for Figure 2.2.9-C

Sleep per hour (*two-way repeated measures ANOVA*):
Between group (*genotype*) → $F_{(2,90)} = 0.410$; $\boldsymbol{p = 0.665}$; $\eta^2 = 0.0006$
Within group (*time*) → $F_{(23,2070)} = 212.200$; $\boldsymbol{p < 0.0001}$; $\eta^2 = 0.642$
Interaction (*genotype × time*) → $F_{(46,2070)} = 3.863$; $\boldsymbol{p < 0.0001}$; $\eta^2 = 0.023$

Table A50. Statistical tests for Figure 2.2.9-D

Sleep per day (*one way ANOVA*): $F_{(2,90)} = 0.410$; $\boldsymbol{p = 0.665}$; $\eta^2 = 0.009$	
R23E10-GAL4 > UAS-Shal^{RNAi} **vs.** *UAS-Shal^{RNAi} /+*	post hoc analyses are not applicable
R23E10-GAL4 > UAS-Shal^{RNAi} **vs.** *R23E10-GAL4/+*	

Table A51. Statistical tests for Figure 2.2.10-A

Sleep per hour (*two-way repeated measures ANOVA*):
Between group (*genotype*) → $F_{(2,93)} = 16.400$; $\mathbf{p < 0.0001}$; $\eta^2 = 0.025$
Within group (*time*) → $F_{(23,2139)} = 148.000$; $\mathbf{p < 0.0001}$; $\eta^2 = 0.532$
Interaction (*genotype × time*) → $F_{(46,2139)} = 5.338$; $\mathbf{p < 0.0001}$; $\eta^2 = 0.038$

Table A52. Statistical tests for Figure 2.2.10-B

Sleep per day (*one way ANOVA*): $F_{(2,93)} = 16.400$; $\mathbf{p < 0.0001}$; $\eta^2 = 0.261$	
R23E10-GAL4 > UAS-hSod1^{WT}, UAS-Hk^{RNAi}, **vs.** *R23E10-GAL4 > UAS-hSod1^{WT}*	$t_{(93)} = 4.917$; $\mathbf{p < 0.0001}$; $d = 0.869$
R23E10-GAL4 > UAS-hSod1^{WT}, UAS-Hk^{RNAi}, **vs.** *R23E10-GAL4 > UAS-Hk^{RNAi}*	$t_{(93)} = 0.086$; $\mathbf{p = 0.932}$; $d = 0.015$

Table A53. Statistical tests for Figure 2.2.10-C

Sleep per hour (*two-way repeated measures ANOVA*):
Between group (*genotype*) → $F_{(2,89)} = 98.860$; $\mathbf{p < 0.0001}$; $\eta^2 = 0.148$
Within group (*time*) → $F_{(23,2047)} = 123.900$; $\mathbf{p < 0.0001}$; $\eta^2 = 0.433$
Interaction (*genotype × time*) → $F_{(46,2047)} = 5.553$; $\mathbf{p < 0.0001}$; $\eta^2 = 0.039$

Table A54. Statistical tests for Figure 2.2.10-D

Sleep per day (*Kruskal-Wallis test*): $H = 61.810$; $\mathbf{p < 0.0001}$	
R23E10-GAL4 > UAS-hSod1^{A4V}, UAS-Hk^{RNAi} **vs.** *R23E10-GAL4 > UAS-hSod1^{A4V}*	$Z > 3.891$; $\mathbf{p < 0.0001}$
R23E10-GAL4 > UAS-hSod1^{A4V}, UAS-Hk^{RNAi} **vs.** *R23E10-GAL4 > UAS-Hk^{RNAi}*	$Z = 3.090$; $\mathbf{p = 0.002}$

Table A55. Statistical tests for Figure 2.2.11-A

Sleep per day (*one way ANOVA*): $F_{(2,92)} = 6.893$; $\boldsymbol{p = 0.002}$; $\eta^2 = 0.130$	
R23E10-GAL4 > UAS-hSod1^{WT}, UAS-Shal^{RNAi} **vs.** *R23E10-GAL4 > UAS-hSod1^{WT}*	$t_{(92)} = 2.036$; $\boldsymbol{p = 0.087}$; $d = 0.360$
R23E10-GAL4 > UAS-hSod1^{WT}, UAS-Shal^{RNAi} **vs.** *R23E10-GAL4 > UAS-Shal^{RNAi}*	$t_{(92)} = 1.686$; $\boldsymbol{p = 0.095}$; $d = 0.300$

Table A56. Statistical tests for Figure 2.2.11-B

Sleep per day (*one way ANOVA*): $F_{(2,85)} = 16.63$; $\boldsymbol{p < 0.0001}$; $\eta^2 = 0.281$	
R23E10-GAL4 > UAS-hSod1^{A4V}, UAS-Shal^{RNAi} **vs.** *R23E10-GAL4 > UAS-hSod1^{WT}*	$t_{(85)} = 2.060$; $\boldsymbol{p = 0.042}$; $d = 0.386$
R23E10-GAL4 > UAS-hSod1^{A4V}, UAS-Shal^{RNAi} **vs.** *R23E10-GAL4 > UAS-Shal^{RNAi}*	$t_{(85)} = 3.475$; $\boldsymbol{p = 0.002}$; $d = 0.645$

Table A57. Statistical tests for Figure 2.2.12

Sleep per day (*one way ANOVA*): $F_{(2,91)} = 48.24$; $\boldsymbol{p < 0.0001}$; $\eta^2 = 0.515$	
R23E10-GAL4 > UAS-Hk^{RNAi}, UAS-Shal^{RNAi} **vs.** *R23E10-GAL4 > UAS-Shal^{RNAi}*	$t_{(91)} = 4.247$; $\boldsymbol{p < 0.0001}$; $d = 0.757$
R23E10-GAL4 > UAS-Hk^{RNAi}, UAS-Shal^{RNAi} **vs.** *R23E10-GAL4 > UAS-Hk^{RNAi}*	$t_{(91)} = 5.510$; $\boldsymbol{p < 0.0001}$; $d = 0.869$